2023

A study of ultrasound neuromodulation mechanisms using crayfish motor axons

BOSTON UNIVERSITY

GRADUATE SCHOOL OF ARTS AND SCIENCES

Dissertation

A STUDY OF ULTRASOUND NEUROMODULATION MECHANISMS USING CRAYFISH MOTOR AXONS

by

FEIYUAN YU

B.S., University of Science and Technology Beijing, 2015
M.A., Boston University, 2017

Submitted in partial fulfillment of the

requirements for the degree of

Doctor of Philosophy

2023

Approved by

First Reader

Jen-Wei Lin, Ph.D.
Associate Professor of Biology

Second Reader

Yoshio Okada, Ph.D.
Professor of Pediatrics
Children's Hospital and Harvard Medical School

Third Reader

Ian Davison, Ph.D.
Associate Professor of Biology

Fourth Reader

Hengye Man, Ph.D.
Professor of Biology

Fifth Reader

Ji-Xin Cheng, Ph.D.
Professor of Biomedical Engineering
Professor of Electrical and Computer Engineering

DEDICATION

I would like to dedicate this dissertation to my beloved family members and all the people who provided help in the completion of this work.

ACKNOWLEDGMENTS

I am deeply indebted to my primary advisor Dr. Jen-Wei Lin for always being supportive and encouraging throughout my Ph.D. study. Words cannot express my gratitude for your detailed instructions, unsurpassed patience, and extensive knowledge. Thank you for leading me into the electrophysiology field and dedicating enormous effort and time to teaching me from zero.

I am also extremely grateful to Dr. Yoshio Okada who serves as a co-advisor in my dissertation project. Your relentless enthusiasm and profound belief in the work have always been inspirational. I gratefully acknowledge your insightful and constructive suggestions on my work. I must also thank all the professors who participated in the project, Dr. Ian Davison, Dr. Hengye Man, Dr. Ji-Xin Cheng, Dr. Michelle Y. Sander, and Dr. Wolfgang S Müller, for your responsive assistance and knowledgeable comments.

I wish to acknowledge the technical help and moral support provided by my classmates and collaborators, Tian Yuan, lab mates, Shaikhah Alshuaib, and staff in the biology department, Christina Honeycutt and Eliza Givens. Special thanks to Linli Shi for your generous help without hesitation whenever I am in need in the academic field and daily life. Many thanks to Xuedong Zhu for generously sharing all the relevant resources in research and experiments.

Lastly, I would like to thank my parents for all your support and motivation during this process. Thanks also to my lovely cats for keeping me and supplying daily joy during this adventure.

A STUDY OF ULTRASOUND NEUROMODULATION MECHANISMS USING CRAYFISH MOTOR AXONS

FEIYUAN YU

Boston University Graduate School of Arts and Sciences, 2023

Major Professor: Jen-Wei Lin, Associate Professor of Biology

ABSTRACT

Focused ultrasound (FUS) mediated neuromodulation has become a trending topic due to its promising attributes that enable precise and transcranial neuromodulation. Despite multiple reports of FUS effects on neurons, nervous systems, and the human brain, the mechanisms underlying such excitation or inhibition remain controversial. In our previous study, we showed that 2.1 MHz FUS induced membrane depolarizations on single crayfish motor axons in the presence of voltage-gated channel blockers, which led to a nanopore hypothesis: FUS triggered lipid molecule reconfiguration and form ion-permeable nanopores on the axonal membrane. Based on this hypothesis, stretching of the axonal membrane due to swelling in low osmolarity should increase the probability of nanopore formation under FUS. As predicted, exposure to 75% hypotonic saline induced significant increases in amplitude and frequency of occurrence of those FUS-induced depolarizations (FUSD) while the onset latency of the FUSD showed a significant decrease. Those results support the hypothesis that FUSD can be modulated by mechanically altering membrane properties.

Since FUS inevitably perturbs cell membranes, we examined the role of mechanosensitive K2P channels at the crayfish opener neuromuscular junction. At

ultrasound intensity lower than those used to evoke FUSD, FUS consistently induced membrane hyperpolarization (FUSH) in motor axons but not muscle fibers, which may lack K2P. Since K2P channels are also thermosensitive, we varied the temperature from 12 to 32 ℃. However, there was no significant correlation between FUSH amplitudes and temperature. Furthermore, FUSH was not inhibited by the K2P channel blockers, although the presence of the channels was confirmed by K2P blockers which increased input resistance and depolarized axonal resting membrane potential. Thus, it is unlikely that K2P channels underlie FUSH.

We also studied the impact of FUS on propagating action potentials (APs) in the crayfish motor axons. APs recorded during FUS took off from a hyperpolarized membrane potential and exhibited larger amplitudes and shorter duration. Three hypotheses were examined and eliminated. The US modulated AP shape changes cannot be due to: (1) alterations in microelectrode characteristics, (2) the increase in the fraction of sodium channels in the closed and not-inactivated state due to the hyperpolarization and (3) US activation of K2P channels which in turn altered AP shapes. One potential mechanism that requires further investigation is that FUS may accelerate the activation of sodium channel opening. Other factors that may indirectly modulate AP shapes are discussed.

In summary, results presented in this thesis suggest that FUS-mediated membrane responses in a single cell could vary depending on the FUS intensity and the type of ion channel a given cell expresses. Furthermore, ultrasound not only evokes changes membrane potential but also modulates action potentials. Collectively, these results

represent significant contribution to the understanding of mechanisms underlying ultrasound neuromodulation at the cellular level.

TABLE OF CONTENTS

DEDICATION iv

ACKNOWLEDGMENTS v

ABSTRACT vi

TABLE OF CONTENTS ix

LIST OF TABLES xiii

LIST OF FIGURES xiv

LIST OF ABBREVIATIONS xxi

CHAPTER 1. INTRODUCTION 1

1.1 Advantages of the FUS neuromodulation technique 1

1.2 Effects of FUS on human studies 3

1.3 Effect of FUS on neuronal tissues in *in vivo* and *in vitro* studies 5

1.4 Mechanisms of FUS neuromodulation 6

1.4.1 Thermal effect 7

1.4.2 Stable cavitation, membrane deformation and capacitance change 7

1.4.3 Activation of mechanosensitive ion channels 9

1.4.4 Nanopore hypothesis and predictions based on manipulations of membrane lipid bilayer organizations 10

1.5 Effects of changing osmolarity and temperature on membrane properties and neuroexcitability 12

1.6 Crayfish motor axon as a model system FUS study 15

1.7 Thesis outlines 16

CHAPTER 2. METHODS 17
2.1 Experimental setup 17
2.1.1 Crayfish preparation 17
2.1.2 Solution preparation and blockers application 18
2.1.3 Setup configuration 19
2.2 Electrophysiology 20
2.3 FUS parameters 21
2.4 Experimental protocols for osmolarity and temperature manipulations 23
2.5 Hodgkin-Huxley model simulation 24
2.6 Data analysis 24
CHAPTER 3. THE EFFECT OF OSMOLARITY ON FUS-INDUCED DEPOLARIZATION 26
3.1 Introduction 26
3.2 Results 28
3.2.1 Basic characteristics of action potentials and FUSD in hypotonic saline 28
3.2.2 Effects of hypotonic saline on properties of FUSD 32
3.2.3 Effects of the osmolarity manipulation on axon morphology 37
3.2.4 Time-dependent variation of FUSD parameters in hypotonic saline 38
3.3 Discussion 40
3.3.1 FUS-specific membrane conductance g_{US} and nanopore hypothesis 40
3.3.2 Potential roles of radiation forces in FUSD 42
3.3.3 Future directions and potential applications to human 44

3.4 Conclusion 44

CHAPTER 4. EFFECTS OF TEMPERATURE ON ULTRASOUND INDUCED NEURONAL RESPONSES IN MOTOR AXONS AND MUSCLE FIBERS OF THE CRAYFISH NEUROMUSCULAR JUNCTION 46

4.1 Introduction 47

4.2 Results 49

4.2.1 Effects of cooling on FUS-induced responses in motor axons 49

4.2.2 Enhancement of FUSH by cooling is specific to axonal responses 51

4.2.3 Summary of cooling effects on FUSH recorded in motor axons and muscle fibers 52

4.2.4 Effects of heating on FUS-induced membrane response in muscle fibers 55

4.2.5 Effects of heating on FUS-induced membrane response in muscle fibers 58

4.2.6 Compilation of data from both cooling and heating does not suggest simple temperature dependence of FUSH 59

4.2.7 Possible role of K2P channels in the temperature dependence of FUSH 60

4.3 Discussion 63

4.3.1 K2P hypothesis for FUSH 63

4.3.2 Sonophore hypothesis for FUSH 65

4.3.3 Effects of changing temperature on mechanical properties of biological membrane 66

4.3.4 Difference between axon and muscle responses to FUS 67

4.4 Conclusion 68

CHAPTER 5. FUS EFFECT ON PROPAGATING ACTION POTENTIALS 70
5.1 Introduction 70
5.2 Results and discussion 72
5.2.1 Effects of FUS on action potentials 72
5.2.2 FUS significantly enhanced the time derivatives of the AP 74
5.2.3 Discussion 75
5.3 Conclusion 79
CHAPTER 6. DISCUSSION 81
6.1 Using crayfish neuromuscular junction as a model system to study FUS neuromodulation 82
6.2 Polymodal FUS effects on crayfish NMJ 82
6.3 Conclusions and perspectives 84
APPENDIX 87
BIBLIOGRAPHY 89
CURRICULUM VITAE 105

LIST OF TABLES

Table 1 Statistical analysis on the physiological parameters of US-induced responses in control and hypotonic saline. Detectable FUSD used for averaging were collected over a period of 45 minutes immediately before and after switching from the control to 75% hypotonic saline. The time windows used for the recovery period varied from 30 to 45 minutes. Values in this table were averaged from the average values calculated from eight axons. One of the eight preparations used sucrose substitution to generate hypotonic saline, two preparations used mannitol substitution while the remaining five used distilled water dilution. 37

LIST OF FIGURES

Figure 1.1 Hypothetical nanopore configurations and transitions induced by FUS on the lipid membrane. The normal stable state of lipid bilayers (state 0) can be interrupted by FUS and possibly transits into an unstable state (state 1) that contains hydrophobic pores created by the lateral movement of lipid molecules. Further perturbation of the external mechanical force may cause a configuration change of the lipid molecules to form a highly unstable transition pore (state 3). The intermediate pores can either reform hydrophobic pores or become semistable hydrophilic pores (state 3) with the realignment of lipids. The configuration of hydrophilic nanopores presents a lower energy level than the transition state, meaning that returning to the initial state required some energy to cross the energy barrier of state 2. Thus, the hydrophilic nanopores, once formed, can remain stable and enable large-conductance permeable through the membrane. Inset: hypothesized mem-brane energy levels for each state and FUS- or radio frequency (RF)-facilitated transitions [83]. 11

Figure 2.1 Experimental configurations and protocols. *A*: illustration of the crayfish opener neuromuscular preparation with two recording electrodes (Rec elec), 1 and 2, respectively, together with ultrasound transducer placements. *B*: detailed 2-electrode current clamp configuration, with 1 electrode at the primary branch (blue) and the second electrode at the secondary branch (red). Also shown is the approximate footprint of a typical US focal area when the transducer is angled at 45° (shaded ellipse). The dimensions of the axon are equivalent to a preparation dissected from a large animal 6 cm in length head to tail. The US focal area coverage, relative to axonal arborization, is likely to be more extensive in some smaller animals used in this study. (C) Timeline of a typical experiment. A 10 nA current injection was alternated with US tone burst. The time gap between the current step and FUS tone burst was 0.5 seconds. FUSD was recorded as 20-s long traces. The time gap between FUS test trace and the next 10 nA current step was 10 second. (D) The FUS tone burst consists of 20 pulses of 50 μs tone bursts (2.1 MHz) delivered at 1 KHz..... 19

Figure 3.1 Effects of hypotonic saline on passive and active membrane properties in crayfish axons. (A) Suprathreshold responses evoked by FUS tone burst. Inset: initial part of US evoked responses displayed in an expanded time scale. The recordings were obtained from the data points marked by inverted red triangles in E. (B) Subthreshold responses evoked by the same US tone bursts. The traces were obtained from the time point marked by red arrows in E. In A and B, the timing of US delivery is marked by the arrowhead in the main graphs and the horizontal bar in the insets. (C) Examples of AP evoked by 10 nA steps recorded in control and hypotonic saline. The recordings were obtained from the time points marked by "*" in E. (D) Arrows identify the time window during which single exponential fits were applied for time constant estimates. This

trace is identical to the black trace in C. (E) Timeline plots of the amplitudes of FUSD ($FUSD_{amp}$) and action potential (AP_{amp}) in control and hypotonic saline (shaded area). Switching to hypotonic saline induced minimal changes in both parameters. (F) Timeline plots of resting membrane potential (RMP) and membrane time constant (Tau). (E) and (F) share the same time axes. Low osmolarity in this experiment was achieved by removing 90 mM mannitol from a "control" saline where 45 mM NaCl had been replaced by 90 mM mannitol.. 31

Figure 3.2 Quantitative analysis of US evoked physiological parameters measured in control and low osmotic saline. (A) Illustration of measurements of amplitude, 50% duration, and delay of US-induced responses (inset). The arrowhead, and the horizontal bar in the inset, indicate the timing of US tone burst delivery. (B) Timeline of the amplitude of FUSD. Red crosses identify suprathreshold responses. (C) Timeline of the delay of US-induced responses. (D) Normalized frequency of occurrence of US-induced responses. The frequency of 1 means US tone burst successfully evoked responses in consecutive trials. (E) Timeline of the half-maximal duration of subthreshold response. The data points in E do not fully correspond to those in B, C, and D because the durations were not measured in trials where the US evoked AP. The number of data points in B, C, and D for control and hypotonic saline was 22 and 29, respectively. The number of data points in E was 20 and 16 for control and hypotonic saline, respectively. 33

Figure 3.3 Compilation of changes in US induced depolarizations as osmolarity was lowered. Average and standard error of means of normalized amplitude (A), delay (B), frequency of occurrence (C) and Dur_{50} (D) plotted in 5-minute blocks. The transition from control (black) to hypotonic (red) saline occurred at 45 minutes. A set of eight preparations were used for statistical analysis in this report. For the preparation of hypotonic saline, one of the eight preparations used sucrose substitution, two used mannitol substitution while the remaining five used distilled water dilution. The sample size for each data point ranged from 4 to 12. For panel A and D, the total number of FUSD events was 73 in control saline and 100 in hypotonic saline. For panel B and C, the sample sizes were 82 in control and 105 in hypotonic saline. Smaller sample sizes in A and D were due to exclusion of trials where FUSD was suprathreshold and evoked AP. 35

Figure 3.4 Illustration of how osmotic stretching of the lipid membrane would affect the hypothetical lipid membrane energy levels, and state transitions caused by US, in comparison to control (=non-stretched) membrane. These changes may explain the observed effects of hypotonic saline on g_{US} opening and closing probabilities. Hypotonic solution stretches the membrane, i.e. loosens the dense packing of the lipid bilayer (from 0-stable to stretched membrane); the increase in surface area corresponds to an increase of the membrane energy level (inset, red level vs. black level 0). From this stretched state the opening of

hydrophobic pores and transition pores requires less absorption of energy than in control (inset: red vs. black uphill arrows 0 → 1 → 2, respectively), so that the probability of transition in response to absorption of US energy is increased. Similarly, the probability of the first step of stable nanopore closing is increased due to a decreased energy gap (inset: 3 → 2 uphill red vs. black arrow, respectively). This change would reduce the mean open time of semi-stable hydrophobic pores 3 and thus duration of g_{US}. 41
Figure 4.1 Effect of cooling on FUS-induced hyperpolarization in a motor axon. (A) US at 2.1 MHz and with a duration of 80 ms induced a small hyperpolarization at 23 °C. (B) The same US tone evoked fluctuating hyperpolarization when the preparation was cooled to 15 °C. (C) Reheating the preparation to control level reduced FUSH. Black traces in (A), (B) and (C) are recordings from individual trials while red traces represent averages. The black bar in (A), (B) and (C) indicates the timing of US. The sample size used for the averages in (A), (B) and (C) were 11, 14 and 9 respectively. (A), (B) and (C) share the same scales. (D) Action potentials were recorded from the same axon as that in (A), (B) and (C) under indicated temperatures. The action potentials recording were single trials and evoked by a suction electrode. (E) Timelines of resting membrane potential (V_m, black) and temperature (red). (F) Timelines of AP amplitude (blue squares) of the motor axons and FUSH (red circles) to highlight the stability and consistency of the recordings..... 50
Figure 4.2 Cooling-induced changes in FUS evoked responses recorded from a muscle fiber. (A), (B) and (C) Intracellular recordings from a muscle fiber obtained from the same preparation, and simultaneously, as those shown in Figure 1. FUS induced small responses with a step-like shape. Black traces represent recordings from individual trials and red traces are averages with a sample size of 11, 14 and 9 for (A), (B) and (C) respectively. (A) (B) and (C) share the same scales. (D) Synaptic potentials were recorded under the temperatures shown in (A) to (C). The synaptic potentials were evoked by a train of eight APs. The EPSP amplitudes increased during the train due to synaptic facilitation. The EPSP traces were averages of 10, 14 and 9 trials. Baselines of EPSP traces have been aligned for comparison. (E) Timeline of resting Vm (black) and temperature (red). (F) Timelines of EPSP amplitude (blue squares) and FUSH (red circles) amplitudes recorded from the muscle fiber are displayed to highlight the stability of the recordings. 52
Figure 4.3 Summary of FUS-induced hyperpolarization upon cooling. (A) Average amplitudes of FUS-evoked responses in motor axons are plotted against the temperatures when the recordings were made. Data points from the same axons are connected. Each preparation is represented by a different symbol. Error bars associated with each data point represent the standard error of means but the temperature variations were typically smaller than the size of the symbols. The dashed line represents a preparation where the changes in

FUS evoked responses were not statistically significant. Sample sizes used for average ranged from 10 to 20. (B) Average amplitudes of FUS-evoked responses recorded from muscle fibers are plotted against the temperatures from which the recordings were made. Data from the same muscle fibers are connected. Each preparation is represented by different symbols. Matching symbols in (A) and (B) mean they were obtained simultaneously from the same preparations. The dashed lines represent preparations where the changes in FUS evoked responses were not statistically significant. 53
Figure 4.4 Effects of heating on FUS-induced responses in a motor axon. (A), (B) Intracellular recordings from a motor axon as the temperature was raised from 23 (A) to 32 °C (B). The heating was accompanied by a minimal change in FUSH amplitude. Black traces in (A) and (B) are recordings from individual trials while the red traces are averages of displayed single trials. The sample size of the averages in (A) and (B) was 17. (A) and (B) share the same scales. (C) An increase in temperature caused membrane potential hyperpolarization and a reduction in AP amplitude and duration in the axon. The leftward displacement of the AP recorded at 32 °C (red) was due to an acceleration of AP conduction velocity. The AP traces were from single trials. (D) Timelines of resting membrane potential (Vm, black) and temperature (red). (E) Timelines of AP amplitude (blue squares) of the motor axons and FUSH (red circles) to highlight the stability of the recordings. 55
Figure 4.5 Heating-induced changes in FUS evoked responses recorded from a muscle fiber. (A) and (B) Intracellular recordings from a muscle fiber obtained from the same preparation, and simultaneously, as those shown in Figure 4. FUS induced small responses with step-like shapes. Black traces represent recordings from individual trials and red traces are averages with sample sizes of 17 for (A), and (B). (A) and (B) share the same scales. (C) Synaptic potentials were recorded under the two temperatures shown in (A) and (B). The synaptic potentials were evoked by a train of eight APs. The EPSP amplitudes increased during the train due to synaptic facilitation. The EPSP traces were averages of 17 trials. Baselines of EPSP traces have been aligned for comparison. (D) Timeline of resting membrane potential (black) and temperature (red). (E) Timelines of EPSP (blue squares) and FUSH (red circles) amplitudes recorded from the muscle fiber are displayed to highlight the stability of the recordings. 57
Figure 4.6 Summary of FUS-induced hyperpolarization upon heating. (A) Average amplitudes of FUS-evoked responses in motor axons are plotted against the temperatures from which the recordings were made. Data from the same axons are connected. Each preparation is represented by a different symbol. Sample sizes used for average ranged from 7 to 20. (B) Average amplitudes of FUS-evoked responses recorded from muscle fibers are plotted against the temperatures from which the recordings were made. Data from the same

muscle fibers are connected. Each preparation is represented by different symbols. The symbols that match those in (A) mean they were obtained simultaneously in the same preparations. The dashed lines represent a preparation where the changes in FUS evoked responses were not statistically significant. 58
Figure 4.7 Compilation of data from heating and cooling experiments. The data points were from axonal recordings shown in Figure 4.3A and 4.6A. The blue line represents a linear fit to the cooling data points, with a slope of 0.25mV/°C. The red line represents a linear fit to the heating data point, with a slope of -0.2 mV/°C. Neither fit represents a statistically significant correlation. (See text). 60
Figure 4.8 Effects of TREK-1 channel blockers on motor axons and FUS evoked responses. (A) Axonal recordings evoked by -5, +5 and +20 nA current steps. Application of 100 μM fluoxetine (red) caused a depolarization of resting membrane potential, by 4 mV, and an increase in input resistance such that the +20 nA step, which was subthreshold in control saline, could trigger AP firing in fluoxetine. Inset: voltage current responses evoked by current steps from -20 to +20 nA in 5 nA increments. The input resistance increased from 0.46 to 0.81 MΩ. (B) FUS evoked hyperpolarization recorded from the same axon as that used in (A). FUSH became larger in fluoxetine (100 μM). Recordings were obtained from single trials. The arrows identify a slight "overshoot" at the termination of FUS tone bursts. Inset: Comparison of averaged FUS-induced hyperpolarization in an expanded time scale. US-induced responses evoked by individual tone bursts showed an increase in amplitudes. Individual hyperpolarization matches the duration of each FUS tone, which lasted for 500 μs. FUS evoked responses ($FUSH_{pp}$) were measured as peak-to-peak amplitudes resulting from individual 0.5 ms tone bursts. (C) Timelines of $FUSH_{pp}$ and input resistance measured from the preparation used in (A) and (B). (D) Timelines of $FUSH_{pp}$ and input resistance were obtained from a different motor axon where norfluoxetine (50 μM) was used to block TREK-1 channels. The blocker effectively raised input resistance but had no impact on $FUSH_{pp}$. Inset: Averaged FUSH recordings obtained before (black) and after (red) addition of norfluoxetine. The number of trials used for averaging were 7 and 9 respectively. 62
Figure 5.1 Effects of focused ultrasound on AP shapes. (A) A train of 8 APs firing at 100 Hz during an 80 ms continuous, 2.1 MHz US tone. (Black bar above), which set off a hyperpolarization (arrow). Control AP (black) and AP recorded ruing FUS (red) are overlaid. The AP train under FUS is also shifted vertically so that the baselines before the first AP are aligned (green). These traces are single trial recordings. (B) The first APs in (A) are displayed in an expanded time scale to detail the changes in AP shape under FUS. Lower traces: time derivative of control AP, to facilitate the illustration of AP delay measurement. Criteria of measurement for parameters defining APs are illustrated. (See text) (C) AP

amplitude (amp), duration (dur), delay (del) and afterdepolarization (adp) from all of the eight APs are measured and plotted. During US application, AP amplitude and durations exhibit significant changes while delay and afterdepolarization showed no change. 74
Figure 5.2 Changes in AP shape are compared in phase plots. Phase plots of control (black) and FUS modulated AP (red) are overlaid. The plot also includes the transients due to stimulus artifacts (arrow). There was minimal difference in stimulus artifact under FUS but the maximal and minimal time derivatives of the AP under FUS are significantly enhanced. Arrowhead identifies the point when the trajectories of the two traces diverge. 75
Figure 5.3 Evaluations of inactivation hypothesis by comparing prediction from the Hodgkin-Huxley model with recordings from the crayfish motor axons. (A) AP calculated from Hodgkin-Huxley (H-H) model. The two APs are fired by 1 ms current steps. AP fired from -98 mV exhibit a larger amplitude and broader duration. (B) Using the H-H model, a comparison of an AP fired from the anodal break (left) and a resting membrane potential of -63 mV (black) was performed. The initial hyperpolarization that set off the anodal break was achieved with a -5 nA and 20 ms current step. The second action potential was activated by a 10 nA and 1 ms current step. (C) Overlay of the two APs displayed in (B) to illustrate the larger amplitude and longer duration of the AP fired from the anodal break. (D) The current step series in a crayfish motor axon demonstrate that despite the larger and longer-lasting hyperpolarization than that shown in (B), no anodal break firing occurred in the crayfish motor axon. (E) Inactivation of I_{Na} recorded from the crayfish axonal terminals. The mid-point of the inactivation curve is -58 mV, adopted from [170]. 77
Figure Appendix 1 A representative example comparing FUS effects in room temperature versus heated temperature. (A) A train of AP without FUS application (black) and during simultaneous FUS (red). The traces were averaged from 23 repeated trials on the same axon. FUS alone induced a small hyperpolarization (blue) on the motor axon. Arrowheads denote the onset and offset of FUS tone burst delivery. The average last AP in the train replot with a higher magnification (right) to illustrate FUS-induced potential fluctuations (inset). (B) Same as (A) but recorded in elevated temperature. Averaged from 19 trials. (C) Phase plots of the last AP in the train with (US) or without (black) FUS at the 2 different temperatures. 87
Figure Appendix 2 Effects of FUS on AP characteristics at different temperatures. (A) Illustration of measurements of ADP. ΔADP = 1st ADP – 7th ADP. (B) Illustration of measurements of amplitude (AMP), 50% duration (DUR_{50}), and delay (DEL) of US-induced responses (inset). (B) Timeline of the temperature of bath saline <0.3 mm away from the electrode recording sites, and the measured parameters of the 8th AP at room temperature (black) and heated temperature (red). Each data point represents the measurement of a single trial. Lighter

colors illustrated data obtained with FUS application at 22.0 ± 1.84 ℃ (grey) and 31.4 ± 1.57℃ (yellow), respectively. The transition period (grey in the temperature timeline) was excluded from calculations of the averages (green, FUS; dark green, control). 88

LIST OF ABBREVIATIONS

ADP	After-Depolarization Potential
AP	Action Potential
ARF	Acoustic Radiation Force
BLS	Bilayer Sonophore
EEG	Electroencephalographic
E_k	Potassium Equilibrium Potential
FDA	Federal Drug Administration
fMRI	Functional magnetic resonance imaging
FUS	Focused Ultrasound
FUSD	Focused Ultrasound-induced Depolarization
FUSH	Focused Ultrasound-induced Hyperpolarization
GABA	γ-Aminobutyric acid
g_{US}	US-induced membrane conductance
HEK	Human Embryonic Kidney
H-H	Hodgkin-Huxley
HIFU	High-Intensity Focused Ultrasound
K2P	Two-Pore-domain Potassium family
NMJ	Neuromuscular Junction
Piezo1	Piezo-type mechanosensitive ion channel component 1
R_m	Membrane Resistance
RMP	Resting Membrane Potential

S1	Primary Somatosensory Cortex
TPS	Transcranial Pulse Stimulation
TRPC1	Transient-Receptor-Potential-Channel 1
US	Ultrasound
VGCC	Voltage-Gated Ca2+ Channels
V_m	Membrane Potential

CHAPTER 1. INTRODUCTION

1.1 Advantages of the FUS neuromodulation technique

FUS is a new-emerging neuromodulation method due to its high spatial resolution and non-invasive features. The neuromodulation technique refers to the modification of neuronal activity by specific modalities, including electric stimulation, magnetic field, optogenetic technique, thermal, pharmacological, and acoustic stimulation [1-3]. These modalities fundamentally change the membrane potentials in selective compartments of neuronal cells to achieve modulatory effects. The neuronal membrane contains ion transporters that separate charged ions in or out of the cell and cause a difference in the charge density of specific ions across the membrane. Therefore, neuromodulation can be achieved by methods that directly act on membrane properties or/and ion-permeable channels on the membrane.

Direct electric stimulation applies voltage or current via electrodes to create a potential gradient across the target cell. As the neuromodulation method with the longest history, the mechanism is well-studied and generally acknowledged. With the implanted electrodes, the signal transmission has the shortest latency (<1 ms) among all neuromodulation modalities with a resolution that depends on the size of the electrode. Current stimulation can also be applied transcranially but with a largely compromised spatial resolution (>500 mm) [2].

Magnetic stimulation creates an effect similar to electric simulation by using a strong magnetic field. The method has been used in humans as a treatment for depression

and peripheral nerve stimulation [4-6]. Transcranial magnetic stimulation requires large equipment and has a spatial resolution of around 10 mm [7].

The Optogenetics technique genetically modified the neuron to express a light-sensitive ion channel and can achieve sub-cellular resolution [8, 9]. However, due to the moral considerations of genetic modification, the method is limited to animal practices only.

Thermal stimulation can be induced by infra-red laser light or microwave, resulting in a change in local transmembrane capacitance and non-uniform changes in ion channel kinetics. A relatively high resolution (~10 μm) can be achieved with optical stimulation [10]. However, thermal-induced tissue damage is a potential risk in neuromodulatory practices [2].

Pharmacological methods modify the chemical environment by changing ionic concentration, and application of neurotransmitters, ion channel blockers, or agonists. The variety of chemical compounds provides numerous modulatory possibilities while the application region may be difficult to be strictly limited due to chemical diffusions.

Acoustic stimulation, especially FUS, was shown to induce a thermal effect to mechanically deform membrane. The deformation could in turn change the membrane capacitance and activate of mechanosensitive ion channels [11, 12]. In addition, FUS could mechanically impact membrane by small gas bubbles (cavitations). Among the non-invasive neuromodulation techniques, FUS could maintain shape focal areas (<1 mm) on the targeted region when applied transcranially, which allows a more precise target [11]. Most neuromodulation studies use low frequency (<3 MHz*) and intensity (<100

mW/cm^2) ultrasound [13, 14], which was not shown to cause considerable thermal increase or cavitation that may induce tissue damage. Thus, low-intensity low-frequency FUS is considered a safe, painless, precise neuromodulation technique for the stimulation of deep areas.

*No uniform standard among literature.

1.2 Effects of FUS on human studies

The potential of using FUS in medical treatment dates back to the 1940s when Lynn et al. found high-intensity ultrasound-induced focal destruction in ex vivo beef liver specimens and reversible cerebral changes in living animals [15]. In 1955, the Fry brothers reported selectively targeted lesions in cat brains with high-intensity focused ultrasound (HIFU) [15, 16]. In the 1990s, HIFU was utilized in the ablation of prostate tumors. With subsequent success in studies, HIFU is now approved for the ablation treatment of various abnormal tissue, including uterine fibroids, osteoid osteoma, and prostate tumors. Researchers also showed the promising application of HIFU-induced thermal ablation in the treatment of various cancers, including retinal, kidney, liver, breast, pancreatic, and brain tumors [17]. With the guidance of magnetic resonance imaging (MRI), FUS was also shown to alleviate the symptoms of neurological disorders such as central neuropathic pain, essential tremor, and Parkinson's disease [18-20].

Despite the well-established clinical application of HIFU and the reported potential of deep brain stimulation, it was not until recently did researchers show interest in low-intensity FUS-induced neuromodulation [21]. In 2002, Clement and Hynynen tested FUS on ex vivo human skulls and demonstrated the feasibility of using FUS in non-invasive

brain stimulation [22]. In 2012, Legon et al. found differential FUS sensitivity of somatosensory fibers when FUS stimulation applied to fingertips was shown to cause functional changes in the cortex, which ignited interest in the potential use of FUS in pain suppression [23]. In 2013, Hameroff et al. first reported improvement in mood after unfocused transcranial ultrasound treatment on the frontal scalp [24]. In 2014, 2 studies reported transcranial FUS effects on the human brain. Legon et al. targeted FUS on the human primary somatosensory cortex (S1) and found alternation in the sensory-evoked brain activity from electroencephalographic (EEG) recordings [25]. In a second study, healthy subjects reported tactile sensation on the hand, which was confirmed with EEG-recorded cortical potential, when applied MRI-guided FUS to the corresponding S1 region [26]. In 2016, a case report showed improvements in a patient with consciousness disorder after FUS thalamic stimulation [27]. Most recently, Beisteiner et al. demonstrated a newly developed Transcranial Pulse Stimulation technique (TPS) using FUS could significantly improve the neuropsychological scores of 35 Alzheimer patients. The improvement was correlated with fMRI data that indicated enhanced connectivity of memory network after a 3-month treatment [28]. A study targeting FUS on the motor cortex induced inhibition of intracortical excitability and reduction in reaction time on behavioral visuomotor task [29]. FUS also allows transcranial stimulation of deeper regions in the brain, supported by a study proposing that FUS activated GABAergic inhibition by preferential activation of interneurons within the superior colliculus [30]. The long-term effects of FUS were evaluated in a study which reported an upregulation of functional coupling persisted a week in the stimulated brain area after repeated TPS based on MRI imaging [31].

Overall, most FUS studies on the human brain demonstrated functional alternations in cortical activity without structural deformations [13, 32], suggesting FUS as a safe and efficient tool for non-invasive deep brain stimulation.

1.3 Effect of FUS on neuronal tissues in *in vivo* and *in vitro* studies

Extensive studies have been done to explore the neuromodulation effects of FUS on animals since the 1950s. However, the excitatory versus inhibitory results were highly variable, likely caused by variances in experimental setup and tested subjects [33], which may involve different neuromodulation mechanisms.

Experiments on the peripheral nervous system mostly showed an inhibition effect of FUS. FUS applied on frog sciatic nerve *in vitro* blocked nerve conduction (2.7 MHz, 1,150 W/cm ^{2}, pulses of 0.14-1.2 s with a 2-3 s interval) [34] and reduced action potential amplitude (0.661 and 1.981 MHz, ~400 W/cm ^{2}, 30 s) [35]. FUS on the sciatic nerves of rabbits also showed conduction blockage (3.2 MHz, 1930 W/cm ^{2}, 5 s) [36]. Transcranial FUS application on rat vagus nerve inhibited compound APs (1.1 MHz, 13.6 – 93.4 W/cm ^{2}, 15 s) [37]. On the *ex vivo* crab leg nerve bundle, however, excitation was induced by FUS (0.67MHz, 66 W/cm^2, and 118.1 W/cm^2, 10kHz PRF, 50% duty cycle, 8 ms total duration) [38].

Studies on the central nervous systems of mice and rats report a mixture of excitatory and inhibitory modulation effects of FUS [39]. Before 2018, multiple previous studies have suggested activation of the motor cortex, hippocampus, thalamus, and visual cortex (varies between 0.25 - 0.69 MHz, 0.25 – 79.02 W/cm ^{2}, 0.5 ms - 40 s sonication duration) [32]. FUS also increased the level of extracellular neurotransmitters, including

dopamine, serotonin, and GABA [40]. In 2018, Guo et al. and Sato et al. reported FUS activation of peripheral auditory pathways in guinea pigs and mouse brains, respectively, suggesting confounding effects of the FUS technique. Later studies confirmed the neuromodulation effects of FUS with deafened animals [41-43]. Auditory masking can also abolish auditory activation in humans during transcranial FUS stimulation [44]. Therefore, precise neuronal pathways by which FUS generate modulation in *in vivo* studies require further investigation. Nevertheless, the nature of FUS cannot be neglected. For example, a recent study on monkeys demonstrated FUS induced a significant reduction of seizures in acute epilepsy (800 kHz, 1.74 MPa, 500 Hz PRF, 36% duty cycle) [45]. In this study, single neuron recording *in vivo* in anesthetized rat somatosensory cortex showed neuron-type selectivity responses to FUS (500 kHz, 1.05 – 158.22 mW/cm ^{2}, 200 μs, 30 – 4,500 Hz PRF, 0.6 – 90% duty cycle) [45]. Studies done *in vitro* on cultured neurons also reported activation of potassium [46], sodium [47], and calcium currents [48]. Therefore, FUS-mediated modulation is well-documented in neuronal tissues and whole animals although the modulation could be either excitatory or inhibitory, depending on preparations and FUS parameters.

1.4 Mechanisms of FUS neuromodulation

Despite numerous reports on FUS-induced neuromodulation, the underling mechanisms in most studies remain unclear. Currently, proposed underling mechanisms of FUS-induced neuromodulation were mainly classified into 2 categories: thermal and non-thermal (mechanical) [11]. Heat generates from the absorption of the acoustic energy transmitted to the medium. Non-thermal effects involve physical processes related to

cavitation, radiation force, streaming, membrane flexoelectricity, and activation of mechanosensitive ion channels [14, 49, 50]. The variety of proposed mechanisms from different studies suggests varying combinations of distinct processes attributed to specific FUS parameters, experimental configuration, and targeted tissue. Further study may need to further explore the FUS mechanism in an application-specific manner.

1.4.1 Thermal effect

Temperature elevation after FUS treatment was well documented in several studies with diagnostic ultrasound [50]. The thermal change result from the absorption of the acoustic energy that converts to heat in the exposed tissue [51], and is a major FUS effect when utilizing high power and long exposure time. Small temperature increases of 0.1°C are sufficient to modulate neuron activity [52, 53] although <4 °C change is within the normal fluctuation range [54] in mammals. Temperature change may interfere with neuronal activity by affecting membrane properties, equilibrium potentials, channel kinetics, and dynamics of thermosensitive ion channels [11]. Some studies attributed FUS-induced inhibition in the nervous tissue to thermal effects [55, 56] while the majority of neuromodulation research avoided significant thermal contribution by settings of low-intensity FUS with short duration (< 0.1°C) [32, 40]. Consequently, rarely was irreversible tissue damage reported among FUS neuromodulation studies [40].

1.4.2 Stable cavitation, membrane deformation and capacitance change

Two major mechanical effects of FUS – cavitation and acoustic radiation force can deform the lipid membrane of the neuronal cells, cause changes in membrane capacitance

and further affect neuronal activity [57-59]. Based on the Hodgkin and Huxley model [60], hydrophobic non-conductive lipid bilayers separate the internal of a neuron and serve as a homogeneous planar capacitor. During the propagation of a nerve pulse, currents flow through the transmembrane ion channels, charging or discharging the membrane capacitor [61]. Several membrane properties, such as curvature and conformational state of the lipids, can affect the membrane capacitance [40] based on the following equation:

$$C_m = \varepsilon \times \frac{A}{d}$$

where ε is the dielectric constant, A is the membrane area and d is the membrane thickness [61]. The generation of capacitive currents was shown to be induced by ultrasound in the artificial pure lipid membrane [62]. Several studies also suggest that capacitance disturbance is sufficient to trigger nerve pulses [40].

Cavitation refers to the phenomenon when acoustic pressure above a certain threshold causes the formation, expansion, oscillation, and collapse of microbubbles in a liquid [11, 62, 63]. The occurrence threshold is affected by several factors, including ultrasound frequency, intensity, exposure duration, gas density, the viscosity of the medium, and especially the availability of cavitation nucleation [64, 65]. Cavitation results in membrane deformation, temperature change, and local velocity fields [66] that generates shear pressure, microstreaming, and microjets[67]. FUS-induced cavitation is classified into 2 common types: inertial cavitation and non-inertial cavitation (also called stable cavitation) [59, 64]. Inertial cavitation describes the unstable and violent collapse of microbubbles, resulting in large local pressure perturbation that is also known as a shock wave [63] and sometimes associates with tissue damage [68, 69]. In contrast, stable

cavitation occurs when applied low acoustic pressure. Microbubbles oscillate symmetrically about the original radius and linearly correlated with acoustic pressure [59], generating more consistent and predictable mechanical disturbance on the lipid membrane.

Acoustic radiation force (ARF) occurs as acoustic wave interfere with materials along the propagation path and causes mechanical displacement [14]. ARF is nonlinearly proportional to the FUS intensity and creates a continuous, non-oscillating pressure on the tissue [70], which leads to membrane deformation [71]. ARF may also cause displacement of microbubbles and interfere with the cavitation effect [59].

Cavitation, ARF, or a combination of both are theoretically capable of causing membrane deformation. The dominance of either mechanism depends on specific ultrasound parameters and medium properties. Capacitive currents were recorded during the application of ultrasound on the artificial lipid membrane [62]. However, despite the existence of multiple measuring techniques for cavitation [72] and ARF-induced displacement [73], only very few studies provided evidence for the contribution of those mechanisms to modulation effects on neuronal tissue [70].

1.4.3 Activation of mechanosensitive ion channels

The mechanical disturbance caused by ARF and/or cavitation may directly or indirectly activate mechanosensitive ion channels on the neuronal membrane. Through a direct activation mechanism, FUS-induced change in membrane tension may cause a conformation change of the ion channel. Indirect activation pathways include: 1) a primary mechanosensory releases a signal molecule that activates the ion channel; 2) a channel open by the force transmitted from the physically attached cytoskeleton and

the extracellular matrix; 3) activation of other mechanosensitive macromolecules that is physically coupled with the ion channel [74]. Studies have shown FUS activation of Na^+, K^+, and Ca^{2+} currents [40]. On *C. elegans*, FUS-mediated responses were absent in mutants without MEC-4, a sensory mechano-electrical transduction channel, while thermosensitive channels are not involved (temperature change <0.05 °C) [75]. Expression of ion channels in the Xenopus oocyte system indicated activation of channels of the two-pore-domain potassium family (K2P), including TREK-1, TREK-2, TRAAK, and $Na_V1.5$ [76, 77]. Low-intensity ultrasound also activated piezo-type mechanosensitive ion channel component 1 (Piezo1) expressed in HEK cells, accompanied by Ca^{2+} influx [78]. In cultured muscle or kidney cells, FUS mechanically activates a Na^+ current mediated by transient-receptor-potential-channel-1 (TRPC1) and further activates downstream voltage-gated Ca^{2+} channels (VGCC) [DOI: 10.7150/thno.33876]. *In vitro* recordings on rodent hippocampus slices suggested activation of Na^+, Ca^{2+} transients [79], and K^+ channels [46, 80]. On cultured murine cortical neurons, a specific Ca^{2+} selective mechanosensitive channel [48]. *In vivo* stimulation on the mouse brain has suggested the involvement of cytoskeleton proteins in FUS-mediated neuron activation [47]. Thus, there has been a variety of experiments suggesting the activation of neuronal channels by modulations on lipid or cytoskeleton.

1.4.4 Nanopore hypothesis and predictions based on manipulations of membrane lipid bilayer organizations.

Our previous data supported a nanopore mechanism (see Figure 1.1 legends for details). The hypothesis is based on several lines of evidence. (1) The duration of a

prolonged US-induced depolarization outlasts the US stimulation. The mechanosensitive channels reported to be US-activated or expressed on crayfish are known to close within milliseconds after the stimulation [81, 82]. (2) US can cause large mem-brane depolarization even after functional VGCs were blocked. (3) The reversal potential (E_{eq} = -8 mV) of US-induced depolarization does not correspond to the E_{eq} of any known selective ion channels and thus suggests a non-selective permeability.

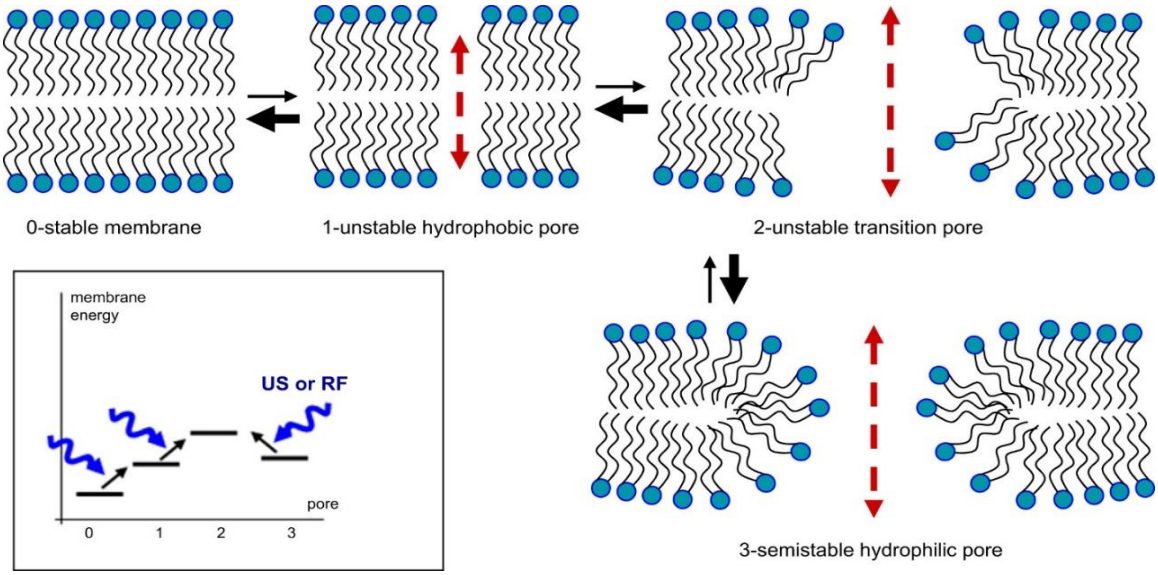

Figure 1.1 Hypothetical nanopore configurations and transitions induced by FUS on the lipid membrane. The normal stable state of lipid bilayers (state 0) can be interrupted by FUS and possibly transits into an unstable state (state 1) that contains hydrophobic pores created by the lateral movement of lipid molecules. Further perturbation of the external mechanical force may cause a configuration change of the lipid molecules to form a highly unstable transition pore (state 3). The intermediate pores can either reform hydrophobic pores or become semistable hydrophilic pores (state 3) with the realignment of lipids. The configuration of hydrophilic nanopores presents a lower energy level than the transition state, meaning that returning to the initial state required some energy to cross the energy barrier of state 2. Thus, the hydrophilic nanopores, once formed, can remain stable and enable large-conductance permeable through the membrane. Inset: hypothesized mem-brane energy levels for each state and FUS- or radio frequency (RF)-facilitated transitions [83].

Since one of the important factors in FUS-induced nanopore formation involves disruption of lipid molecule organization in the membrane, manipulations that could stress lipid molecule organization is likely to alter the probability of nanopore formation.

Changes in osmolarity may be one of these manipulations. Extracellular osmolarity change is known to induce surface area regulation or altered membrane tension in most cells [84]. The expansion of cell membranes or increased membrane tension in a hypoosmotic solution may facilitate the US-induced lateral movement of lipid molecules [85] and may increase the likelihood of nanopore creation. The temperature change may affect the mechanical properties of the membrane by modifying its fluidity based on the phase states of lipid organization in the cell membrane. Over a smaller range, especially near the phase transition temperature, temperature-dependent changes in the cell membrane may influence the probability of nanopore formation under US.

1.5 Effects of changing osmolarity and temperature on membrane properties and neuroexcitability

The biological membrane has a degree of both elasticity and rigidity. Membrane rupture occurs when reaching the elastic limit with a stretching force, which could be induced by osmotic pressure. When challenged by osmotic pressure, membrane tension of pure lipid liposomes depends on their size and curvature. Large and less curved liposomes will have bigger in-plane membrane tension and are more susceptible to lysis [86]. Animal cells can adapt to osmotic changes with pumping and leaking osmolytes to keep the tension within the rupture threshold. The cytoskeleton under the plasma membrane, including actin and myosin, also modulates stress on the membrane [86]. Despite these experimental studies, details in intermediate lipid organization leading up to nanopore formation require molecular dynamic simulations. In simulation studies, artificial lipid bilayers form transient and semistable water-permeable hydrophilic pores without rupture under

mechanical force [87]. Under osmotic pressure, pore formation in giant unilamellar vesicles was reported to be stochastic [88]. The lifetime of those pores ranged from nanoseconds to milliseconds [89]. Our previous study suggested stable pores, lasting a few seconds, can be induced by the mechanical effects of the US [90]. The large discrepancy in duration could be due to complex lipid composition and mechanical support provided by surrounding tissue in the biological membrane.

Temperature affects the fluidity of lipid bilayers (the phase of the bilayer). Lipid molecules are diffusible in the liquid phase and relatively stable in the gel/solid-state. At a critical temperature, lipids go through a transition from one phase to another, which is accompanied by a profound change in the mechanical properties of the membrane. Changes in the fluidity of the membrane, after it has undergone the phase transition, can alter membrane function by affecting membrane elasticity, permeability, and the movements of proteins and other lipid components [91-93].

The transition temperature largely depends on the composition of the lipid molecules. An increased concentration of long-chain phosphatidylcholines in the bilayer shifted the liquid-to-gel phase transition to a higher temperature [94]. Cholesterol, rich in the membrane of biological tissue, is well known to stabilize the lipids in the intermediate liquid-gel condition [95]. The biological membrane has “rafts” of cholesterol-rich domains that have membrane phase-separated from surrounding cholesterol-poor regions [86]. This uneven distribution of cholesterol may induce a local change of function at a different temperature. Cholesterol depletion resulted in increased temperature of the gel-liquid phase transition of the bovine hippocampus membrane. The level of increase showed high

dependency on the extent of cholesterol depletion [96]. Additionally, anesthetic drugs generally increase the membrane fluidity and decrease the temperature required for phase transition [97]. However, the role of temperature-dependent changes in membrane mechanisms has not been investigated in the context of FUS modulation.

Temperature effects on neuronal excitability have been studied extensively, only representative examples are outlined below. The resting potential of the squid giant axon was slightly affected by temperature, while the duration of spikes increased at lower temperatures. The amplitude of APs remained relatively constant at -1 to 30℃. Above 35℃, heat shock started to appear. The falling phase of the APs had a higher temperature coefficient than the rising phase [98]. In guinea-pig hippocampus CA1 pyramidal neurons, cooling from 37℃ to between 33 and 27℃ increases input resistance, amplitude, and duration of APs. In addition to the impact of changing the temperature on channel kinetics, some temperature-dependent changes in membrane excitability could be attributed to slowed $Ca2^{+}$ removal from the cytoplasm [99]. Rat visual cortical cells also showed a lower spiking threshold with cooling from 35℃ to 7℃. In this case, the changes were attributed to a changed ratio between K^{+} and Na^{+} conductance at a lower temperature [100].

A temperature increase of as little as 0.1℃ has been shown to affect neuronal activity and function [52, 53, 101, 102]. In the medical application of deep brain stimulation, it has been suggested that thermal effects were adequate to cause additional neuronal modulation in addition to the treatment itself. The temperature changes are dependent on specific stimulation/tissue parameters such as stimulation waveform, electrode lead selection, blood perfusion, and brain metabolism. Thus, the thermal effects

of the US should be taken into consideration when intended to use the technique in practical therapy.

In addition, the mechanosensitive K2P channels especially TREK and TRAAK, recently known to be activated by FUS [76], are also sensitive to thermal changes [103, 104]. Those hyperpolarizing background K^+ channels in mammalian peripheral nerve have an optimal opening probability at body temperature. Heating or cooling causes progressive to inhibit channel opening, reducing the hyperpolarization contribution from K2P channels [104], thus affecting neuronal excitability.

In summary, temperature affects membrane fluidity, ion channel conductance, enzyme activities, and equilibrium potential. Manipulation of osmolarity, temperature, and cholesterol levels could alter the mechanical properties of the membrane and, in turn, sensitivity to US pressure waves.

1.6 Crayfish motor axon as a model system FUS study

Crayfish opener preparation has morphological and technical advantages for this purpose. It is a relatively simple system that contains two motor axons, one excitatory and one inhibitory, neuromuscular synaptic junction (NMJ), and muscle fibers that control the opening of the claws. The two axons are juxtaposed with each other. They both branch and form synaptic contacts with all the muscle fibers to control the movement of the claw of the first walking leg. The axons and muscles have large diameters for easy electrode penetration [105]. The preparation is sturdy and remains functionally stable in physiological saline for up to 36 hr [106]. Previous studies have characterized pharmacology and spatial distributions of voltage-gated channels (VGCs) in the axons

[107-109]. Overall, the crayfish preparation is well characterized and provides an ideal model to study US effects on single-axon excitability and synaptic transmission.

1.7 Thesis outlines

Chapter 1 provided the background of current neuromodulation techniques, specifies the advantages and potential application of FUS, and pointed out current gaps in understanding underlying modulation mechanisms via alternation in neuronal membrane properties. Chapter 2 listed detailed methodology to achieve research goals in the following chapters. Chapter 3 described the effects of hypoosmotic pressure on FUS-mediated membrane depolarizations on crayfish axons and states the consistency in the previously proposed nanopore hypothesis. Chapter 4 showed the effects of temperature change o FUS-evoked membrane responses and discusses possible mechanisms in the absence of the involvement of K2P channels. Chapter 5 demonstrated the effects of FUS on propagating AP on the crayfish axon and discussed potential mechanisms. Chapter 6 summarized the work and offered future interests in some of the research topics.

CHAPTER 2. METHODS

The first walking leg of crayfish, *Procambarus clarkii*, was dissected to expose the motor axons and fixed to a recording dish. The two-electrode current clamp was performed on one of the axons to monitor membrane potential responses in each trial. Both electrodes and a ~1.4 mm long axon segment were covered by FUS with an intensity of the spatial peak temporal average of around 0.94 mW/cm^2. Current injection trials were performed to test axon excitability or trigger action potentials (APs). FUS application trial includes the application of a train of 20 FUS pulses (2.1 MHz) delivered at 1 kHz with a 5% duty cycle or a continuous wave with a duration of 80 ms. Osmotic and thermal controls were achieved by circulating saline of specific osmolarity and temperature in the dish until remaining in a plateau state for at least 15 minutes. Data acquisition and analysis were performed with IGOR pro customized macros.

2.1 Experimental setup

2.1.1 Crayfish preparation

Crayfish, *Procambarus clarkii*, were purchased from Niles Biological Supplies (Sacramento, CA, USA). Small animals of both sexes, 5-7 cm head to tail, were maintained in tap water at room temperature (22°C). All experiments were performed at the same temperature. The first walking leg was removed by autotomy and fixed with cyanoacrylate (KG86648R, Elmer's products, Westerville, OH, USA) to a 60-mm diameter plastic petri dish (430589, Corning, NY, USA). The opener axon-muscle preparation was dissected in saline. Recordings from both excitatory and inhibitory axons were polled for statistical analysis in this study because previous imaging and electrophysiological studies have

shown that the two axons are similar in their basic structural and physiological properties [110, 111].

2.1.2 Solution preparation and blockers application

The bathing medium was a physiological saline with the following composition (in mM): 195 NaCl, 5.4 KCl, 13.5 $CaCl_2$, 2.6 $MgCl_2$, and 10 HEPES, titrated to pH 7.4 with NaOH. The saline was circulated by a peristaltic pump at a rate of 1.5 ml/min. Five pharmacological stock solutions were prepared: (1) 4-aminopyridine (4-AP, 1M), which blocks the dominant low-threshold potassium channels [112], was dissolved in distilled water; (2) TTX (1 mM), which blocks sodium channels, was dissolved in distilled water; (3) ZD7288 (50 mM), which blocks hyperpolarization-activated cation channels, was dissolved in DMSO;（4) Fluoxetine stock solution was dissolved in DMSO to 50 mM and diluted into saline to a final concentration of 100 μM; (5) Norfluoxetine stock solution was dissolved in DMSO to 50 mM and diluted into saline to a final concentration of 50 μM. The stock solutions were stored at -20C° and added to the saline directly after each solution reached room temperature. ZD7288 and fluoxetine was purchased from TOCRIS Bioscience (Bristol, UK). Norfluoxetine was from Cayman Chemical (Ann Arbor, MI, USA). All other chemicals were from Sigma-Aldrich (Burlington, MA, USA). The perfusion inlet was positioned within 5 mm of, and aimed at, the preparation such that the change of solution at the axons was nearly instantaneous when channel blockers or hypotonic saline reached the recording dish [90].

2.1.3 Setup configuration

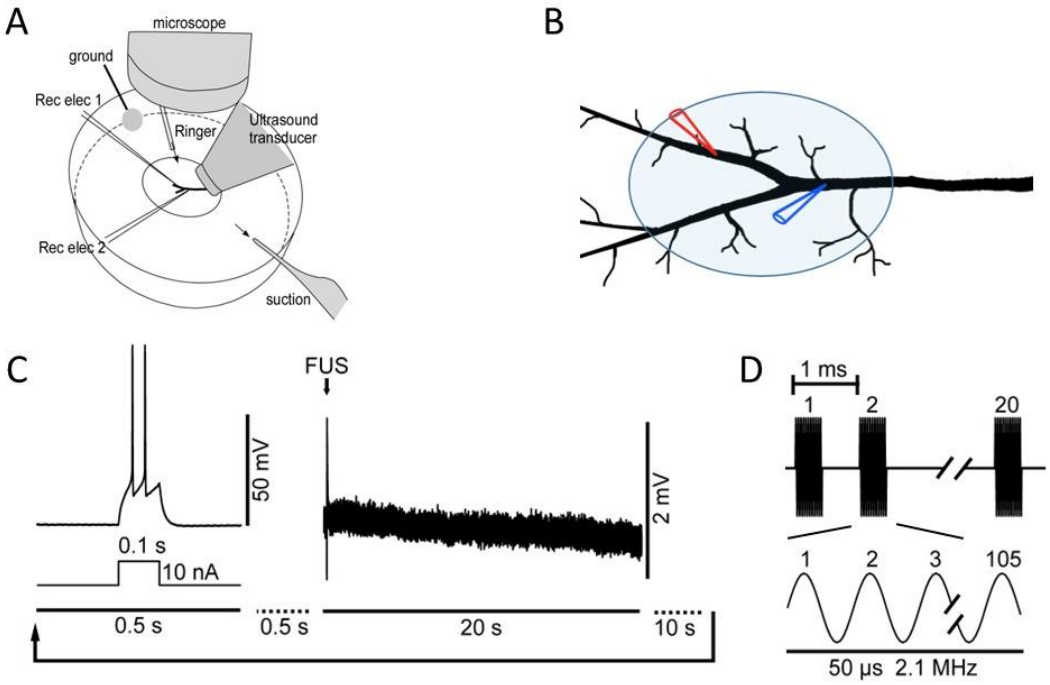

Figure 2.1 Experimental configurations and protocols. *A*: illustration of the crayfish opener neuromuscular preparation with two recording electrodes (Rec elec), 1 and 2, respectively, together with ultrasound transducer placements. *B*: detailed 2-electrode current clamp configuration, with 1 electrode at the primary branch (blue) and the second electrode at the secondary branch (red). Also shown is the approximate footprint of a typical US focal area when the transducer is angled at 45° (shaded ellipse). The dimensions of the axon are equivalent to a preparation dissected from a large animal 6 cm in length head to tail. The US focal area coverage, relative to axonal arborization, is likely to be more extensive in some smaller animals used in this study. (C) Timeline of a typical experiment. A 10 nA current injection was alternated with US tone burst. The time gap between the current step and FUS tone burst was 0.5 seconds. FUSD was recorded as 20-s long traces. The time gap between FUS test trace and the next 10 nA current step was 10 second. (D) The FUS tone burst consists of 20 pulses of 50 µs tone bursts (2.1 MHz) delivered at 1 KHz.

Experimental configurations have been detailed in a previous study [90] and is illustrated in Figure 2.1 for visualization. Briefly, the two electrodes for two electrode current clamp approached axons from the same distal-to-proximal direction while the FUS transducer approached the preparation from the opposite direction (Fig. 2.1A). Recordings

shown in Chapter 3 were mainly obtained from the secondary branches (Fig. 2.1B red) of both excitor and inhibitor. In Chapter 4, the two electrodes in current clamp mode were inserted in a motor axon and a muscle fiber, respectively. Axonal recordings provided in Chapter 4 were obtained mainly from the primary branch of the excitor axon. Axon penetrations were performed under a 40×/0.80w water immersion lens (LUMPlanFl/lR, Olympus, Tokyo, Japan) which was then removed to make room for the FUS transducer. The transducer was angled at 45°, and microelectrodes at 28°, to the horizontal plane (Fig. 2.1A). The FUS transducer was brought as close to the preparation as possible, with the lower edge of the FUS transducer cone ~1 mm from the bottom of the recording dish. The distance was estimated visually in most experiments, but it had been verified by digital readouts of a motorized manipulator (MP-285, Sutter Instrument, Novato, CA, USA). For optimal localization of the transducer, the transducer was moved horizontally until the amplitude of a hyperpolarization transient was maximal [90]. The localization coincided with having most of the axonal arborization enclosed within the diameter of the US focal point (~1 mm x 1.4mm) (Lin et al. 2019). This procedure ensured that FUS-induced responses could be triggered by the lowest possible intensity.

2.2 Electrophysiology

Two DC amplifiers (IE-210, Warner Instruments, Hamden, CT, USA) were used to perform a two-electrode current clamp. Voltage signals were low pass filtered at a cut-off frequency of 5 KHz and digitized at 50 KHz. Data were digitally sampled with a NI 6251 board (National Instruments, Austin, TX, USA) and analyzed with IGOR (Wavemetrics, Lake Oswego, OR, USA). Microelectrodes for axonal recording were filled

with 500 mM KCl and had a resistance of 40-60 MΩ. Microelectrode for muscle recordings was filled with 3 M KCl and had a resistance of 10-20 MΩ. The typical axonal resting membrane potential (V_m) was ~-70 mV and muscle V_m was ~ -80 mV.

Each preparation represents a recording session from a motor axon dissected from an animal. A recording session typically lasted 2-4 hrs. In Chapter 3, the preparations can be grouped into two subsets based on pharmacological conditions. Group 1 (n=5): FUS-evoked responses were recorded without channel blockers. Groups 2 (n=3): preparations were treated with TTX (1 μM), 4-AP (200 μM), and ZD7288 (50 μM). While three of the eight preparations used in statistical analysis were studied in the presence of channel blockers, most FUSD were subthreshold to AP initiation and were minimally affected by these drugs. Therefore, parameters characterizing FUSD from both sets of preparations, with and without blockers, were pooled for data analysis.

2.3 FUS parameters

The active element of the transducer was a spherical piezo cup from Steminc Piezo (SMSF20C30F21, Steiner & Martins, Davenport, FL, USA). The piezo cup was driven by a mini-circuit amplifier (LZY-22+, Mini-Circuits, Brooklyn, NY, USA) which in turn was modulated by a function generator (DG1022, Rigol, Beijing, China). The cup had a diameter of 20 mm and a spherical radius 30 mm, which was also the focal length of the conical ultrasound beam from the cup. Rexolite (C-Lec Plastics, Philadelphia, PA, USA), a cross-linked polystyrene with low ultrasound absorption (impedance =2.48 MRayl) and a low reflection coefficient from soft tissues, was machined into a conical shape with the large end fitting exactly to the inside of the piezo cup. FUS sound waves passed through

the cone, and reached the tip of the cone, which was machined down to a concave sphere to increase the focus and FUS power. The tip pulled the original focal point closer to the transducer when it was submerged in saline. The Rexolite-to-saline interface formed a lens that made the focal spot smaller. As characterized previously, a focused FUS beam with a circular cross-section of 1 mm diameter and at a 45° angle should project an elliptic focal image on the preparation with minor and major axes of 1 and 1.44 mm respectively (Fig. 2.1B). The lowest possible FUS pressure capable of triggering FUSD, in ~10% of the trials, was chosen for each preparation. Based on calibrations of the same transducer reported previously [90], the pressure typically ranged from 0.1 to 0.3 MPa, which was well below the maximal pressure (0.75 MPa) the transducer was capable of delivering. Taking into account Rexolite impedance and duty cycle (1 ms total burst duration/20 s), the intensity of the spatial peak temporal average (I_{SPTA}) of FUS at the focal point should be 0.94 mW/cm^2. The intensity is lower than the FDA safety limit for the applied temporal average energy level of <720 mW/cm^2 [113].

FUS-induced responses in Chapter 3 were evoked by a train of 20 FUS pulses (2.1 MHz), each pulse lasting for 50 μs (Fig. 2.1D), delivered at 1 KHz. In other words, each pulse train lasted for 20 ms with a duty cycle of 5%. A typical experimental cycle included a test current step to trigger AP, to monitor axonal excitability (Fig. 2.1C left), followed by a trial testing effect of the FUS tone burst (Fig. 2.1C right). Responses evoked by a single train of 20 FUS pulses were recorded in a trace lasting 20 seconds. There was then a 10-s gap after the end of the US monitor traces and before the next test current was injected

(Fig. 2.1C). Both APs evoked by current steps (500 ms in recording duration) and FUS evoked responses (20 s in recording duration) were sampled at the rate of 50 kHz.

FUS-induced responses used in Chapter 4 and Chapter 5 were evoked by a continuous, 2.1 MHz US wave with a duration of 80 ms. In these experiments, one electrode was in the motor axon while the second electrode was in a muscle fiber. A typical cycle contains three trials, FUS alone, AP train alone, FUS and AP train simultaneously. There was a 10-sec rest between trials. The cycle repeated as the temperature changed. A different US transducer, of the same construction but had the maximal output at 2 MHz, was used in K2P channel blocker experiments. The US pulse pattern was composed of 30 pulses at a 1 kHz repeating rate with a 50% duty cycle. Th K2P blocking series of experiments placed two electrodes in the motor axons to achieve a two-electrode current clamp configuration. A typical cycle contained 8 current steps, four hyperpolarizing and four depolarizing, to assess input resistance and excitability of motor axons. There was a 2-second resting time between individual current steps.

2.4 Experimental protocols for osmolarity and temperature manipulations

Reduction in osmolarity was achieved in two ways. First, the circulating saline was diluted with distilled water to 75% of this original osmolarity. Since the dilution reduced concentrations of ions, we also use a second saline preparation to mitigate this confound. In the second saline preparation, NaCl in the control saline was reduced from 195 to 150 mM, which is ~75% of total NaCl, and 90 mM sucrose or mannitol was added to restore the osmolarity. The reduction in osmolarity was achieved by the same saline in the absence of sucrose or mannitol. Sucrose-substituted experiments were tested in eight preparations

and mannitol in three. Osmolarity was measured, using Osmometer 3D3 (Advanced Instruments, Norwood, MA, USA) and in quadruplicates, from these solutions were (in mOsm): control saline (429±5.4), control saline diluted with distilled water (326±1.6), mannitol substituted saline (444±7.5), sucrose substituted saline (455±10.8) and sugar-free saline (350±4.7). The percentage reduction of osmolarity of the three saline variants ranged from 75 to 78%.

Temperature control was accomplished by manually adjusting the power supply output to the Peltier. Bath temperature was monitored with a probe in the dish (Physitemp Model BAT-12) and the temperature readout was digitized simultaneously with electrophysiological recordings. With the room temperature varied between 19 to 23 ˚C and the peristaltic pump circulating the saline at 1ml/minute, this configuration allowed reliable cooling of the preparation to ~10 ˚C and heating to 40 ˚C.

2.5 Hodgkin-Huxley model simulation

HHsim (http://www.cs.cmu.edu/~dst/HHsim/) was used in simulation studies. This model is similar to that developed for the squid giant axon [114]. However, the model does not incorporate the morphology of an axon. Instead, current flow and AP firing were calculated based on a spherical cell with an input resistance of 5.1 MΩ. Simulations performed in this study used default kinetic parameters similar to those of the squid giant axon at 6.5 °C.

2.6 Data analysis

Statistical results presented in graphs were presented as averages and standard deviation (SD) or standard errors of means (SEM). Statistical significance was determined

with paired Student's *t*-test. Estimates of membrane time constant used a single exponential curve fitting routine in IGOR.

CHAPTER 3. THE EFFECT OF OSMOLARITY ON FUS-INDUCED DEPOLARIZATION

We have previously identified a novel non-selective membrane conductance (g_{US}) opened by focused ultrasound (FUS) in crayfish motor axons. In this report, we studied g_{US} properties further by comparing FUS-evoked depolarization (FUSD) in control and hypotonic saline with 75% of control osmolarity. The FUS was a train of 20 FUS bursts (2.1 MHz and 50 μs per burst) delivered at 1 kHz. The amplitude, onset latency, frequency of occurrence, and duration of FUSD were compared in a 15-minute time window before and after switching to hypotonic saline. Significant increases were observed for amplitude ($p<0.001$) and frequency of occurrence ($p<0.01$) while the onset latency showed a significant decrease ($p<0.001$). FUSD duration was not significantly different. These results support predictions based on our hypothesis that g_{US} is mediated by the opening of nanopores in the lipid bilayer and that stretching of the axonal membrane due to swelling in low osmolarity should increase the probability of nanopore formation under FUS. The FUSD parameters, in addition, exhibited time-dependent trends if the window of observation was expanded to 45 minutes in each saline. Statistical significance of amplitude and duration differed between 15 vs 45-minute time windows, indicating the presence of adaptive responses of the axonal membrane to osmotic manipulation.

3.1 Introduction

Focused ultrasound (FUS) is increasingly recognized as a promising modality for noninvasive neural modulation because of its ability to stimulate deep brain areas with fine spatial resolutions and power levels within the U.S. Federal Drug Administration (FDA)

safety limits [115-117]. In comparison to transcranial magnetic stimulations or transcranial electrical stimulations, FUS has the advantage of deeper penetration while maintaining a fine, millimeter, resolution [118].

The mechanisms of FUS-based neuromodulation are being actively studied to help advance the application of FUS approaches for brain activation [40, 119-122]. While mechanical impacts generated by US on target neurons could be mediated through multiple physical processes, FUS-generated mechanical disturbance ultimately may influence neuronal activity by modulating mechano-sensitive domains of voltage-gated channels [76, 123] or mechanosensitive channels [76, 124, 125]. FUS may alter membrane excitability by stretching and compressing the lipid bilayer and thus generating capacitive currents [62].

In our previous study using single motor axons [90], we found that FUS-induced depolarization (FUSD) could best be explained by a non-selective conductance (g_{US}). The membrane depolarization induced by g_{US} could reach a maximum of 50 mV in amplitude with a long duration (2.1 s average and 200 s maximum) and a relatively fast onset time (mean 3.4 ms). The reversal potential was estimated to be -8.4 mV, suggesting that the conductance was non-selective to ions. The potential contribution of voltage-gated channels to FUSD was ruled out because this depolarization was recorded in the presence of blockers of voltage-gated channels. Mechanosensitive channels or capacitive current, due to membrane stretching or compression, were also considered unlikely because FUSD persisted for seconds, long after millisecond-long FUS tone bursts had ended. The combination of these characteristics and the fact that g_{US} was non-selective led us to

propose that nanopores in the axonal membrane, i.e. lipid ion channels [119], should be the most likely mechanism underlying g_{US}.

In this study, we characterized g_{US} further in the crayfish motor axons. Molecular dynamic simulations have suggested that electroporation and stretch of membrane lipid bilayers could increase the probability of the formation of hydrophilic pores that could be semi-stable [126, 127]. In this report, we use hypotonic saline to induce cell swelling, increase lateral tension of the axonal membrane, and examine whether the occurrences, as well as other characteristics of, FUSD may be enhanced as predicted from the nanopore hypothesis.

3.2 Results

3.2.1 Basic characteristics of action potentials and FUSD in hypotonic saline

FUSD was evoked by applying a brief train of 20 US pulses (2.1 MHz and 50 μs induration) delivered at 1 kHz. FUSD occurred stochastically as reported previously. The depolarizations were suprathreshold for eliciting action potentials (APs) in some trials (Fig. 3.1A) while subthreshold in others (Fig. 3.1B). In the examples shown in Fig. 3.1A and B, FUSD traces recorded in hypotonic saline (red) exhibited larger amplitudes and shorted delays compared to those recorded in control saline (black). Insets in A and B show the same traces with a faster time scale and FUS delivery periods are indicated by the black bars. Subthreshold FUSDs typically exhibited a rapid rising phase with a prolonged decay, Fig. 3.1B. The stability of the electrode recording was monitored during the experiment by a 10 nA current step delivered between FUS trials (Fig. 1C and Fig.2C). Arrows in Fig. 3.1D, using the same trace as the black one in Fig. 3.1C, identify the time window used to

determine the membrane time constant. Fig. 3.1E and 3.1F show the timelines of four parameters of the FUSD and AP measured during a typical experimental session over a period of 90 minutes: (1) amplitudes of FUSD (Fig. 3.1E left axis), (2) AP amplitude evoked by current steps (Fig. 3.1E right axis), (3) resting membrane potential (Fig. 3.1F left axis) and (4) membrane time constant (Fig. 3.1F right axis). (Red symbols in Fig. 3.1E identify the trials from which traces in (A), (B), and (C), with corresponding symbols, were obtained.) The time during the control saline is on white background, and during the hypotonic saline condition in pink background. Due to the stochastic nature of the FUS-induced responses, the density of data points corresponding to FUSD (Fig. 3.1E, filled circles) was not as high as that evoked by step current injections (Fig. 3.1F grey triangles). FUSD exhibited slightly higher incidences of occurrence after transitioning into hypotonic saline while AP amplitudes evoked by current steps did not show appreciable change. There was a slight drift in resting membrane potential (RMP), but lowering osmolarity did not disrupt the continuous drift in RMP (Fig. 3.1F filled circles). Although time constants appeared to decline after switching to hypotonic saline in this preparation, this change was not a consistent finding. The RMP was measured during 20 ms baseline before the current step or FUS was delivered in each digitized trace. In each preparation, the RMP was averaged across all the trials during a 15-minute time window before and after lowering osmolarity. Averaged RMP values from eight preparations were: -68.4 ± 3.4 mV before and -68.0 ± 5.7 mV after switching to hypotonic saline. This change represents a continuous drift in the DC level not related to osmolarity because there was no stepwise change in this parameter associated with the reduction of osmolarity. The time constant of

the membrane, measured using the same 15-minute time windows as those of RMP, remained the same when the osmolarity was decreased: 10.2 ± 1.13 ms before and 10.2 ± 1.11 ms after (n=7) switching to hypotonic saline, respectively. (The sample size for time constant was 7 because 10 nA test current steps were not used in one preparation.) Overall, these results indicate that the hypotonic solution did not noticeably alter the passive nor active membrane properties of the axon.

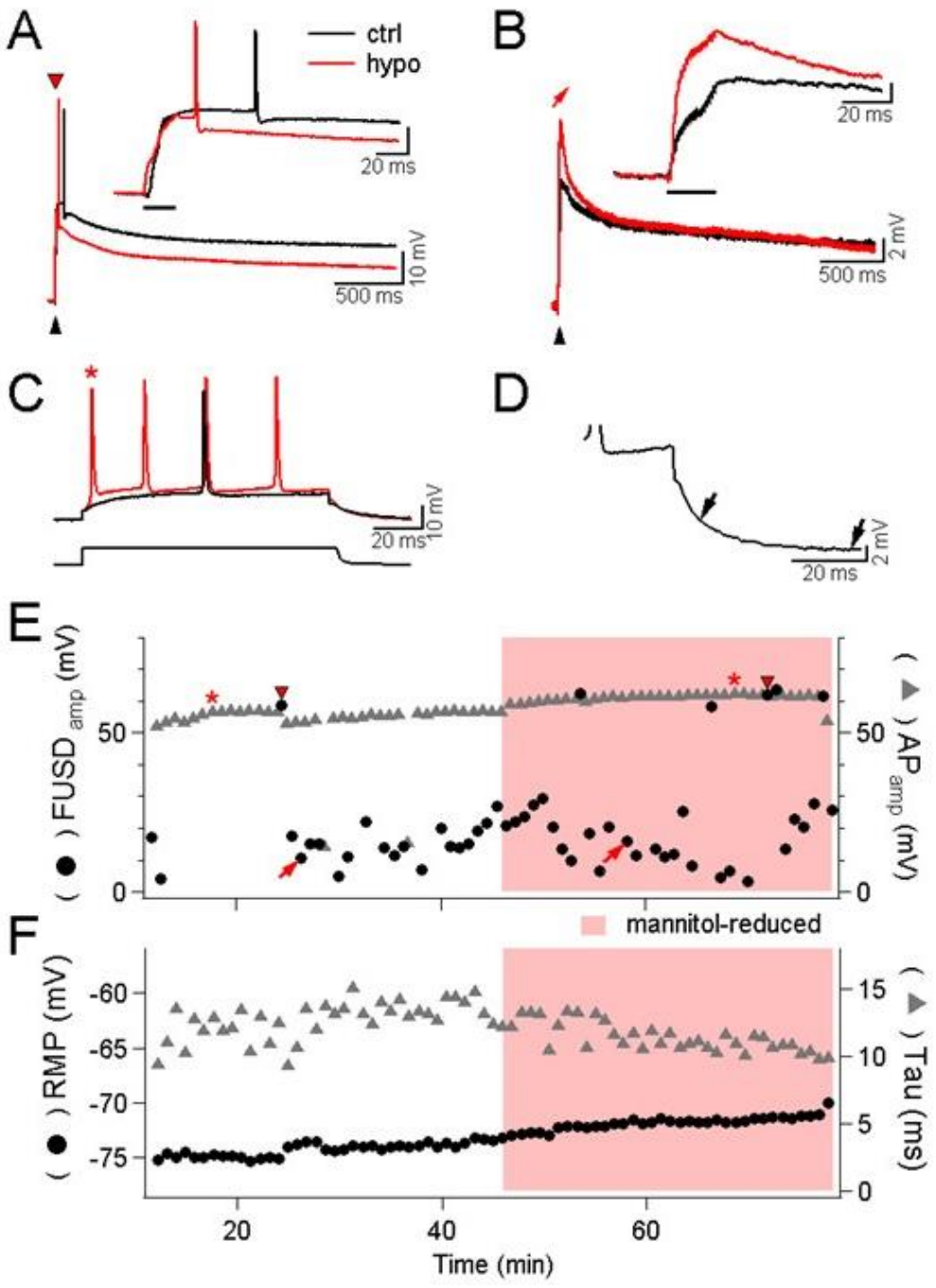

Figure 3.1 Effects of hypotonic saline on passive and active membrane properties in crayfish axons. (A) Suprathreshold responses evoked by FUS tone burst. Inset: initial part of US evoked responses displayed in an expanded time scale. The recordings were obtained from the data points marked by inverted red triangles in E. (B) Subthreshold responses evoked by the same US tone bursts. The traces were obtained from the time point marked by red arrows in E. In A and B, the timing of US delivery is marked by the arrowhead in the main graphs and the horizontal bar in the

insets. (C) Examples of AP evoked by 10 nA steps recorded in control and hypotonic saline. The recordings were obtained from the time points marked by "*" in E. (D) Arrows identify the time window during which single exponential fits were applied for time constant estimates. This trace is identical to the black trace in C. (E) Timeline plots of the amplitudes of FUSD ($FUSD_{amp}$) and action potential (AP_{amp}) in control and hypotonic saline (shaded area). Switching to hypotonic saline induced minimal changes in both parameters. (F) Timeline plots of resting membrane potential (RMP) and membrane time constant (Tau). (E) and (F) share the same time axes. Low osmolarity in this experiment was achieved by removing 90 mM mannitol from a "control" saline where 45 mM NaCl had been replaced by 90 mM mannitol.

3.2.2 Effects of hypotonic saline on properties of FUSD

Figure 3.2 illustrates the analysis of four parameters used to characterize FUSD. Figure 3.2A illustrates how the amplitude, duration, and delay of the FUSD were defined. The duration was defined as the width of the subthreshold depolarization at 50% of maximal amplitude (Dur_{50}). Delay (Del) of FUSD was defined as the time between the onset of FUS pulse train to the time when FUSD crossed a threshold of 2 mV (Fig. 3.2A inset). The time axis in Fig. 3.2B-E is bracketed such that the equal times (45 minutes) are displayed before and after switching to low osmolarity as in Fig. 3.1. Hypotonic saline enhanced the amplitude (Fig. 3.2B) and frequency of occurrence of FUSD (Fig. 3.2D). The FUSD became suprathreshold for eliciting AP in most of the trials during the first 15 min after switching from normal to hypo-osmolar saline (Fig. 3.2B, red crosses). The delay of FUSD was consistently reduced, immediately after switching the solution to 75% osmolarity (Fig. 3.2C). The instantaneous frequency of occurrence of FUSD for each FUSD was defined as 1 when there was an FUSD in the preceding trial. The frequency was 0.5 and 0.3 when the previously detected FUSD was observed at 2 or 3 trials before the FUSD in question. As shown in Fig. 3.2D, FUS succeeded in eliciting a depolarization in every trial, with a frequency of one, after switching to hypotonic saline in this preparation. The depolarization duration Dur_{50} varied considerably in the control and hypotonic saline

and this parameter did not exhibit any noticeable change when the osmolarity was lowered. (Note that the number of data points in Fig. 3.2E is lower than those in panels B, C, and D because Dur_{50} was not measured on trials that evoked APs.)

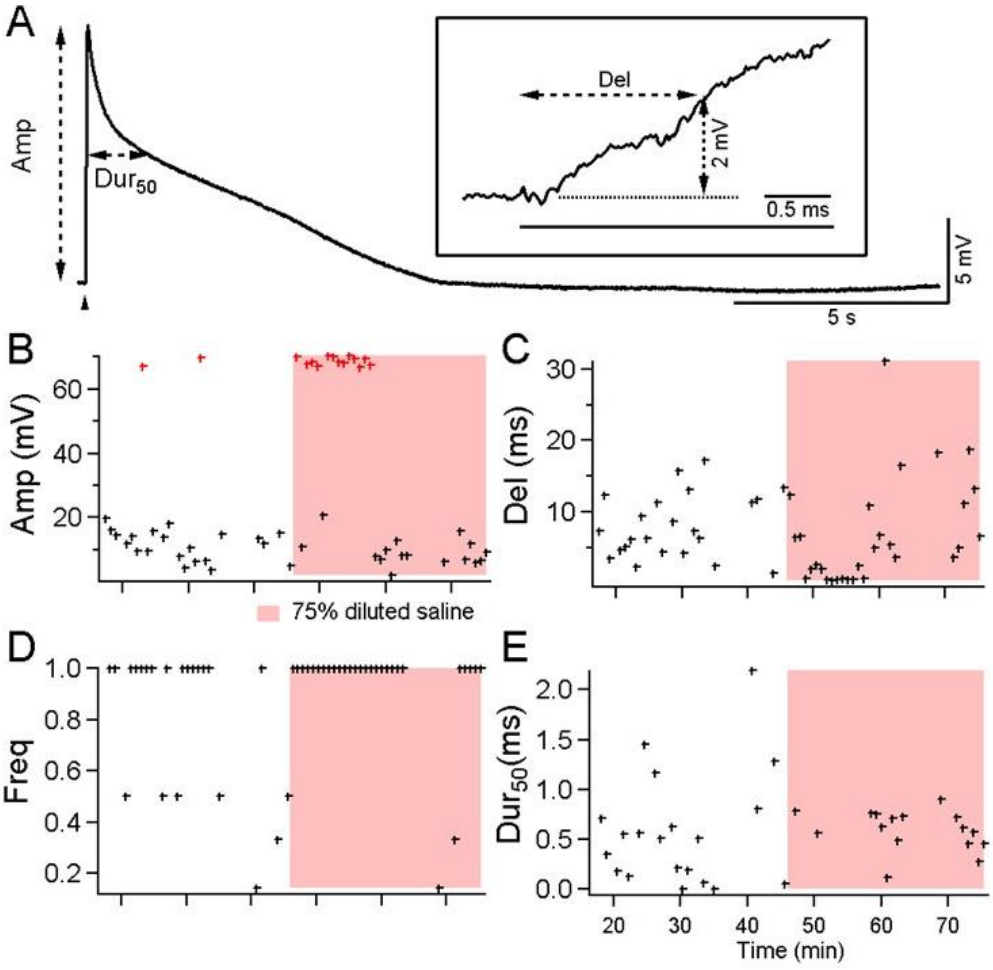

Figure 3.2 Quantitative analysis of US evoked physiological parameters measured in control and low osmotic saline. (A) Illustration of measurements of amplitude, 50% duration, and delay of US-induced responses (inset). The arrowhead, and the horizontal bar in the inset, indicate the timing of US tone burst delivery. (B) Timeline of the amplitude of FUSD. Red crosses identify suprathreshold responses. (C) Timeline of the delay of US-induced responses. (D) Normalized frequency of occurrence of US-induced responses. The frequency of 1 means US tone burst successfully evoked responses in consecutive trials. (E) Timeline of the half-maximal duration of subthreshold response. The data points in E do not fully correspond to those in B, C, and D because the durations were not measured in trials where the US evoked AP. The number of data points in B, C, and D for control and hypotonic saline was 22 and 29, respectively. The number of data points in E was 20 and 16 for control and hypotonic saline, respectively.

In order to evaluate the statistical significance of changes induced by hypotonic saline, the parameters shown in Fig.3.2 from eight preparations were normalized first before being combined. Specifically, in each preparation, values measured from every detectable FUSD trial in control saline were averaged. The average was then used to scale all the trials, including those in hypotonic saline, such that the average value for all the control trials was one. The normalized data from all eight preparations were then merged into a single composite timeline.

Figure 3.3A shows the composite timeline of the amplitude of subthreshold FUSD, in 5-minute time blocks, over a period of 90 min with error bars representing standard error of means. The amplitude timeline exhibits an abrupt jump when hypotonic saline was introduced, despite a declining trend during the control period (Fig. 3.3A). The FUSD delay exhibited a step decrease upon switching to hypotonic saline (Fig. 3.3B). The instantaneous frequency of occurrence of FUSD increased after the switch (Fig. 3.3C). The duration (Dur_{50}) did not show a significant change immediately after switching to hypotonic saline.

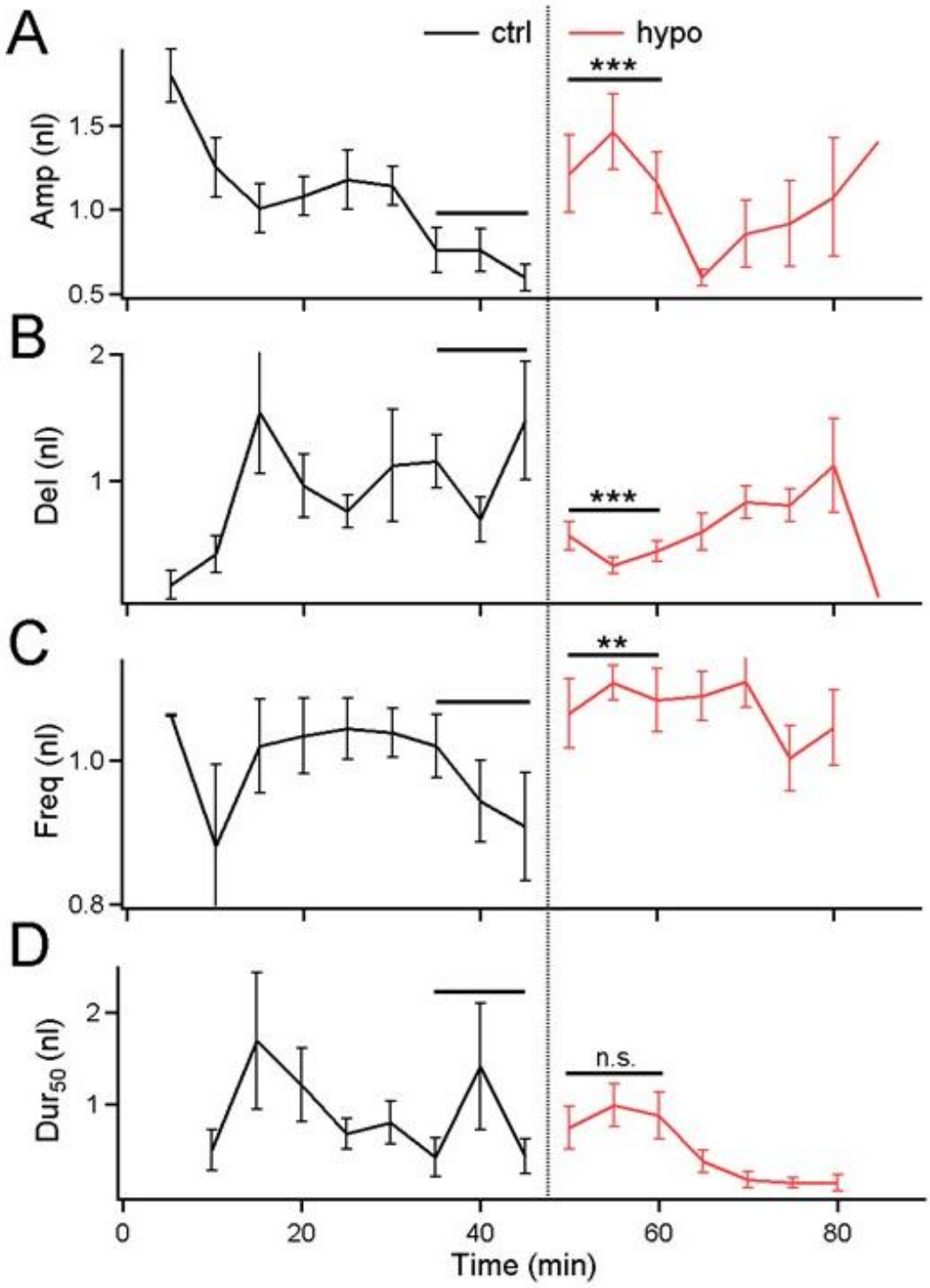

Figure 3.3 Compilation of changes in US induced depolarizations as osmolarity was lowered. Average and standard error of means of normalized amplitude (A), delay (B), frequency of occurrence (C) and Dur_{50} (D) plotted in 5-minute blocks. The transition from control (black) to

hypotonic (red) saline occurred at 45 minutes. A set of eight preparations were used for statistical analysis in this report. For the preparation of hypotonic saline, one of the eight preparations used sucrose substitution, two used mannitol substitution while the remaining five used distilled water dilution. The sample size for each data point ranged from 4 to 12. For panel A and D, the total number of FUSD events was 73 in control saline and 100 in hypotonic saline. For panel B and C, the sample sizes were 82 in control and 105 in hypotonic saline. Smaller sample sizes in A and D were due to exclusion of trials where FUSD was suprathreshold and evoked AP.

These qualitative trends were analyzed statistically by comparing the parameters during the 15-min period (three data blocks) before and after the switch to the hypotonic medium. The normalized subthreshold amplitude increased from 0.71±0.07 to 1.28±0.12 (*t*-test, $p=4*10^{-5}$) after lowering the osmolarity. The delay of FUSD was significantly shorter after the saline switch, from 1.13±0.18 to 0.44±0.05 (*t*-test, $p=1.8*10^{-4}$). The frequency of occurrence increased from 0.97±0.03 to 1.09±0.02 (*t*-test, $p=1.4*10^{-3}$). There was no significant change in Dur_{50} (0.72±0.21 vs 0.89±0.13 (*t*-test, p=0.28) during the 15-min time window before and after lowering osmolarity.

Although the changes in these parameters were clearly significant during the 15-min period after the switch compared to the same period just before the switch, the pattern of data was more complex over the entire 45 min period before and after the switch. Statistical analysis was carried out over the entire 45-min period before and after the switch (Table 1). Amplitude averaged over 45 min did not change significantly in the 75% hypotonic saline compared to the control. The average delay over the 45-min remained significant lower as for the 15-min time window. The significant increase in frequency of FUSD seen during the first 15-min period remained during the 45 min period**.** Although Dur_{50} did not significantly decrease with the first 15-min time window, the decrease over the entire 45 min was significant. The RMP and membrane time constant, which are two basic indicators of the stability of passive membrane properties, did not exhibit any

significant change as the preparations were switched in and out of hypotonic saline (Table 1).

	Amp. (mV) †	Freq. (nl) §	Delay (ms)	Dur_{50} (ms)	RMP (mV)	Time constant (ms)
Control (n=8)	18.5±3.3	0.77±0.11	11.9±4.9	598±154	68.4±3.4	10.2±1.13
p values	p=0.447	**p=0.025**	**p=0.034**	**p=0.03**	p=0.437	p=0.483
75% hypotonic	19.0±4.0	0.85±0.09	8.0±3.2	341±97	68.0±5.7	10.2±1.11
p values	p=0.268	p=0.447	p=0.348	p=0.146	p=0.290	p=0.086
Recovery	21.5±3.5	0.87±0.05	5.5±1.6	577±210	67.7±3.9	8.21 ±0.85

Table 1 Statistical analysis on the physiological parameters of US-induced responses in control and hypotonic saline. Detectable FUSD used for averaging were collected over a period of 45 minutes immediately before and after switching from the control to 75% hypotonic saline. The time windows used for the recovery period varied from 30 to 45 minutes. Values in this table were averaged from the average values calculated from eight axons. One of the eight preparations used sucrose substitution to generate hypotonic saline, two preparations used mannitol substitution while the remaining five used distilled water dilution.

Bold p values indicate a statistically significant difference.

†: subthreshold FUSD responses only.

§: frequency was normalized to the maximum of 1, when US evoked responses in every trial.

3.2.3 Effects of the osmolarity manipulation on axon morphology

The hypotonic saline had small effects of the crayfish motor axon morphology. When motor axon diameter was monitored with imaging, following fluorescence dye

injection, no consistent increase in axonal diameter was detected (n=4) in hypotonic saline (data not shown). Previous electron microscopic studies have shown that the crayfish motor axons are encased in glia cells and extracellular matrix [128, 129]. The latter could serve as a "brace" that prevents excessive swelling and rupture. In support of this unique resilience of the motor axon, the same hypotonic saline applied to the crayfish giant axons, in the central nervous system, caused measurable swelling (Yu et al. unpublished data). Furthermore, the crayfish giant axons showed reduced AP amplitude and hyperpolarization of RMP in hypotonic saline while none of these parameters of motor axons was changed by low osmolarity. Therefore, the "resilience" of the motor axons in hypotonic saline may be uniquely relevant to peripheral neural tissues. The freshwater environment for crayfish means that any injury to the exoskeleton may result in a significant reduction in osmolarity locally. The extensive extracellular matrix that could contain excessive swelling of the axon may be part of the reason that swelling in motor axons was difficult to resolve microscopically in hypotonic saline. Results reported here may be applicable to vertebrate peripheral nerve tissues where axons typically are surrounded by a protective sheath such as perineurium and epineurium.

3.2.4 Time-dependent variation of FUSD parameters in hypotonic saline

The parameters of FUSD showed consistent changes that correlated with reduced osmolarity within a 15-min time window. However, the changes did not remain steady over the period of 45 min in hypotonic saline. Specifically, FUSD amplitude exhibited a large fluctuation within the 45-min period in hypotonic saline while FUSD duration gradually declined in the same period. As a result, averaged over a period of 45 minutes, FUSD

amplitude in hypotonic saline was no longer statistically different from that of control saline while duration became significantly shorter in low osmolarity. Changes in FUSD parameters were not reversed within the duration of our study, ~30 min after the osmolarity was returned to the control saline.

This complexity may be due not only to the unique morphology of the extracellular matrix surrounding the crayfish motor axon but also to cellular adaptation. Studies of membrane mechanics in other preparations provide clues to possible explanations. When a laser tweezer was used to stretch the membrane and monitor the membrane tension of rat basophilic leukemia cells, it was shown that the cells adapted to the tweezer stretching by inserting the membrane over a period of 20 min [130, 131]. Furthermore, the plasma membrane and its linkage to the submembranous cytoskeleton have been shown to change as the osmolarity of bathing saline was altered [86]. The processes of insertion and retrieval of the cell membrane as well as disrupted linkage between the membrane and submembranous cytoskeleton could all take time to develop and recover. These cellular processes are relatively slow and could be the cause of the delayed reduction of Dur_{50} (Fig. 4D) and recovery in FUSD amplitude (Fig. 4A) as well as the absence of recovery of all parameters after switching back to control saline (Table 1). While amplitude, onset delay, frequency of occurrence, and duration were used to characterize FUSD, these parameters may differentially be controlled by different cellular processes under stresses introduced by changing osmolarity. Therefore, while FUS may create nanopores in the lipid bilayer, the ability of cells to add and retrieve membrane as well as breaking or forming linkages

between membrane lipids and molecules inside or outside of the membrane may all influence the formation and duration of nanopores.

3.3 Discussion

We examined the effect of lowering osmolarity on FUSD in crayfish motor axons. Lowering osmolarity to 75% of the control level did not change the passive and active properties of the axon but altered the characteristics of FUSD produced by FUS tone bursts. Statistically significant changes in FUSD parameters were observed when comparing recordings from a 15-minute time window before and after switching to hypotonic saline. Specifically, the amplitude and frequency of the FUSD occurrences increased, while the delay of FUSD decreased in hypotonic saline. The duration of the FUSD, however, did not show statistical differences in a 15-minute time window. These changes are consistent predictions based on the nanopore hypothesis. Expanding the time window of comparison to 45 min changed the status of statistical significances of FUSD amplitude, from significant to insignificant, and duration, from insignificant to significant, while the statistical significance of delay and frequency of occurrence were unaffected by the time windows selected for the comparison.

3.3.1 FUS-specific membrane conductance g_{US} and nanopore hypothesis

As reviewed in the Introduction, the application of FUS to an axonal membrane leads to an increase in membrane conductance (g_{US}) which underlies FUSD [90]. Biophysical properties of g_{US}, namely non-selective permeability, and long duration, together with pharmacological properties, namely absence of sensitivity to voltage-gated channel blockers, of FUSD led to the hypothesis that g_{US} may be mediated by nanopores

formed in the axonal membrane. In molecular dynamic simulations, similar lipid channels have been suggested to occur under electroporation and strong mechanical stretch [126, 127, 132-134]. Furthermore, low-intensity FUS may also cause pore formation at the membrane protein-lipid interface [135]. Therefore, the data presented here correspond well with characterizations based on quantitative simulations at an atomic level.

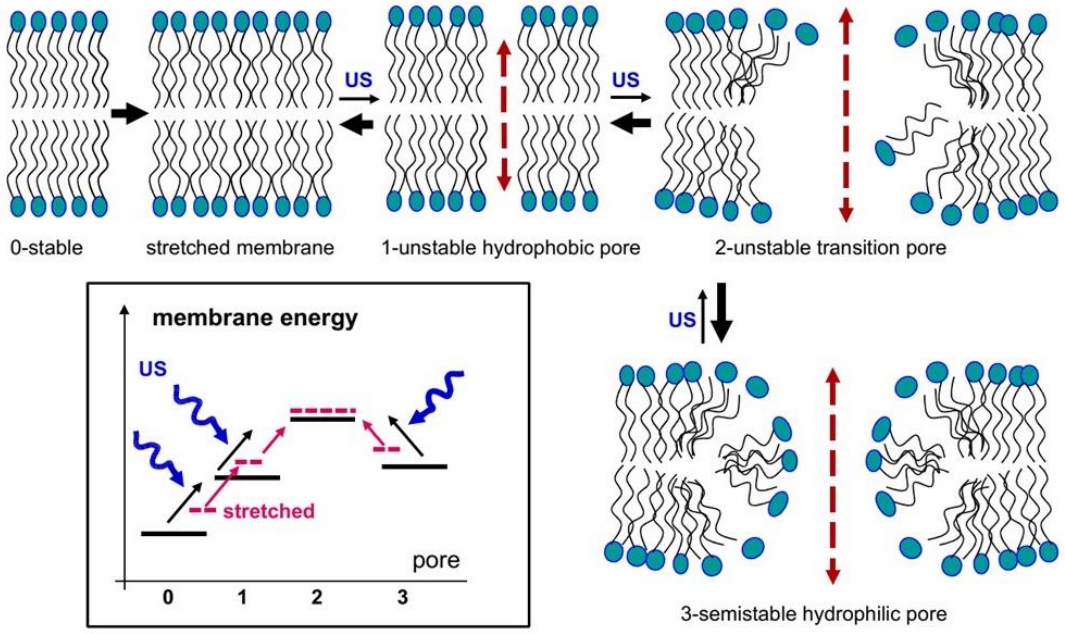

Figure 3.4 Illustration of how osmotic stretching of the lipid membrane would affect the hypothetical lipid membrane energy levels, and state transitions caused by US, in comparison to control (=non-stretched) membrane. These changes may explain the observed effects of hypotonic saline on g_{US} opening and closing probabilities. Hypotonic solution stretches the membrane, i.e. loosens the dense packing of the lipid bilayer (from 0-stable to stretched membrane); the increase in surface area corresponds to an increase of the membrane energy level (inset, red level vs. black level 0). From this stretched state the opening of hydrophobic pores and transition pores requires less absorption of energy than in control (inset: red vs. black uphill arrows $0 \rightarrow 1 \rightarrow 2$, respectively), so that the probability of transition in response to absorption of US energy is increased. Similarly, the probability of the first step of stable nanopore closing is increased due to a decreased energy gap (inset: $3 \rightarrow 2$ uphill red vs. black arrow, respectively). This change would reduce the mean open time of semi-stable hydrophobic pores 3 and thus duration of g_{US}.

A schematic illustration of nanopore formation in the context of the stretched membrane is shown in Figure 3.4 to help the interpretation of results in this paper. A FUS-

mediated mechanical disturbance was assumed to disrupt the lipid organization of the axonal membrane, which leads to the opening of hydrophilic pores. The mechanical disturbance could cause lipid molecules to transition through a series of intermediate states (states 1 and 2) before settling in a relatively stable state (state 3) where the hydrophilic pores are well formed. These transitions could also be presented as a series of energy levels associated with the reorganization of the phospholipids (inset). According to molecular dynamic simulations, the stability of nanopores is influenced by the balance between membrane surface tension and line tension of open pores [136]. The line tension in turn is influenced by the organization of lipid tails as well as electrostatic interactions among ions, water molecules and charged head groups of lipid molecules around an open pore. It is therefore reasonable to anticipate that increases in membrane tension due to lowered osmotic pressure could enhance the probability of nanopore formation by way of decreasing the energy barriers between states and making transitions between states faster (red potential levels in Fig. 3.4 inset). The increase in the probability of nanopore formation may underlie the increase in FUSD amplitude and frequency of occurrence while the faster forward transitions could explain the reduction in FUSD delay. The reduction in FUSD duration could also be explained by the decreased energy difference between states 2 and 3 (Fig.3.4 inset) such that the close rate of the open pores is increased in hypotonic saline.

3.3.2 Potential roles of radiation forces in FUSD

The design of experiments presented in this report was not intended to distinguish different US-generated physical processes—such as forces generated by streaming, cavitation, or radiation—underlying FUSD. However, the preparation used here, being a

neuromuscular junction, could provide insights into the potential contributions of radiation forces. We have examined and could not detect movement of the motor axons under a 40X water immersion lens during FUS application, with the FUS transducer positioned below the preparation (Unpublished data). Displacement in the range of ~1 μm should be visible under a 40X lens. Furthermore, being a neuromuscular preparation, strong stimulation of the motor axons triggers muscle contractions, which also move the motor nerves attached to it. In neurophysiological studies, we have recorded from muscle fibers and axons under the condition of mild contraction (≈100 μm in displacement), which generated small changes in membrane potential that persisted only during movement and were not stochastic. In contrast, FUSD was stochastic and had a duration of seconds in response to millisecond US tone bursts. Finally, we penetrated the axons with two electrodes routinely. The process of penetration invariably moved and deformed the axonal membrane. During the penetration of the second electrode, the first electrode, which was intracellular already, only detected small changes in membrane potential roughly coinciding with, but never out-lasting, the movement of the second electrode.

In summary, while radiation force may be important in certain preparations and experimental configurations, we believe that the movement of the membrane due to radiation forces is unlikely to be the cause of FUSD at the crayfish neuromuscular preparation. The radiational force, however, may be altering the structure of the axonal membrane at a spatial scale <1 μm that cannot be easily observed under an optical microscope. However, this hypothesis would require a separate experimental approach, such as using optical techniques to detect small membrane displacement, to resolve.

3.3.3 Future directions and potential applications to human

We believe our finding on g_{US} from crayfish motor axons can be applicable to other predations including neurons in the human brain because the basic membrane structure and physiological properties are conserved across an evolutionary scale. Although we use 2MHz FUS while 400-700 kHz are typically used for humans, FUS across the entire range of the frequencies from 0.4 to 2 MHz should be cable of altering the lateral surface tension between phospholipids in the lipid membrane, in the human central and peripheral nervous systems, with the radiation force of FUS. In addition, the FUS pressure in this study is significantly below the FDA safety limit. Thus, the phenomena we found can be produced using low-intensity safe values of FUS for humans.

In the long run, this study could prove relevant to situations where osmotic pressure is reduced in the human brain, such as during traumatic brain injuries or controlled reductions of osmolarity in circulating blood or cerebrospinal fluid. Furthermore, given the complexity of neuronal morphology, changes in US sensitivities of different neuronal compartments—such as soma, dendrites, axons, and synaptic terminals—under low osmolarity should be examined.

3.4 Conclusion

Focused ultrasound-evoked membrane depolarization can be modulated by the osmolarity of the physiological saline surrounding the cell. The reduced osmolarity of the saline bathing the crayfish motor axon increased the amplitude, reduced the onset latency, and increased the frequency of occurrence of FUSD immediately after osmolarity was lowered. The results support our hypothesis that FUSD may be generated by non-selective

FUS-specific lipid ion channels whose activities are influenced by lateral surface tension in the membrane.

CHAPTER 4. EFFECTS OF TEMPERATURE ON ULTRASOUND INDUCED NEURONAL RESPONSES IN MOTOR AXONS AND MUSCLE FIBERS OF THE CRAYFISH NEUROMUSCULAR JUNCTION

Applications of ultrasound (US) in humans include imaging and modulation of target tissues. Although multiple physical and biological processes have been proposed as the mechanistic underpinning of US-mediated neuromodulation, the final step invariably involves mechanical perturbation of the cell membrane. One likely target of the perturbation is mechanosensitive channels, which could be either excitatory or inhibitory depending on the ion permeability of the channel activated, i.e. cation or potassium. In this report, we examined the role of K2P channels in US modulation. Since this channel is sensitive to both US and temperature, we varied temperature to titrate the baseline K2P channel activities and examined the effects of focused ultrasound (FUS) on intracellular responses recorded from motor axons and muscle fibers of the crayfish opener neuromuscular junction. Although FUS consistently induced membrane hyperpolarization (FUSH) in motor axons, simultaneously recorded responses in muscle fibers were minimal. Over the range of 12 to 32 °C, there was no significant correlation between FUSH amplitudes, recorded in the motor axons, and temperature. Therefore, the temperature dependence of FUSH amplitudes was independent of the background K2P channel. Furthermore, FUSH was not inhibited by the K2P channel blockers although the presence of the channels in motor axons was confirmed by K2P blockers which increased input resistance and depolarized resting membrane potential. We conclude that it is unlikely that K2P channels underlie FUSH. Possible mechanisms underlying FUSH are discussed.

4.1 Introduction

Multiple physical modalities—such as infrared, and ultrasound (US) as well as electromagnetic and microwave radiations—have been used to deposit energy onto neural tissues to achieve neuromodulation. Among these modalities, US has a unique combination of attributes that offer promising potential for human application. US can accomplish non-invasive and precision targeting of any brain area due to its ability to penetrate the cranium and to narrowly focus on small regions deep inside the human brain. Therefore, the application of ultrasound technology in a clinical context has received considerable attention [137, 138].

Several physical processes have been proposed to explain US-induced mechanical interactions with neurons, including cavitation, radiation, and streaming (see [67] for review). Forces generated by these processes interact with biological membranes and evoke electrophysiological events [139]. Results of mechanical perturbations of the neuronal membrane include: (1) activation of mechanosensitive ion channels [76, 140-142], (2) formation of ion-permeable lipid nanopores in the neuronal membrane [90, 143, 144] (3) changes in membrane capacitance that is altered either by stretching or by thickening of the membrane due to intramembrane cavitation [62, 145] and (4) alterations in voltage-gated channels kinetics due to US mediated changes in lipid environment surrounding the channels [76, 123, 146]. These diverse mechanisms could result in a multitude of effects, including either excitation or inhibition, depending on the ion channels present in a given neuron.

The K2P channels family comprises a large number of K channels that share a common topology where a channel is formed by two subunits each of which contains two pore-lining domains [147]. K2P channels are of interest in the context of US-mediated neuromodulation because some members of this channel family are mechano-sensitive [148-150] and have been shown to be activated by US [76, 141]. In addition to mechano-sensitivity, some K2P channels, such as members of TREK/TRAAK family, are also temperature sensitive [151, 152]. The presence of K2P channels, most likely TREK-1 channels, at the crayfish motor axons, has been suggested in a previous study where an infrared laser was used to raise temperature transiently [153]. Furthermore, while K2P channels have been mainly investigated in temperature range relevant to mammalian tissues, 24-32 ℃ [151], studies of this channel in the context of pain perception and in heterogenous expression systems have tested TREK-1 and TRAAK channel activities down to 12 ℃ [154, 155]. In this report, we leveraged the dual sensitivity of K2P channels to explore the effects of temperature variations on FUS-induced responses. In theory, temperature could titrate the fraction of K2P channels in a close state. If US could activate K2P channels closed by low temperature, US-induced responses mediated by K2P channels should exhibit a temperature dependence consistent with that of K2P channels.

In this study, we examined whether US-induced membrane responses in crayfish motor axons would change as the preparation is cooled or heated. We focus on a FUS-induced membrane hyperpolarization (FUSH) in the crayfish motor axon, which typically required US intensity slightly lower than those used to evoke FUS induced depolarization

(FUSD) [90, 144]. FUS-evoked responses were interpreted in the context of the effects of temperature variations on K2P channels.

4.2 Results

4.2.1 Effects of cooling on FUS-induced responses in motor axons

Figure 4.1 illustrate a representative experiment where US evoked responses were recorded at room temperature (24 °C) first (A) followed by cooling to 15 °C (B) and finally back to room temperature (23 °C) (C). The ultrasound parameter was an 80 ms continuous burst. At room temperature, a single FUS burst consistently triggered small hyperpolarization. Figure 1A displays overlaying traces from individual trials (black) and the averaged trace (red). The average of FUS evoked responses at room temperature shows a small hyperpolarization during US applications (black bar) that is followed by a slow recovery (Fig.4.1A red). Upon cooling, the US-evoked responses transitioned into fluctuating hyperpolarization (Fig.4.1B). The average of trials recorded at 15 °C shows ~ 6 mV hyperpolarization during the US tone burst (red). When the temperature returned to room temperature, amplitudes of FUSH were reduced from those recorded at 15 °C (Fig.4.1C) but did not return to the control level.

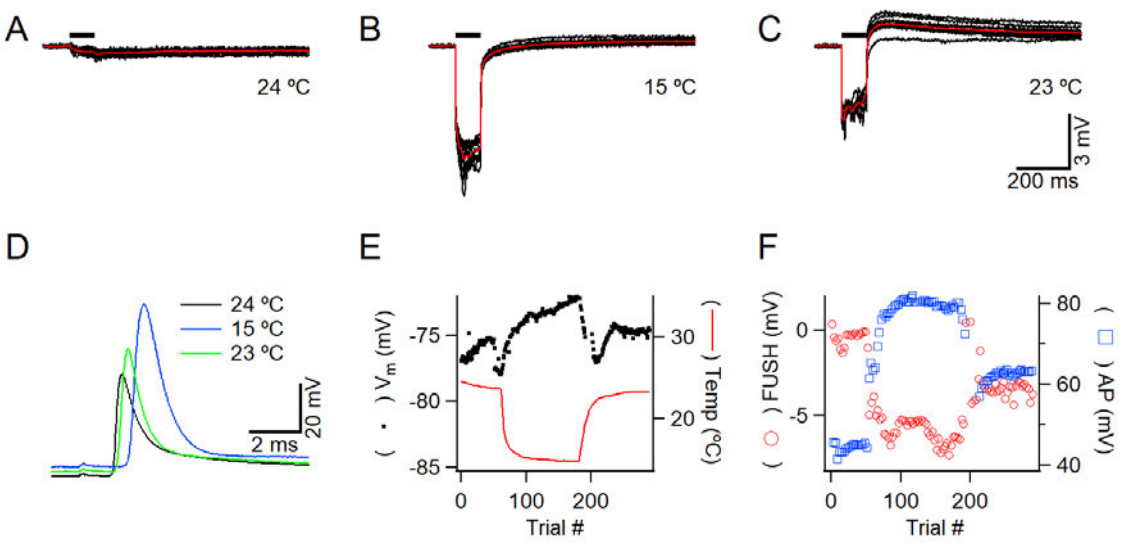

Figure 4.1 Effect of cooling on FUS-induced hyperpolarization in a motor axon. (A) US at 2.1 MHz and with a duration of 80 ms induced a small hyperpolarization at 23 °C. (B) The same US tone evoked fluctuating hyperpolarization when the preparation was cooled to 15 °C. (C) Reheating the preparation to control level reduced FUSH. Black traces in (A), (B) and (C) are recordings from individual trials while red traces represent averages. The black bar in (A), (B) and (C) indicates the timing of US. The sample size used for the averages in (A), (B) and (C) were 11, 14 and 9 respectively. (A), (B) and (C) share the same scales. (D) Action potentials were recorded from the same axon as that in (A), (B) and (C) under indicated temperatures. The action potentials recording were single trials and evoked by a suction electrode. (E) Timelines of resting membrane potential (V_m, black) and temperature (red). (F) Timelines of AP amplitude (blue squares) of the motor axons and FUSH (red circles) to highlight the stability and consistency of the recordings.

To ensure that the quality of the axonal recording was not adversely affected by the cooling or FUS, we monitored action potentials (APs) between US trials. Figure 1D shows APs recorded at 24 (black), 15 (blue), and back to 23 °C (green), respectively. These APs are propagating action potentials evoked by a suction electrode placed proximal to the axonal recording site, ~ 10 mm away. Cooling depolarized resting membrane potential (RMP) of the motor axon and increased AP amplitude and duration (Fig.4.1D black vs blue). Rightward displacement of the AP at 15 °C was due to the slowing of AP conduction velocity at the low temperature. Return to room temperature partially reversed all of the temperature-sensitive electrophysiological parameters. These temperature-dependent

changes are consistent with typical neuronal responses reported previously [156, 157]. Timelines of the temperature changes (red), and resting V_m (black) are displayed in figure 4.1E. AP amplitudes (blue circles) as well as FUSH (red circles) amplitudes, measured as averaged potential during US application, are displayed in Figure 1F. Neither AP amplitude nor FUSH amplitudes recovered completely. While AP amplitude was fully reversible in most preparations, FUSH recovery was incomplete in all preparations, suggesting the hysteresis of this parameter.

4.2.2 Enhancement of FUSH by cooling is specific to axonal responses

The FUS-induced hyperpolarization resulting from cooling is specific to motor axons. Figure 4.2 illustrates intracellular recordings from a muscle fiber obtained simultaneously with the axonal recordings shown in Figure 4.1. In this case, deflections in membrane potential during FUS application exhibited stepwise changes, suggestive of FUS-induced artifact in microelectrodes. The membrane potential deflections recorded during FUS were small in amplitude and typically less than 0.5 mV (Fig.4.2 A, B and C). Black traces in Figure 4.2 (A) to (C) represent individual trials while red traces are averages. The integrity of the muscle recordings was monitored by examining excitatory postsynaptic potentials (EPSP) evoked by the APs of the motor axon. EPSPs, triggered by a train of 8 APs at 100 Hz, exhibited strong facilitation, which is characteristic of this synapse. Cooling increased EPSP amplitude (Fig.4.2D blue), due to the increase in the amplitude and duration of presynaptic APs (Fig.4.1D). (The EPSP baselines were aligned for comparison.) Returning to room temperature restored EPSPs to their control levels (Fig.4.2D green). The resting V_m of the muscle fiber depolarized by 8 mV upon cooling

(Fig.4.2E dots). The timeline of the maximal EPSP indicates a clear temperature dependence (Fig.4.2F blue squares.) However, FUSH amplitudes (red circles) recorded in the muscle fiber suggest no apparent trend as the temperature was lowered and returned.

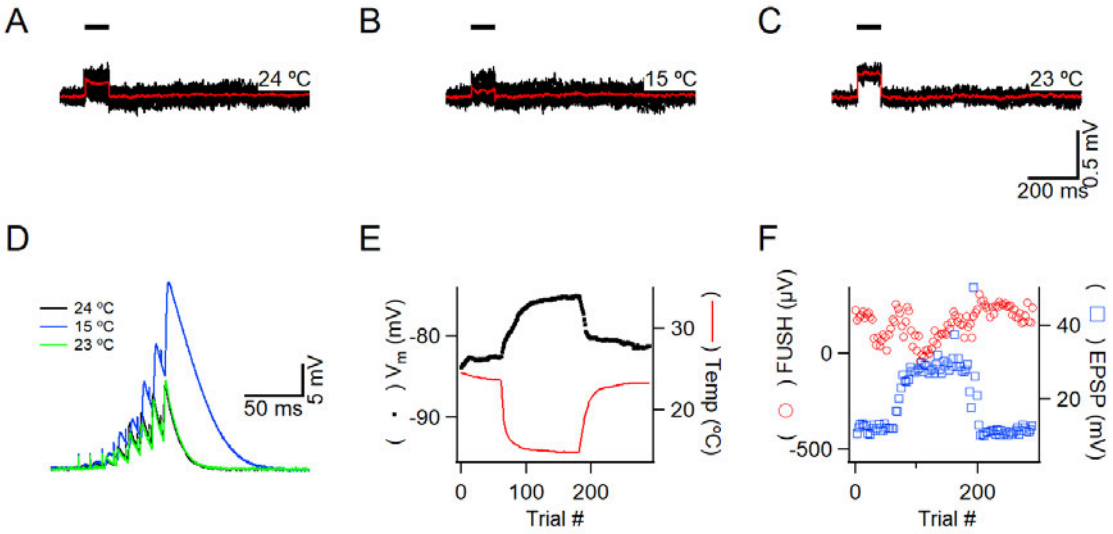

Figure 4.2 Cooling-induced changes in FUS evoked responses recorded from a muscle fiber. (A), (B) and (C) Intracellular recordings from a muscle fiber obtained from the same preparation, and simultaneously, as those shown in Figure 1. FUS induced small responses with a step-like shape. Black traces represent recordings from individual trials and red traces are averages with a sample size of 11, 14 and 9 for (A), (B) and (C) respectively. (A) (B) and (C) share the same scales. (D) Synaptic potentials were recorded under the temperatures shown in (A) to (C). The synaptic potentials were evoked by a train of eight APs. The EPSP amplitudes increased during the train due to synaptic facilitation. The EPSP traces were averages of 10, 14 and 9 trials. Baselines of EPSP traces have been aligned for comparison. (E) Timeline of resting Vm (black) and temperature (red). (F) Timelines of EPSP amplitude (blue squares) and FUSH (red circles) amplitudes recorded from the muscle fiber are displayed to highlight the stability of the recordings.

4.2.3 Summary of cooling effects on FUSH recorded in motor axons and muscle fibers

The enhancement of FUSH in motor axons upon cooling was a consistent observation. Figure 4.3A summarize results obtained from six axons where five exhibited a significant increase in FUSH while the sixth showed non-significant changes (Fig.4.3A dashed). FUS-evoked responses recorded from muscle fibers simultaneously in the same preparations exhibited significantly smaller amplitudes (Fig.4.3B). (Figure 4.3 A and B use

the same vertical scale.) Motor axons and muscle fibers recorded simultaneously used the same symbols in A and B. Furthermore, cooling did not cause a consistent trend in FUS-induced responses in muscle fibers. Four preparations did not exhibit statistically significant changes (Fig.4.3B dashed) while the remaining two showed significant depolarization and hyperpolarization respectively (Fig.4.3B solid).

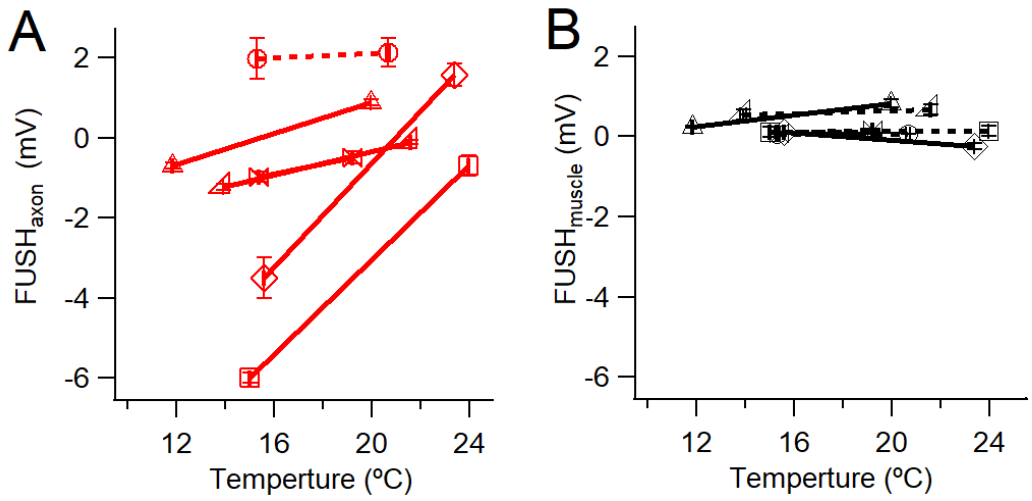

Figure 4.3 Summary of FUS-induced hyperpolarization upon cooling. (A) Average amplitudes of FUS-evoked responses in motor axons are plotted against the temperatures when the recordings were made. Data points from the same axons are connected. Each preparation is represented by a different symbol. Error bars associated with each data point represent the standard error of means but the temperature variations were typically smaller than the size of the symbols. The dashed line represents a preparation where the changes in FUS evoked responses were not statistically significant. Sample sizes used for average ranged from 10 to 20. (B) Average amplitudes of FUS-evoked responses recorded from muscle fibers are plotted against the temperatures from which the recordings were made. Data from the same muscle fibers are connected. Each preparation is represented by different symbols. Matching symbols in (A) and (B) mean they were obtained simultaneously from the same preparations. The dashed lines represent preparations where the changes in FUS evoked responses were not statistically significant.

When a burst of US is applied to a motor axon with a pressure of 0.1-1 MPa (2.1 MHz, 1 mm focal area diameter), it initially produces hyperpolarization. This is followed by a depolarization when the pressure is higher than about 0.3 MPa [90, 158]. To focus on FUSH in this study, we typically used pressures below 0.3 MPa (see Methods) such that

the depolarization is rarely seen, in <5% of the trials. Therefore, only some preparations exhibited averaged FUSD at room temperature but lowering the temperature consistently enhanced FUSH (Fig.4.3A). These results could be due to an increase in US-activated K2P channels upon cooling. Specifically, US-activated channels were increased at a lower temperature because the channels closed by cooling increased the pool of channels available to be activated by US. We therefore examine whether heating could lead to the opposite effect on FUSH.

4.2.4 *Effects of heating on FUS-induced membrane responses in motor axons*

Figure 4.4 illustrates a heating experiment using the same preparation shown in Figure 4.1 and 4.2. Representative responses recorded in the control temperature, 23 °C, are shown in Figure 4.4A which exhibit similar characteristics to those in Figure 4.1C. (The black traces in Figure 4.4A, while recorded from the same recording session as those in Figure 4.1C, were sampled from different trials than those used in Figure 4.1C). When the saline was heated to 32 °C, there was only a slight change in FUSH (Fig.4.4B). Black traces represent recordings from individual trials while the red traces are the averages of the black ones. The heating did not adversely affect the preparation. The motor axon hyperpolarized upon heating. In addition, both AP amplitude and duration exhibited a clear reduction at 32 °C (Fig.4.4C). The leftward shift in the AP recorded after heating was due to a faster conduction velocity. These changes in AP parameters are characteristics of excitable cells when the temperature was raised [159, 160]. Timelines of resting V_m, AP, and FUSH amplitudes are displayed in Figure 4.4D and 4.4E respectively. Fluctuations in FUSH

amplitude were more pronounced momentarily upon heating but this parameter settled back to a more stable state later.

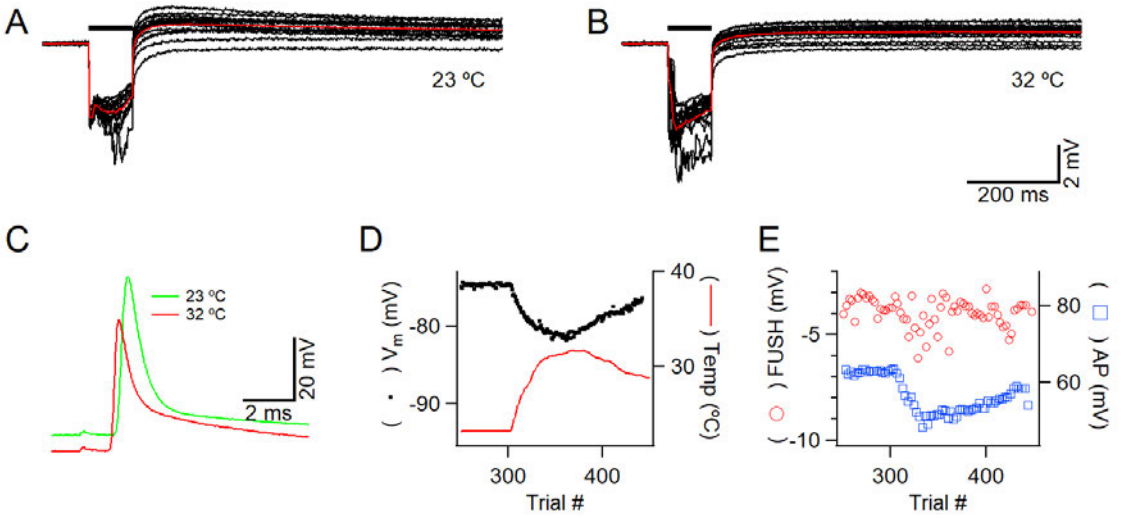

Figure 4.4 Effects of heating on FUS-induced responses in a motor axon. (A), (B) Intracellular recordings from a motor axon as the temperature was raised from 23 (A) to 32 °C (B). The heating was accompanied by a minimal change in FUSH amplitude. Black traces in (A) and (B) are recordings from individual trials while the red traces are averages of displayed single trials. The sample size of the averages in (A) and (B) was 17. (A) and (B) share the same scales. (C) An increase in temperature caused membrane potential hyperpolarization and a reduction in AP amplitude and duration in the axon. The leftward displacement of the AP recorded at 32 °C (red) was due to an acceleration of AP conduction velocity. The AP traces were from single trials. (D) Timelines of resting membrane potential (Vm, black) and temperature (red). (E) Timelines of AP amplitude (blue squares) of the motor axons and FUSH (red circles) to highlight the stability of the recordings.

4.2.4 Effects of heating on FUS-induced membrane response in muscle fibers

Figure 4.5A and B illustrate intracellular recordings from a muscle fiber obtained simultaneously with the axonal recordings shown in Figure 4.4. Similar to the observation made during cooling (Fig. 4.2A and B), deflections in membrane potential during FUS application exhibit stepwise changes with small amplitudes, <0.5 mV (Fig.4.5 A and B). The integrity of the muscle recordings was monitored by examining EPSPs evoked by the AP train of the motor axon. EPSPs exhibited strong facilitation during the eight AP trains.

Consistent with the reduction in AP amplitude and duration during heating (Fig.4.4C), EPSP exhibited a clear decrease in amplitude (Fig.4.5C). Resting V_m of the muscle fiber exhibited a clear hyperpolarization, with a timeline mirroring that of temperature change (Fig.4.5D black). While the timeline of the maximal EPSP (Fig.4.5E blue squares) indicates a clear temperature dependence, FUSH amplitudes (Fig.4.4E red circle) recorded in the muscle fiber suggest no apparent trend.

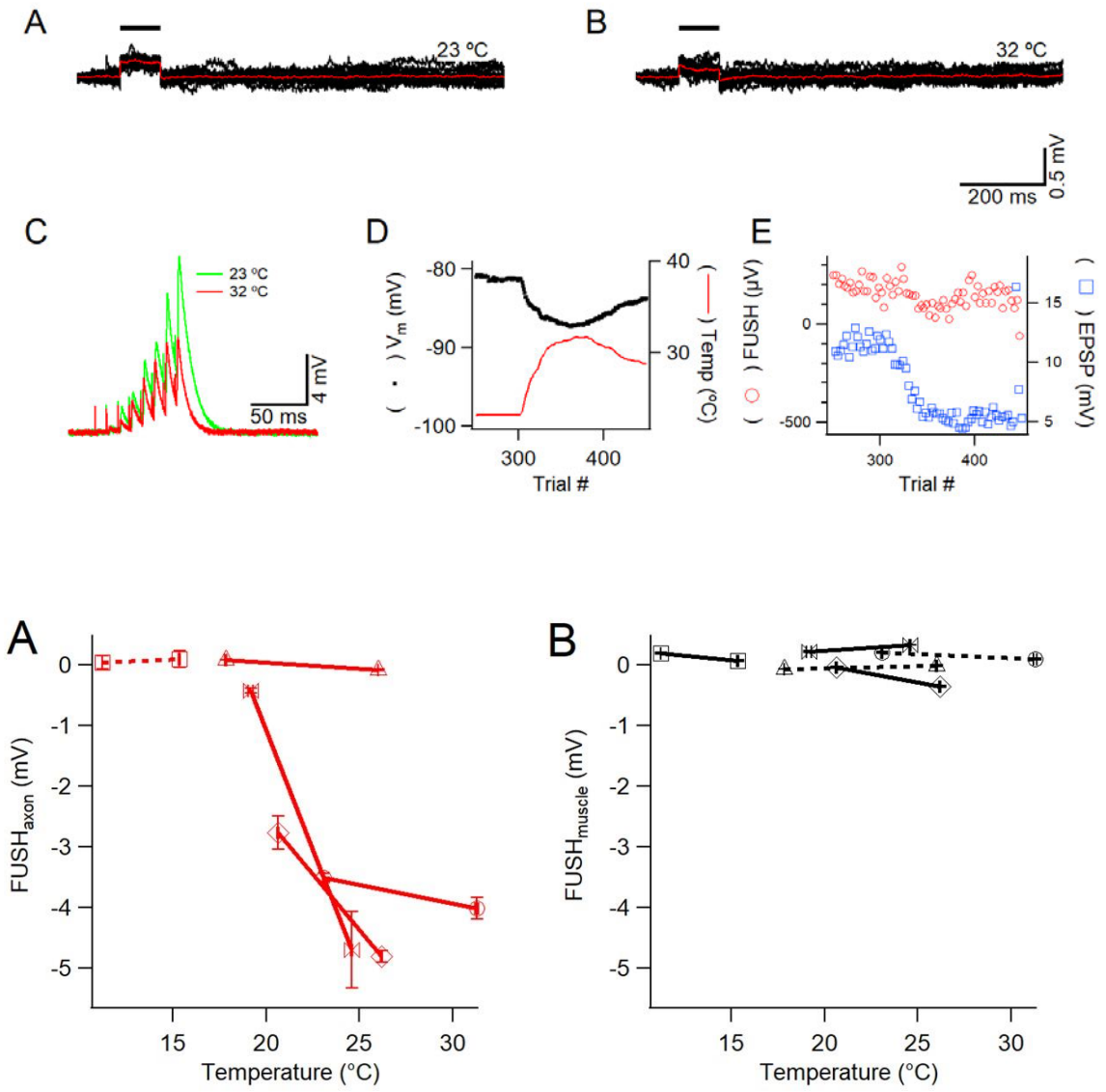

Figure 4.5 Heating-induced changes in FUS evoked responses recorded from a muscle fiber. (A) and (B) Intracellular recordings from a muscle fiber obtained from the same preparation, and simultaneously, as those shown in Figure 4. FUS induced small responses with step-like shapes. Black traces represent recordings from individual trials and red traces are averages with sample sizes of 17 for (A), and (B). (A) and (B) share the same scales. (C) Synaptic potentials were recorded under the two temperatures shown in (A) and (B). The synaptic potentials were evoked by a train of eight APs. The EPSP amplitudes increased during the train due to synaptic facilitation. The EPSP traces were averages of 17 trials. Baselines of EPSP traces have been aligned for comparison. (D) Timeline of resting membrane potential (black) and temperature (red). (E) Timelines of EPSP (blue squares) and FUSH (red circles) amplitudes recorded from the muscle fiber are displayed to highlight the stability of the recordings.

4.2.5 Effects of heating on FUS-induced membrane response in muscle fibers

There was no apparent temperature-dependent trend in axonal FUSH amplitude. In seven axons examined during heating, five exhibited significant increases and two significant decreases in FUSH amplitudes (Fig.4.6A). Similar to the situation with cooling, changes in FUSH were specific to motor axons. Simultaneously recorded muscle responses to FUS exhibited much smaller amplitudes and showed no consistent trend (Fig.4.6B). Specifically, four muscle fibers exhibited no statistically significant change in FUS-induced responses (Fig.4.6B dashed), while the remaining three exhibited small but significant changes. Therefore, the temperature dependence of FUSH in motor axons during heating did not follow the same trajectory as that of cooling. FUS-evoked responses recorded in muscle fibers are significantly smaller than those of motor axons and do not suggest a temperature dependence.

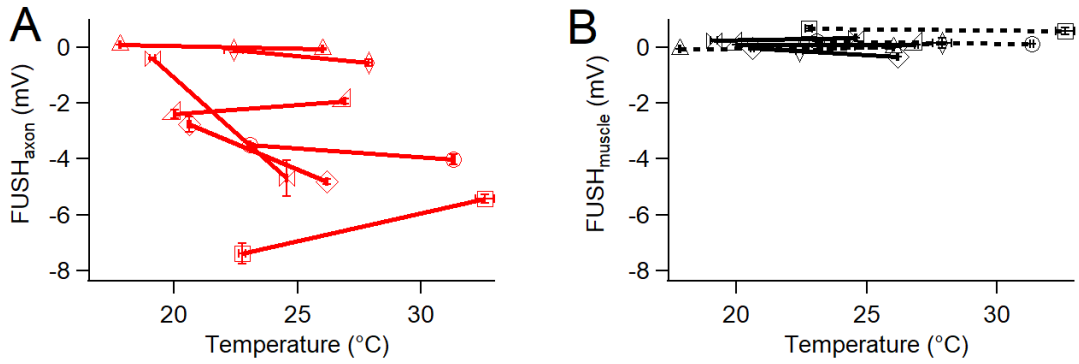

Figure 4.6 Summary of FUS-induced hyperpolarization upon heating. (A) Average amplitudes of FUS-evoked responses in motor axons are plotted against the temperatures from which the recordings were made. Data from the same axons are connected. Each preparation is represented by a different symbol. Sample sizes used for average ranged from 7 to 20. (B) Average amplitudes of FUS-evoked responses recorded from muscle fibers are plotted against the temperatures from which the recordings were made. Data from the same muscle fibers are connected. Each preparation is represented by different symbols. The symbols that match those in (A) mean they were obtained simultaneously in the same preparations. The dashed lines represent a preparation where the changes in FUS evoked responses were not statistically significant.

4.2.6 Compilation of data from both cooling and heating does not suggest simple temperature dependence of FUSH

Figure 7 combines the heating and cooling data point of FUSH recorded from crayfish motor axons (Fig.4.3A and Fig.4.6A). While cooling (blue) suggested an predominantly increase in FUSH, the linear fit to the entire data set (blue line) gave a correlation coefficient of 0.42 which is not statistically significant (p=0.16). However, when a *t*-test was performed by comparing the cooling-induced changes in FUSH amplitudes from individual preparations against the null hypothesis of zero change in amplitudes, cooling significantly increase FUSH amplitude only when one-tailed distribution was assumed (p=0.03, one-tail). Linear regression performed for heating experiments gave rise to a negative slope and a correlation coefficient of 0.37 (p=0.19). Results from the *t*-test suggested no significant changes in FUSH amplitude upon heating (p=0.19, one-tail). In summary, while cooling experiments suggest weak temperature dependence of FUSH, heating did not support the same trend. Since K2P channel activities exhibit a monotonous rise in temperature-dependent activation over the temperature range tested here [161], one would expect a continuous trend in the temperature dependence of FUSH if K2P channels are the dominant process underlying FUSH. Therefore, the scatter plot in Figure 4.7 does not support the hypothesis that FUS activation of K2P channels underlies FUSH.

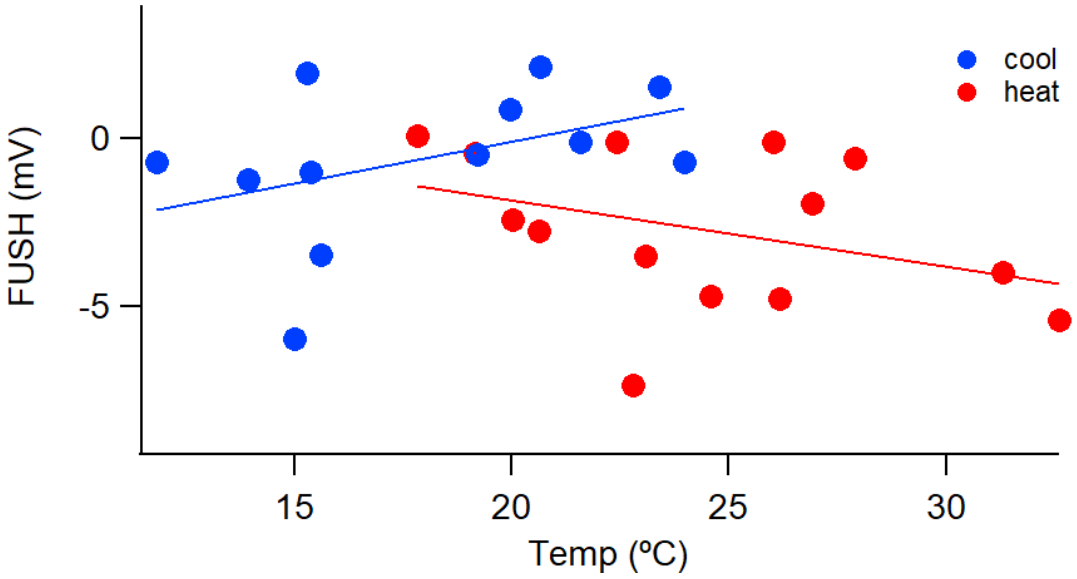

Figure 4.7 Compilation of data from heating and cooling experiments. The data points were from axonal recordings shown in Figure 4.3A and 4.6A. The blue line represents a linear fit to the cooling data points, with a slope of 0.25mV/°C. The red line represents a linear fit to the heating data point, with a slope of -0.2 mV/°C. Neither fit represents a statistically significant correlation. (See text).

4.2.7 Possible role of K2P channels in the temperature dependence of FUSH

To verify the presence of K2P channels in motor axons, we tested these K2P channel blockers: Fluoxetine (100 µM), norfluoxetine (50 µM), and Ba^{2+} (2 mM) on electrophysiological properties of motor axons. Figure 8A shows that 100 µM fluoxetine depolarized the resting membrane potential and increased the input resistance. A series of current steps that evoked subthreshold membrane responses in control saline were recorded first (Fig. 4.8A black), the membrane responses to the same current steps increased after the introduction of 100 µM Fluoxetine (Fig.4.8A red). Voltage-current relationship measured from subthreshold responses showed a 1.8-fold increase in input resistance after fluoxetine (Fig.4.8A inset). The combined effects of blocking K2P channels, namely membrane depolarization and increase in input resistance, resulted in AP firing trigger by

a +20 nA current step in some trials which was subthreshold before the blocker (Fig.4.8A red). However, the application of fluoxetine did not block FUSH. In the same axon in which K2P channels had been blocked, we also examined FUSH before and after fluoxetine (Fig.4.8B). Representative FUSHs from single trials showed an increase in FUSH amplitude after the blocker (Fig.4.8B). The FUSHs were triggered by FUS tone bursts containing 30 2MHz tones, each of which had a duration of 0.5 ms and a 50% duty cycle. Details of averaged FUSHs, at the beginning of the tone burst, are shown in Figure 8B inset. Here, each US tone, 2 MHz with 500 μs duration, triggered a membrane hyperpolarization. The same US tone triggered a larger hyperpolarization in fluoxetine (red). Timelines of FUSH amplitude (red circles), measured as the peak-to-peak amplitude of the hyperpolarizing transient (Fig.4.8B inset $FUSH_{pp}$), and input resistance (blue squares) of the motor axon are displayed in Figure 8C. Fluoxetine increased both parameters. Norfluoxetine, which is a metabolite of fluoxetine but has a higher affinity for TREK-1 channels [150, 162], did not change the amplitude of $FUSH_{pp}$ (Fig.4.8D red circles and inset) but effectively increase input resistance (Fig.4.8D blue square). We tested three blockers in six motor axons at room temperature: fluoxetine (n=3; 100 μM), norfluoxetine (n=1; 50 μM), and Ba^{2+} (n=2; 2 mM). K2P blockers significantly increased $FUSH_{pp}$ in three preparations and did not alter $FUSH_{pp}$ in the remaining three. In the absence of K2P blocker-mediated FUSH inhibition, we propose that K2P channels do not play a significant role in FUSH at the crayfish opener axons.

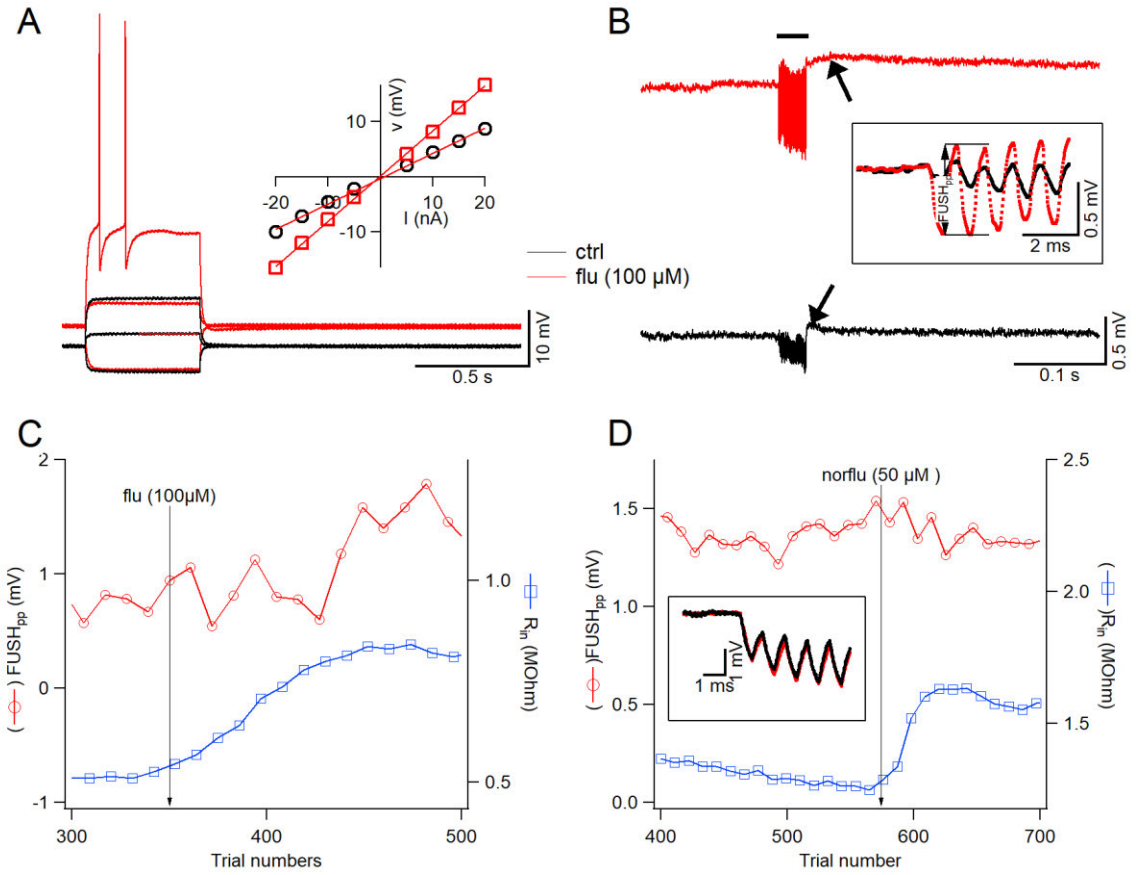

Figure 4.8 Effects of TREK-1 channel blockers on motor axons and FUS evoked responses. (A) Axonal recordings evoked by -5, +5 and +20 nA current steps. Application of 100 µM fluoxetine (red) caused a depolarization of resting membrane potential, by 4 mV, and an increase in input resistance such that the +20 nA step, which was subthreshold in control saline, could trigger AP firing in fluoxetine. Inset: voltage current responses evoked by current steps from -20 to +20 nA in 5 nA increments. The input resistance increased from 0.46 to 0.81 MΩ. (B) FUS evoked hyperpolarization recorded from the same axon as that used in (A). FUSH became larger in fluoxetine (100 µM). Recordings were obtained from single trials. The arrows identify a slight "overshoot" at the termination of FUS tone bursts. Inset: Comparison of averaged FUS-induced hyperpolarization in an expanded time scale. US-induced responses evoked by individual tone bursts showed an increase in amplitudes. Individual hyperpolarization matches the duration of each FUS tone, which lasted for 500 µs. FUS evoked responses ($FUSH_{pp}$) were measured as peak-to-peak amplitudes resulting from individual 0.5 ms tone bursts. (C) Timelines of $FUSH_{pp}$ and input resistance measured from the preparation used in (A) and (B). (D) Timelines of $FUSH_{pp}$ and input resistance were obtained from a different motor axon where norfluoxetine (50 µM) was used to block TREK-1 channels. The blocker effectively raised input resistance but had no impact on $FUSH_{pp}$. Inset: Averaged FUSH recordings obtained before (black) and after (red) addition of norfluoxetine. The number of trials used for averaging were 7 and 9 respectively.

4.3 Discussion

In this report, we use motor axons and muscle fibers of the crayfish opener neuromuscular preparation to examine the effects of temperature variations on FUS-induced responses. Cooling weakly enhanced FUSH while heating results did not suggest temperature dependence of FUSH. The presence of FUSH was specific to motor axons because FUS-induced responses in muscle fibers exhibited significantly smaller amplitudes and showed no consistent trend with temperature variations. Results from the temperature experiments do not support the hypothesis that K2P channels underlie FUSH despite the dual thermos- and mechano- sensitivity of this channel class. While the presence of the K2P channel in the motor axons was confirmed by specific blockers, these blockers failed to block FUSH at room temperature. Temperature dependence of FUSH and pharmacological results both suggest that K2P channels are unlikely to underlie FUSH.

4.3.1 K2P hypothesis for FUSH

In excitable cells, hyperpolarization is typically attributed to potassium channels. We consider the role of K2P channels in FUSH because TREK-1 and TRAAK channels, both members of the K2P family, have been shown to be activated by US [76, 141]. Furthermore, K2P channels have been implicated in a hyperpolarization evoked by temperature rises triggered by infrared pulses in the crayfish motor axons [153]. These factors in combination make K2P channels compelling candidates for FUSH.

To increase the response amplitudes of a neuron, either an increase in input currents or input resistance (R_{in}) was expected. R_{in} of a neuron was determined by cytoplasmic resistance and membrane resistance. In the context of US-mediated modulation, we mainly

consider the effects of FUS on membrane resistance (R_m). R_m is determined by the resistance of the lipid bilayer and ion channels arranged in parallel. Resistance of lipid bilayer is known to increase with cooling and decrease with heating [163, 164]. In neurons, as the temperature is raised or lowered, K2P channels open or close which in turn dictate temperature-dependent changes in V_m and R_{in}. In the context of this report, FUSH enhancement by cooling could be explained by assuming that K2P channels that were closed by reduced temperature could still be open by US. (K2P hypothesis) Therefore, cooling could increase the pool of K2P channels available for opening by US. However, this hypothesis would predict a decrease in FUSH upon heating, due to a decrease in the fraction of channels available for opening by US and a decrease in membrane resistance. The absence of a temperature-dependent decrease in FUSH upon heating contradicts the K2P hypothesis. Finally, both specific (fluoxetine and norfluoxetine) and nonspecific (Ba^{2+}) K2P channel blockers failed to inhibit FUSH at the crayfish motor axons. Therefore, neither the physiological nor pharmacological results reported here support the K2P hypothesis. Although it remains possible that mechano-sensitivities of K2P channels may have a temperature dependence that could explain the results reported here, there has been no published information that could guide informed speculations. In conclusion, the K2P hypothesis for FUSH is not viable in this preparation, and that potential contributions from other K^+ channel types should be considered.

A standard approach to test the possible contribution of a potassium channel in neuronal responses is to shift membrane potential and examined whether the responses could be inverted at potassium equilibrium potential (E_K) [153]. However, shifting

membrane potential by current injection did not invert FUSH in motor axons (Data not shown). Recording configurations used in this study could at least partially be the reason why FUSH could not be inverted. Specifically, a current injection could only change membrane potential around the segment of the axon near the current injection electrode. On the other hand, FUSH is likely to appear in the entire axonal arborization because the FUS focal area is large enough to enclose most of the preparation. As a result, FUSH could not be easily inverted if membrane potential is shifted only near the current injection electrode. Therefore, the absence of data demonstrating that FUSH reverses polarity at E_K does not conclusively rule out potassium channels as a potential contributor to FUSH.

4.3.2 Sonophore hypothesis for FUSH

It has been proposed that ultrasound-mediated neuromodulation could arise from intramembrane cavitation, namely that gas bubbles form and collapse within the lipid bilayer (Sonophore hypothesis) [145, 165]. It was suggested that membrane expansion due to the intramembrane cavitation could reduce membrane capacitance transiently and generate a hyperpolarizing capacitive current. The hyperpolarization could have a sufficiently large amplitude to drive inward sodium and potassium currents through leak channels. Cumulative effects, from multiple US cycles, of the inward currents were proposed to generate excitation. While this process has been explored by simulation [166], there has been no published experimental evaluation of this process. Since we have ruled out the potential contribution of K2P channels, the sonophore hypothesis represents a viable alternative. FUSHs presented in this report were typically less than 10 mV and were not large enough to drive significant inward currents through leak channels. However, the

FUSH could be the result of filtering by passive properties of microelectrodes, which has a time resolution of ~5 KHz, while the voltage transients due to cavitation that is synchronized to US cycling at 2.1 MHz may be much larger. Cumulative effects of the inward current generated by sonophore could account for the overshoots that occurred at the end of the US tone burst (Fig.4.8B arrows). The overshoots were often observed in our recording configuration and have been noted previously [90]. Finally, sonophore hypothesis is consistent with the fact that we could not invert FUSH at E_K by shifting membrane potential in the axons. While the motor axon recordings are consistent with the sonophore hypothesis, recordings from muscle fibers did not exhibit significant FUSH and, therefore, do not conform to the hypothesis. See the section comparing motor axons and muscle fibers below for further discussion.

4.3.3 Effects of changing temperature on mechanical properties of biological membrane

Physical processes underlying temperature dependence of lipid molecule reorganization in membrane bilayers have been studied extensively. Studies using artificial lipid bilayers suggested that the organization of lipid molecules in the membrane can transition from a highly organized gel phase to a disorganized liquid phase as a specimen is heated (Phase transition). The actual temperature at which the phase transition happens depends on the type of lipid molecules and the presence of cholesterol [163]. While temperature-dependent changes in the mechanical properties of artificial membranes have been characterized [167], the significance of these changes in the context of US-membrane interaction remains to be articulated. Nevertheless, changes in lipid organization due to temperature variation could contribute to the temperature-dependent behavior of FUSH

reported here. In the crayfish axon, attempts to examine phase transition using Laurdan, a fluorescence reporter of the state of water penetration into the bilayer membrane [168], were hampered by strong background fluorescence. Thus, whether the temperature range examined in this report could cause reorganization of lipid molecules, and whether the resulting reorganization would change the mechanical interactions between US and the motor axons remain to be further investigated. For now, we suggest that phase transition is not the dominant parameter shaping the temperature dependence of FUSH because this mechanism should result in a temperature dependence of FUSH with similar trajectories for both heating and cooling.

4.3.4 Difference between axon and muscle responses to FUS

The comparison of simultaneously recorded axon and muscle responses provided a clear demonstration that FUSH is specific to motor axons of the crayfish opener neuromuscular preparation. The focal area of the FUS used in this study is large enough to enclose the entire preparation. The separation between the two electrodes was 200-400 μm within a 1x1.4 mm US focal area. Therefore, axon and muscle recording sites are unlikely to be subjected to different US pressure. Therefore, the specificity is more likely to be due to the difference in the ion channels expressed in the two cell types. The motor axons have characteristics of typical excitable cells that fire action potentials and have spatially nonuniform distributions of sodium and potassium channels [112, 169, 170]. In contrast, muscle fibers at the crayfish opener neuromuscular preparation do not fire APs. Muscle contraction in this preparation is graded by the amplitude of EPSP. Thus, the main difference between the cell types is the absence of voltage-dependent Na^+ and K^+ channels

with fast kinetics which typically underlie APs. In other words, the qualitative difference in ion channels expressed in motor axons and muscle fibers may explain the data reported here. Finally, muscle fibers contract actively while motor axons attached to them are pulled passively during locomotion. The two modes of movement may involve a difference in lipid compositions of the cell membrane or sub-membranous scaffolds such that intramembrane cavitation may not occur readily in muscle fibers.

In addition to differences in ion channel expressions, the morphological difference between the two cell types should also be noted. In the case of the crayfish opener neuromuscular preparation, muscle fibers are typically cylindrical and 3-5 times wider in diameter than that of the primary branch of motor axons, typically 20-30 μm. Furthermore, motor axons branch repeatedly and end in strings of varicosities. The varicosities are typically 1-5 micrometers in diameter and strung together by sub-micrometer connecting axons. The role of neuronal morphology in US-mediated modulation is difficult to evaluate at present. This question has just begun to be explored [165, 166].

4.4 Conclusion

In our previous studies using the crayfish motor axons, we showed that FUS at sufficiently high intensity evoked a prolonged depolarization, which was mediated by a non-selective cationic conductance. This conductance was more than ten times larger than the resting leak conductance of the axons and can activate persistent AP firing. In this report, we demonstrate the presence of a FUS-induced hyperpolarization at a US intensity lower than that used to evoke FUSD. The multitude of biological effects evoked by ultrasound is not surprising. US pressure waves at different intensities may preferentially

bring forth the effects of one particular type of US-membrane interaction. Specifically, high-intensity US causes lipid sonoporation while lower intensities activate different US-membrane interactions which generate hyperpolarization. Furthermore, as our comparison between motor axons and muscle fibers suggests, different neurons may respond to the same US perturbation differently due to their unique composition of ion channels expressed. Therefore, investigation of cellular responses to US perturbation is likely to uncover a large variety of distinct US-activated responses that are specific to the target neuronal cell types and US stimulus regimes. We believe that information on the US sensitivity of individual cell types in combination with optimal US delivery regimes for each type of response should form the basis of selective modulation of specific neural or muscle tissues. These considerations should expand the versatilities of US applications in humans.

CHAPTER 5. FUS EFFECT ON PROPAGATING ACTION POTENTIALS

Ultrasound (US) mediated neuromodulation is under intense exploration because of its potential in non-invasive human applications. Mechanisms underlying the modulation have been investigated at multiple levels. Studies on mechanisms of US modulation at the cellular level have mainly focused on mechanosensitive channels or the mechanical perturbation of cell membranes. Investigations on the effects of US on action potentials have only started recently. Here, we use intracellular recordings to study the effects of US on propagating action potential in the crayfish motor axons. AP recorded during a continuous US tone (2.1 MHz) took off from a hyperpolarized membrane potential and exhibited larger amplitudes and shorter duration. We have examined and eliminated three hypotheses. The US modulated AP shape changes cannot be due to: (1) alterations in microelectrode characteristics, (2) the increase in the fraction of sodium channels in the closed and not-inactivated state due to the hyperpolarization and (3) US activation of K2P channels which in turn altered AP shapes. One potential mechanism that requires further investigation is that US may accelerate the activation of sodium channel opening. Other factors that may indirectly modulate AP shapes are discussed.

5.1 Introduction

Ultrasound has been considered a promising modality for neuromodulation in human applications due to its ability to penetrate the cranium and to narrowly focus on small regions deep in the human brain [116, 171]. In the area where US is focused, US pressure waves interact with neurons through physical processes such as cavitation, radiation or streaming [67]. These processes mechanically interact with the neuronal

membrane, change membrane potential and lead to the modulation of neuronal activities [139].

While the efficacy of *in vivo* US applications have been demonstrated using EEG or EMG recordings [12], mechanistic understanding of these effects requires techniques that monitor neuronal activities at a single cell level. Calcium imaging, current clamp, and voltage clamp recordings from neurons or cell lines expressing ion channels have been used for this purpose. Cellular level studies have shown that US can modulate neuronal activities by (1) modulation of mechanosensitive ion channels [76, 77], (2) formation of lipid nanopores in neuronal [90, 143, 144], and (3) generation of capacitive currents, by stretching membrane or by membrane thickening due to intramembrane cavitation [62, 145, 165]. These processes can generate subthreshold activities which in turn can alter neuronal firing. However, the possibility that US modulation may directly modulate action potentials has recently started to be examined in detail.

Investigations of US-mediated impacts on action potentials (AP) have been conducted at multiple levels. Extracellular recording has been the main technique used to examine US-mediated neuromodulation and has made a significant contribution to the field [172, 173]. However, this technique does not provide sufficient resolution to unravel the mechanisms underlying the modulation. Current clamp studies on US modulation of AP firing, using brain slices or primary cultures, have consistently demonstrated a reduction in AP duration, which was accompanied by accelerations of rising and falling phases of APs [174-177]. Some studies further reported a reduction in membrane resistance and time constant during US application [174, 175, 177]. In addition, US applications during

repetitive firing activated by current steps have been shown to increase firing frequency and depolarization of after-hyperpolarizing potentials [174-177]. Using the voltage clamp, it has been reported that activation and inactivation of cardiac Na^+ channels (Nav1.5) can be accelerated by membrane stretching [123] or by US at 10 MHz [76]. The changes in firing frequency, Na^+ channel kinetics, AP shapes, and passive membrane properties represent a wide spectrum of neuronal properties. These changes are unlikely to be attributable to a common mechanism. Thus, while US modulation of AP represents an area of active interest, there exist many unresolved questions that would require the use of a large variety of preparations and approaches. The studies reviewed so far used current steps to trigger AP at neuronal soma, which approximates processes underlying AP triggered by synaptic integrations. However, effects of US on propagating AP along an axon represents a different functional context and has not been investigated with high resolution intracellular recordings. In this report, we use the crayfish motor axons to examine effects of 2.1 MHz focused US on propagating AP.

5.2 Results and discussion

5.2.1 Effects of FUS on action potentials

Effects of US application on action potentials (AP) were examined by applying US tone burst during a train of forward propagating action potential. Figure 5.1A illustrate a typical experiment where a train of 8 APs firing at 100 Hz was compared in the absence (black) and presence (red) of FUS which was a continuous tone for 80 ms (Fig.5.1A black bar). AP firing during the US tone took off from a hyperpolarized membrane potential. The trace with US treatment was also shifted vertically (green) such that the baseline before the

first AP was aligned with that of the control trace. Details of the FUS-induced changes in the first AP are shown at an expanded time scale in Figure 1B. There is an increase in AP amplitude and a reduction in AP duration under FUS. AP parameters analyzed quantitatively are also defined in Figure 5.1B. AP amplitude (amp) is defined as the difference between the minimal point before AP onset and the peak of the AP. AP duration (dur) is measured as the width at 50% of AP amplitude. Afterdepolarizing potential (adp) is measured as the difference between the minimal point before AP onset and the potential 8 ms after the minimum. AP conduction delay (del) is measured from the onset of the stimulus artifact to the maximum of the time derivative of the AP.

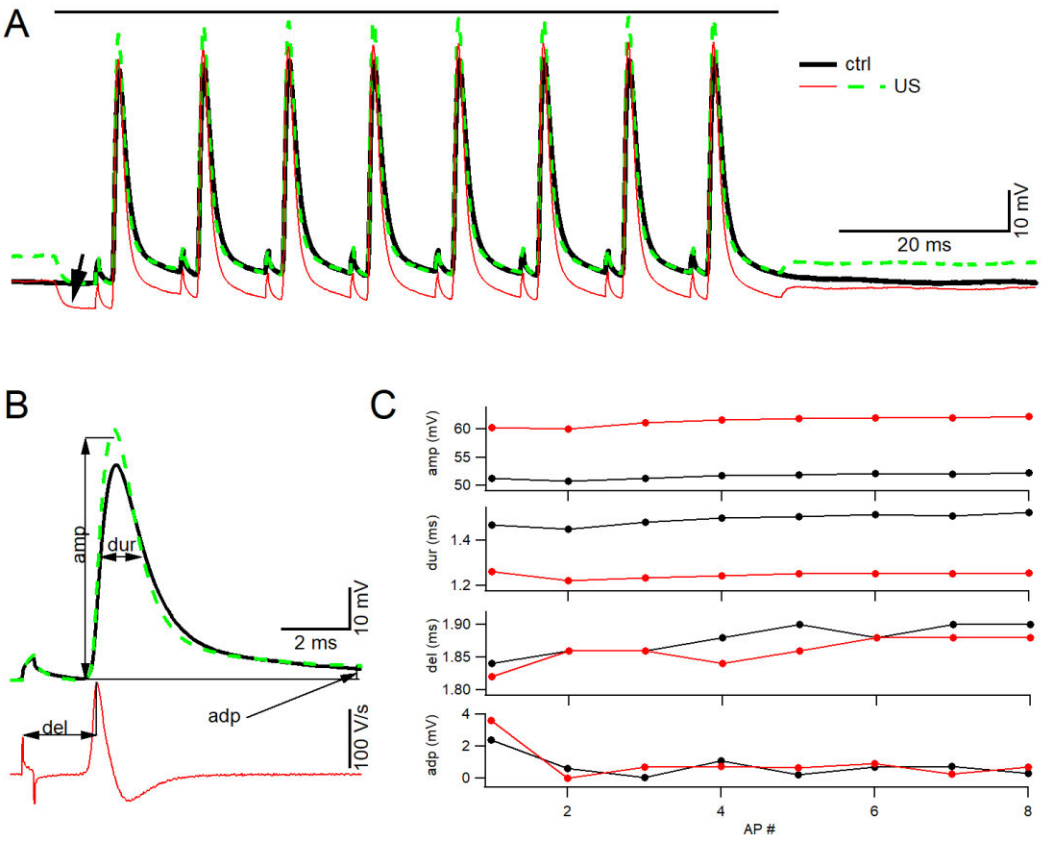

Figure 5.1 Effects of focused ultrasound on AP shapes. (A) A train of 8 APs firing at 100 Hz during an 80 ms continuous, 2.1 MHz US tone. (Black bar above), which set off a hyperpolarization (arrow). Control AP (black) and AP recorded ruing FUS (red) are overlaid. The AP train under FUS is also shifted vertically so that the baselines before the first AP are aligned (green). These traces are single trial recordings. (B) The first APs in (A) are displayed in an expanded time scale to detail the changes in AP shape under FUS. Lower traces: time derivative of control AP, to facilitate the illustration of AP delay measurement. Criteria of measurement for parameters defining APs are illustrated. (See text) (C) AP amplitude (amp), duration (dur), delay (del) and afterdepolarization (adp) from all of the eight APs are measured and plotted. During US application, AP amplitude and durations exhibit significant changes while delay and afterdepolarization showed no change.

Comparison between control and US-treated APs is summarized by plotting AP amplitude (amp), duration (dur), conduction delay (del), and after-depolarizing potential (adp) for the eight APs shown (Fig.5.1C). The main parameters altered by US are AP amplitude (increase) and duration (decrease). AP conduction velocity was not changed. While adp was not changed in this preparation, this parameter was variable among preparations (data not shown).

5.2.2 FUS significantly enhanced the time derivatives of the AP

A representative pair of first APs from the train in Figure 5.1, with and without FUS, were normalized to eliminate the difference in RMP. A phase plot was drawn to further investigate the detailed changes in the AP kinetics and the artifacts caused by the AP-triggering electric stimulation applied on the proximal end of the axon. FUS caused an increase in the rising and falling rate besides the increase in the AP amplitude. The increase in the AP raising rate became obvious when the membrane was depolarized for about 5 mV (arrowhead in Fig.5.2) while the difference in falling rate became minimal when the membrane potential was recovered to approximate +10 mV from RMP. FUS included a maximum of ~30% increase in the time derivative (dv/dt).

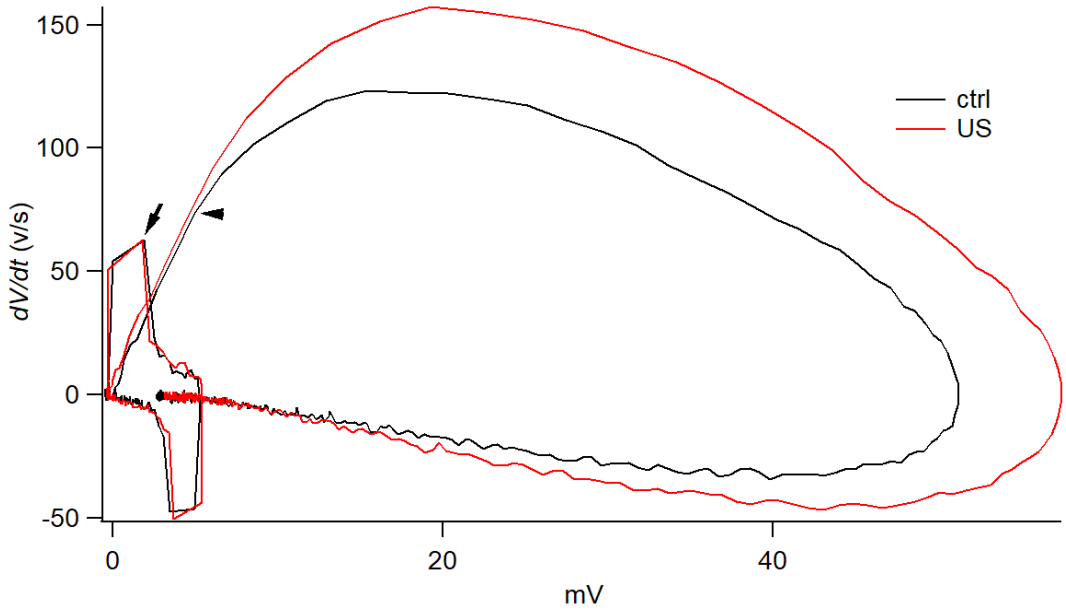

Figure 5.2 Changes in AP shape are compared in phase plots. Phase plots of control (black) and FUS modulated AP (red) are overlaid. The plot also includes the transients due to stimulus artifacts (arrow). There was minimal difference in stimulus artifact under FUS but the maximal and minimal time derivatives of the AP under FUS are significantly enhanced. Arrowhead identifies the point when the trajectories of the two traces diverge.

5.2.3 Discussion

First, we investigated the possibility that US may alter microelectrode characteristics such that AP measurements are no longer accurate (Microelectrode hypothesis). If the microelectrode characteristics are altered by FUS, it is expected that the alteration should be similar for AP and for stimulus artifacts, which exhibit voltage time courses comparable in speed to that of APs. In the overlaid APs in Figure 1B, stimulus artifacts overlap nearly perfectly between control (black) and under US (green) traces, but AP recorded under US was 13% larger in amplitude, and duration was reduced by 20%. The comparison was also evaluated using phase plots of the two APs shown in Figure 5.1B. There was a ~30% increase in dv/dt maximum of the AP recorded under FUS, derivatives

of the artifacts did not reveal any changes (Fig.5.2 arrow). Therefore, the increase in AP amplitude under FUS is unlikely to be due to changes in electrode characteristics.

Second, there is an obvious membrane hyperpolarization during FUS application, Fig.5.1A arrow. We consider the possibility that the hyperpolarization could shift the Na^+ channel out of an inactivated state such that an increase in Na channel availability could contribute to an enhanced AP amplitude (Inactivation hypothesis). This hypothesis is best illustrated by the Hodgkin-Huxley model of AP firing from control and hyperpolarized levels. The model uses kinetic parameters similar to those of the squid giant axon at 6.5 °C. Figure 5.3A illustrates that AP initiated by a 1 ms current step from -98 mV (red) exhibits a larger amplitude and longer duration than the AP initiated from -63 mV (black). Axons that exhibit these characteristics also can be fired by the anodal break (Fig.5.3B). AP fired due to the anodal break started from hyperpolarization of -9 mV and 20 ms in duration. The black AP to the right in Figure 5.3B represents an AP fired from the control resting membrane potential of -63 mV. The AP fired from the anodal break exhibits a larger amplitude and longer duration than that fired from the resting membrane potential of -63 mV (Fig.C). However, crayfish motor axons don't display these characteristics. Figure 5.3D shows a representative current clamp recording from a crayfish motor axon where hyperpolarization of -16 mV for 0.5 seconds did not trigger rebound AP. Therefore, there appear to be few Na^+ channels in the inactivated state at the resting membrane potential of -68 mV in this motor axon. This conclusion is consistent with the Na^+ channel inactivation curve in crayfish axon terminals published previously [170] which indicated that nearly 100% of the Na^+ channel should be in a closed and not inactivated state at a resting

membrane potential more negative than -70 mV. Furthermore, H-H model suggests that AP fired from hyperpolarized membrane potentials should have a longer duration which is inconsistent with the narrower AP recorded during US shown in Figure 5.1 and data published by other studies [174-177]. Therefore, the increased AP amplitude under FUS in the crayfish motor axons could not be explained by the inactivation hypothesis.

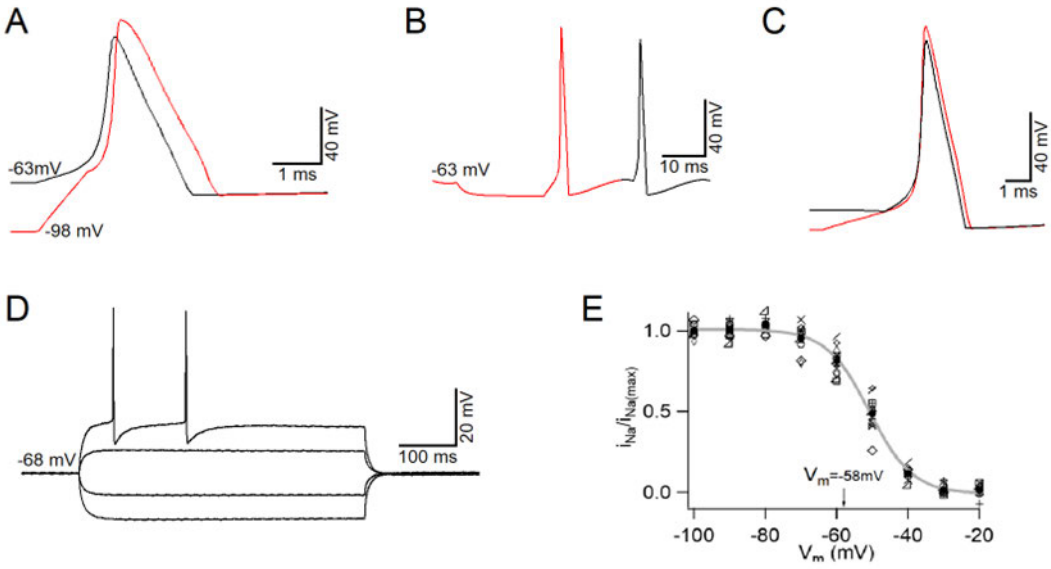

Figure 5.3 Evaluations of inactivation hypothesis by comparing prediction from the Hodgkin-Huxley model with recordings from the crayfish motor axons. (A) AP calculated from Hodgkin-Huxley (H-H) model. The two APs are fired by 1 ms current steps. AP fired from -98 mV exhibit a larger amplitude and broader duration. (B) Using the H-H model, a comparison of an AP fired from the anodal break (left) and a resting membrane potential of -63 mV (black) was performed. The initial hyperpolarization that set off the anodal break was achieved with a -5 nA and 20 ms current step. The second action potential was activated by a 10 nA and 1 ms current step. (C) Overlay of the two APs displayed in (B) to illustrate the larger amplitude and longer duration of the AP fired from the anodal break. (D) The current step series in a crayfish motor axon demonstrate that despite the larger and longer-lasting hyperpolarization than that shown in (B), no anodal break firing occurred in the crayfish motor axon. (E) Inactivation of I_{Na} recorded from the crayfish axonal terminals. The mid-point of the inactivation curve is -58 mV, adopted from [170].

Third, the reduction in AP duration may be due to FUS-activated TREK or TRAAK channels that are known to be mechanosensitive (K2P channel hypothesis). TREK and TRAAK channels belong to the K2P channel family and some member of this K channel

family has been shown to be thermally and mechanically sensitive [150]. TREK-1 and TRAAK channels are the main K conductance at the mammalian nodes of Ranvier and are responsible for AP repolarization in APs recording in the myelinated axons [178, 179]. The Block of TREK-1 and TRAAK channels has been shown to increase AP duration. It is possible that the effect of US on APs recorded in the crayfish motor axons, especially the reduction in AP duration and FUS-induced hyperpolarization, could potentially be explained by FUS-activated K2P channel opening. However, while this hypothesis explains the reduction in AP duration and the hyperpolarization under US, it cannot explain the increase in AP amplitudes shown in Figure 1, especially given our conclusion that the inactivation hypothesis does not apply to our observations. The presence of TREK-1 channels in the crayfish motor axons has been confirmed by membrane depolarization and increased input resistance after specific and non-specific TREK-1 blockers [144, 153]. Importantly, these blockers failed to block FUS-induced membrane hyperpolarization (FUSH) [144]. In conclusion, although the roles of TREK-1 channels on AP have not been investigated explicitly in the crayfish motor axons, failures of the blockers to inhibit FUSH strongly suggest that K2P channels are unlikely to underlie US mediated modulation of AP shapes shown in Figure 5.1.

Forth, to explain the US-induced increase in AP amplitude, mechanical impact mediated by FUS may directly interact with Na^+ channels such that the activation kinetics of Na^+ channels is accelerated. (Activation hypothesis) Previous studies in cardiac Na channels (Nav1.5) demonstrated an accelerated channel activation which increased I_{Na}, when the membrane was stretched [123] or under ultrasound [76]. Therefore, if US

pressure waves enhance Na^+ channels activation in the crayfish motor axon, this process should be able to accelerate the maximal rate of rise as well as the peak amplitude of APs. Indirect support for this hypothesis can be gleaned from the phase plot in Figure 5.2. Here the initial rising part of the plot overlapped before diverging (arrowhead). The initial rise that overlaps is typically attributed to the charging current from approaching APs. This component, being relatively small and may in part be driven by approaching AP from axons outside of US focal area, may not be significantly different in control vs US modulated APs. The part of the phase plot here the two APs diverge could be due to accelerated I_{Na}. Direct evaluation of this hypothesis required patch clamp analysis of sodium current in this preparation [170].

5.3 Conclusion

In this study, we have evaluated four hypotheses for the impact of FUS on the shapes of propagating AP. The rejections of the microelectrode hypothesis and inactivation hypothesis are based on clear experimental data and could be considered conclusive. The K2P hypothesis, while considered unlikely at present, cannot be discarded completely because of uncertainties regarding the pharmacology of crayfish K2P channels. In the absence of genomic information that can predict molecular structures of the crayfish K2P channels, we cannot exclude the possibility that the blockers we have used did not completely block the crayfish K2P channels in the crayfish that are sensitive to US. Finally, the activation hypothesis remains viable mainly because of the lack of experimental data specifically designed to test this hypothesis.

This report represents the beginning of exploring US ion channel interactions in the context of action potentials. In the future, potential contributions from other ion channels, such as potassium channels and mechanosensitive channels, or mechanical properties of lipid bilayers should also be incorporated to fully understand US modulation of action potentials.

CHAPTER 6. DISCUSSION

In this thesis, I showed that FUS-induced membrane responses in crayfish motor axons can be modulated by physical conditions that alter membrane properties. Lowering osmolarity to 75% changes FUSD characteristics in ways that supports the nanopore hypothesis. Specifically, low osmolarity enhances FUSD amplitude, frequency and reduced FUSD delays. These changes are expected from a stretched lipid bilayer which is more sensitive to US induced membrane poration. This study further examined the role of K2P channels on FUSH. A previous study had established the presence of this channel in crayfish motor axons. In addition, this channel is known to be US sensitive. Using temperature to titrate the availability of closed K2P channels to US activation, an enhanced FUSH in low temperature and an inhibition upon cooling are expected. Results from temperature dependence of FUSH did not conform to the prediction. Furthermore, specific K2P blockers, while effective in changing resting membrane potential and input resistance as the result of blocking K2P channels did not block FUSH. in combination, these results did not favor the contribution of K2P channel activation. At room temperature, FUS caused an increase in AP amplitude, suggesting an accelerating modulation of Na^+ channels. Meanwhile, the reduction in AP duration and the hyperpolarized shift in ADP during cooling indicated the activation of K^+ channels. In sum, FUS-induced responses on the crayfish axons most likely involve multiple mechanisms. The variance in the evoked mechanism may be caused by differences in the FUS parameters, including intensity,

duration, and intervals. Future investigation will need to understand tissue-specific mechanisms under certain FUS settings to fully control and optimize FUS effects.

6.1 Using crayfish neuromuscular junction as a model system to study FUS neuromodulation

In this report, the motor axons of the crayfish opener NMJ were used to investigate US-mediated neuromodulation under the conditions that could change membrane properties. The crayfish nerve-muscle preparation is one of the classical model systems that has contributed to the understanding of basic neurophysiological mechanisms of membrane excitability and synaptic transmission [180, 181]. The simplicity and hardiness of this preparation have been exploited for the initial implementations of new technologies such as calcium uncaging and calcium imaging [182, 183]. In the context of studies of US neuromodulation, the hardiness of this preparation allows for collection of large data sets for quantitative analysis of FUSD, which occurs stochastically. This preparation has also proved useful, in other biomedical applications of new technologies, such as microwave and infrared laser, in neuromodulation [90, 184].

6.2 Polymodal FUS effects on crayfish NMJ

Despite the stochastic nature of occurrence, FUSD was consistently activated with the same experimental setup on multiple crayfish preparations. Results in previous work [90] led to the nanopore hypothesis that a non-selective conductance was activated. Our further study [158] with hypotonic saline showed major predicted changes in FUSD, which supported the nanopore hypothesis (see Chapter 3). Besides the FUSD, FUSH was also recorded from the motor axons at the crayfish opener NMJ. The results (see Chapter 4)

suggested a sonophore hypothesis that the hyperpolarization resulted from the reduction of membrane capacitance. Finally, FUS effects on propagating APs indicated modulation of Na^+ channel kinetics (see Chapter 5).

In this study, the frequency of the ultrasound was consistently 2.1 MHz (except 2 MHz in experiments with fluoxetine application), but the duration of FUS application varied. In experiments when FUS mostly induced membrane depolarizations, we used a train of 20 pulses, each lasting for 50 μs, with a total application time of 20 ms (Fig. 2.1D). On the contrary, a continuous 80 ms FUS mostly evoked FUSH. A longer FUS application duration usually caused a larger temperature elevation due to the absorption of the acoustic energy [51]. The thermal increase could accelerate Na^+ inactivation and K^+ activation [185], causing a hyperpolarization of the membrane potential[186]. Although in this experiment temperature increase was <2℃ during FUS application at room temperature (data not shown), the thermal effect could be an alternative explanation of FUSH (see appendix). However, the rate of FUSH recovery was faster than that of temperature dissipation previously reported after the specimen has been heated by infrared laser transiently [184]. Therefore, despite the absence of direct of temperature measurement in our preparation, the temperature hypothesis is considered unlikely. Besides, FUS duration might also affect the capacitance current on the membrane resulting from tissue displacement-induced increase of membrane area [187]. The results in Chapter 4 also did not fully rule out the possible contribution of a K^+ channel, including or excluding K2P channels, to FUSH on the axon membrane. It is very likely that FUSH co-exist when only FUSD was observed if the large depolarization fully masked the small hyperpolarization.

To sum up, the results suggested: 1) US simultaneously activates multiple mechanisms on the same preparation; 2) the dominant FUS effects may depend on FUS application parameters; 3) activated mechanisms can be sensitive to manipulations on the membrane properties. Although the data points out the complexity of FUS-evoked responses and brings up confounds in practical applications, it also reveals possibilities of investigating different underlying mechanisms on an individual animal/neuron model. Future studies could focus on understanding involving mechanisms with optimized parameters to utilize FUS in the treatment of different purposes.

6.3 Conclusions and perspectives

This dissertation evaluates mechanisms underlying ultrasound mediated neuromodulation by examining impacts of membrane stretching and temperature on the efficacy of the neuromodulation. In addition, ultrasound modulation of action potentials was also investigated. We conclude the subject of mechanistic understanding of ultrasound mediated neuromodulation should be considered in two separate functional contexts. First, ultrasound can alter neuronal membrane potential from their resting state by at least two distinct mechanisms. High intensity ultrasound tends to generate lipid nanopores in neuronal membrane which leads to excitation due to the cationic permeability of the nanopores. Medium intensity ultrasound can generate membrane hyperpolarization, which is assumed to be mediated by a potassium channel although potential roles of K2P channels have been ruled out. Alternative hypotheses for the hyperpolarization, such as intramembrane cavitation, have been discussed. The conclusion from these considerations is that ultrasound could alter neuronal excitability by multiple processes depending on

ultrasound intensity and the ion channels present in the target tissues. Second, results presented in this thesis suggest that ultrasound can modulate action potentials, by making them larger and narrower. After eliminating multiple hypotheses, we proposed that the modulation of action potentials most likely involve changes in sodium channel kinetics. The interaction of ultrasound with ion channel kinetics presents a complex question because it needs to take into consideration impacts of ultrasound on lipid molecule organization in neuronal membrane, ion channels and lipid-channel interface. Future studies of this topic would require a combination of biophysical experiments with molecular dynamics simulations.

In conclusion, understanding of ultrasound mediated neuromodulation needs to take into consideration on how ultrasound could impact: (1) lipid bilayer of neuronal membrane, (2) mechanosensitive ion channels and (3) voltage gated ion channels. Depending on neuronal types—with different ion channel compositions and lipid molecules in neuronal membrane—and ultrasound application regimes, ultrasound could potentially trigger different neuronal responses. While the diverse responses appear confusing, in depth understanding of processes underlying these responses offers an opportunity to achieve specificity in modulation, excitation vs inhibition, and targeting of neuronal types in future human applications.

Manipulations on the membrane properties undoubtfully altered FUS effects on neuronal membranes, which provides a potential direction to study the underlying mechanisms of FUS-induced neuromodulations in specific applications. Besides, the results also suggest that under pathological conditions that involves osmolarity or

temperature change, such as hydrocephalus and inflammation [188, 189], US application in patients may not provide the same outcomes as those observed in healthy individuals. On the other hand, osmolarity manipulations in combination with temperature controls may expand the effectiveness of US application in human.

APPENDIX

FUS (2.1 MHz, continuous application of 80 ms) induced a small hyperpolarization on the membrane of the isolated crayfish opener axon. To test the effects on APs, a train of 8 APs was triggered by electric stimulations applied at the proximal end of the axon. FUS slightly increased the amplitudes of all the APs in the train despite the AP taking off from the FUSH. Compared to trials without FUS, a large variation in the membrane potential, which became more significant during the repolarization phase. Heating enhanced the FUSH but reduced the FUS-induced potential fluctuations. Heating also hyperpolarized RMP and decreased AP amplitude as predicted. In general, FUS increased dv/dt in both temperatures but the effect is more obvious at the higher temperature.

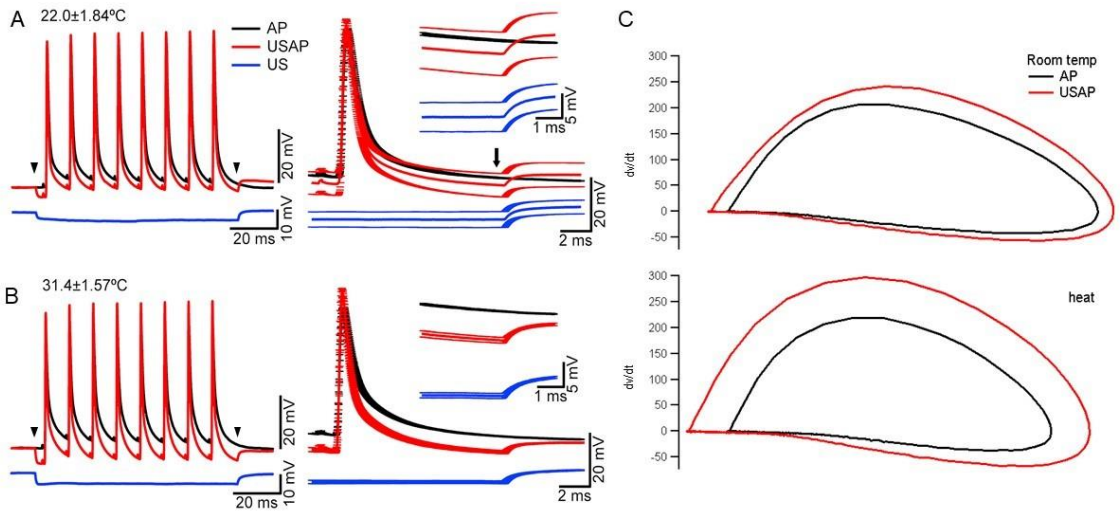

Figure Appendix 1 A representative example comparing FUS effects in room temperature versus heated temperature. (A) A train of AP without FUS application (black) and during simultaneous FUS (red). The traces were averaged from 23 repeated trials on the same axon. FUS alone induced a small hyperpolarization (blue) on the motor axon. Arrowheads denote the onset and offset of FUS tone burst delivery. The average last AP in the train replot with a higher magnification (right) to illustrate FUS-induced potential fluctuations (inset). (B) Same as (A) but recorded in elevated temperature. Averaged from 19 trials. (C) Phase plots of the last AP in the train with (US) or without (black) FUS at the 2 different temperatures.

Figure Appendix 2 illustrates the analysis of four parameters used to characterize the last AP in the train. Heating reduced AP AMP, DEL, DUR_{50}, and the difference between the first and last ADP. FUS significantly increased AMP and decreased DUR_{50} but did not cause significant changes in DEL and ΔADP. Heating reduced FUS effects on AP AMP but enhanced that on ΔADP.

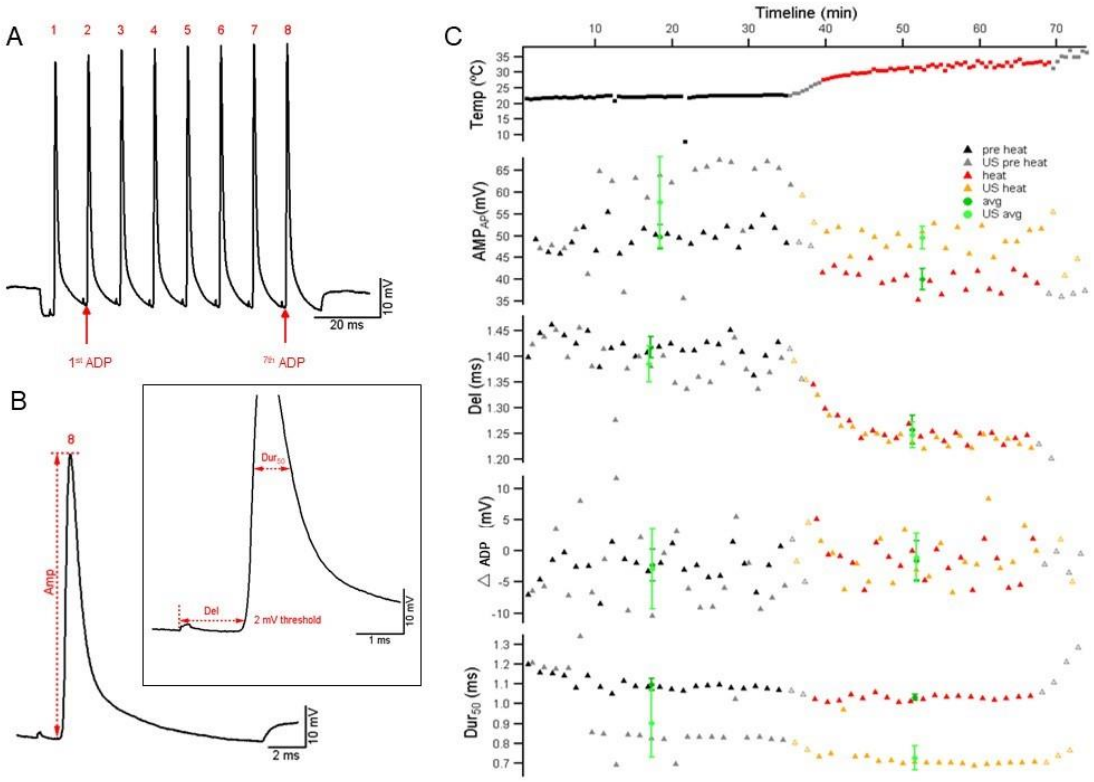

Figure Appendix 2 Effects of FUS on AP characteristics at different temperatures. (A) Illustration of measurements of ADP. ΔADP = 1st ADP – 7th ADP. (B) Illustration of measurements of amplitude (AMP), 50% duration (DUR_{50}), and delay (DEL) of US-induced responses (inset). (B) Timeline of the temperature of bath saline <0.3 mm away from the electrode recording sites, and the measured parameters of the 8th AP at room temperature (black) and heated temperature (red). Each data point represents the measurement of a single trial. Lighter colors illustrated data obtained with FUS application at 22.0 ± 1.84 ℃ (grey) and 31.4 ± 1.57℃ (yellow), respectively. The transition period (grey in the temperature timeline) was excluded from calculations of the averages (green, FUS; dark green, control).

BIBLIOGRAPHY

1. Lewis, P.M., et al., *Brain Neuromodulation Techniques: A Review.* Neuroscientist, 2016. **22**(4): p. 406–421. https://doi.org/10.1177/1073858416646707

2. Luan, S., et al., *Neuromodulation: present and emerging methods.* Frontiers in Neuroengineering, 2014. **7**: p. 27. https://doi.org/10.3389/fneng.2014.00027

3. Meng, Y., et al., *Chapter Ten - Focused ultrasound neuromodulation*, in *International Review of Neurobiology*, E. Moro, M. Polosan, and C. Hamani, Editors. 2021, Academic Press. p. 221–240.

4. Hallett, M., *Transcranial magnetic stimulation and the human brain.* Nature, 2000. **406**(6792): p. 147–150.

5. Hallett, M., *Transcranial Magnetic Stimulation: A Primer.* Neuron, 2007. **55**(2): p. 187–199.

6. Kobayashi, M. and A. Pascual-Leone, *Transcranial magnetic stimulation in neurology.* The Lancet. Neurology, 2003. **2**(3): p. 145–156.

7. Passera, B., et al., *Exploring the spatial resolution of TMS-EEG coupling on the sensorimotor region.* NeuroImage, 2022. **259**: p. 119419.

8. Karunarathne, W.K., P.R. O'Neill, and N. Gautam, *Subcellular optogenetics – controlling signaling and single-cell behavior.* Journal of Cell Science, 2015. **128**(1): p. 15–25. https://doi.org/10.1242/jcs.154435

9. Rost, B.R., et al., *Optogenetic Tools for Subcellular Applications in Neuroscience.* Neuron, 2017. **96**(3): p. 572–603.

10. Richter, C.P., et al., *Neural stimulation with optical radiation.* Laser & Photonics Reviews, 2011. **5**(1): p. 68–80. https://doi.org/10.1002/lpor.200900044

11. Darrow, D.P., *Focused Ultrasound for Neuromodulation.* Neurotherapeutics, 2019. **16**(1): p. 88–99.

12. Tyler, W.J., S.W. Lani, and G.M. Hwang, *Ultrasonic modulation of neural circuit activity.* Current Opinion in Neurobiology, 2018. **50**: p. 222–231.

13. Wang, P., et al., *Brain Modulatory Effects by Low-Intensity Transcranial Ultrasound Stimulation (TUS): A Systematic Review on Both Animal and Human Studies.* Frontiers in Neuroscience 2019. **13**: p. 696. https://doi.org/10.3389/fnins.2019.00696

14. Darmani, G., et al., *Non-invasive transcranial ultrasound stimulation for neuromodulation.* Clinical Neurophysiology, 2022. **135**: p. 51–73.

15. Lynn, J.G., et al., *A new method for the generation and use of focused ultrasound in experimental biology.* Journal of General Physiology 1942. **26**(2): p. 179–193. https://doi.org/10.1085/jgp.26.2.179

16. Fry W.J., Barnard, J.W., et al., *Ultrasonic lesions in the mammalian central nervous system.* Science, 1955. **122**(3168): p. 517–518.

17. Copelan, A., et al., *High-Intensity Focused Ultrasound: Current Status for Image-Guided Therapy.* Seminars in Interventional Radiology, 2015. **32**(4): p. 398–415. https://doi.org/10.1055/s-0035-1564793

18. Fishman, P.S. and V. Frenkel, *Focused Ultrasound: An Emerging Therapeutic Modality for Neurologic Disease.* Neurotherapeutics, 2017. **14**(2): p. 393–404.

19. Kubanek, J., *Neuromodulation with transcranial focused ultrasound.* Neurosurgical Focus, 2018. **44**(2): p. E14. https://doi.org/10.3171/2017.11.focus17621

20. Ghanouni, P., et al., *Transcranial MRI-Guided Focused Ultrasound: A Review of the Technologic and Neurologic Applications.* AJR. American Journal of Roentgenology, 2015. **205**(1): p. 150–159. https://doi.org/10.2214/ajr.14.13632

21. Beisteiner, R.A., *Human Ultrasound Neuromodulation: State of the Art.* Brain Sciences, 2022. **12**(2): p. 208. https://doi.org/10.3390/brainsci12020208

22. Clement, G.T. and K. Hynynen, *A non-invasive method for focusing ultrasound through the human skull.* Physics in Medicine and Biology, 2002. **47**(8): p. 1219–1236. https://doi.org/10.1088/0031-9155/47/8/301

23. Legon, W., et al., *Pulsed ultrasound differentially stimulates somatosensory circuits in humans as indicated by EEG and FMRI.* PLoS One, 2012. **7**(12): p. e51177. https://doi.org/10.1371/journal.pone.0051177

24. Hameroff, S., et al., *Transcranial Ultrasound (TUS) Effects on Mental States: A Pilot Study.* Brain Stimulation, 2013. **6**(3): p. 409–415.

25. Legon, W., et al., *Transcranial focused ultrasound modulates the activity of primary somatosensory cortex in humans.* Nature Neuroscience, 2014. **17**(2): p. 322–329.

26. Lee, W., et al., *Image-Guided Transcranial Focused Ultrasound Stimulates Human Primary Somatosensory Cortex.* Scientific Reports, 2015. **5**(1): p. 8743.

27. Monti, M.M., et al., *Non-Invasive Ultrasonic Thalamic Stimulation in Disorders of Consciousness after Severe Brain Injury: A First-in-Man Report.* Brain Stimulation, 2016. **9**(6): p. 940–941.

28. Beisteiner, R.A., et al., *Transcranial Pulse Stimulation with Ultrasound in Alzheimer's Disease – A New Navigated Focal Brain Therapy.* Advanced Science, 2019. **7**(3): p. 1902583. https://doi.org/10.1002/advs.201902583

29. Fomenko, A., et al., *Systematic examination of low-intensity ultrasound parameters on human motor cortex excitability and behavior.* eLife, 2020. **9**: p. e54497.

30. Guerra, A.A., et al., *Effects of Transcranial Ultrasound Stimulation on Trigeminal Blink Reflex Excitability.* Brain Science, 2021. **11**(5): p. 645. https://doi.org/10.3390/brainsci11050645

31. Matt, E., et al., *First evidence of long-term effects of transcranial pulse stimulation (TPS) on the human brain.* Journal of Translational Medicine, 2022. **20**(12): p. 26. https://doi.org/10.1186/s12967-021-03222-5

32. Baek, H., K.J. Pahk, and H. Kim, *A review of low-intensity focused ultrasound for neuromodulation.* Biomedical Engineering Letters, 2017. **7**(2): p. 135–142.

33. Blackmore, J., et al., *Ultrasound Neuromodulation: A Review of Results, Mechanisms and Safety.* Ultrasound in Medicine & Biology, 2019. **45**(7): p. 1509–1536. https://doi.org/10.1016/j.ultrasmedbio.2018.12.015

34. Young R.R. and E. Henneman, *Reversible block of nerve conduction by ultrasound.* Archives of Neurology, 1961. **4**: p. 83–89. https://doi.org/10.1001/archneur.1961.00450070085009

35. Colucci, V., et al., *Focused ultrasound effects on nerve action potential in vitro.* Ultrasound in Medicine & Biology, 2009. **35**(10): p. 1737–1747. https://doi.org/10.1016/j.ultrasmedbio.2009.05.002

36. Foley, J.L., J.W. Little, and S. Vaezy, *Image-guided high-intensity focused ultrasound for conduction block of peripheral nerves.* Annals of Biomedical Engineering, 2007. **35**(1): p. 109–119.

37. Juan, E.J., et al., *Vagus Nerve Modulation Using Focused Pulsed Ultrasound: Potential Applications and Preliminary Observations in a Rat.* International Journal of Imaging Systems and Technology, 2014. **24**(1): p. 67–71. https://doi.org/10.1002/ima.22080

38. Wright, C.J., J. Rothwell, and N. Saffari, *Ultrasonic stimulation of peripheral nervous tissue: an investigation into mechanisms.* Journal of Physics: Conference Series, 2015. **581**(1): p. 012003.

39. Zhang, T., et al., *Transcranial Focused Ultrasound Neuromodulation: A Review of the Excitatory and Inhibitory Effects on Brain Activity in Human and Animals.* Frontiers in Human Neuroscience, 2021. **15**: p. 749162. https://doi.org/10.3389/fnhum.2021.749162

40. Blackmore, J., et al., *Ultrasound Neuromodulation: A Review of Results, Mechanisms and Safety.* Ultrasound in Medicine & Biology, 2019. **45(7)**: p. 1509–1536.

41. Mohammadjavadi, M., et al., *Elimination of peripheral auditory pathway activation does not affect motor responses from ultrasound neuromodulation.* Brain Stimulation, 2019. **12**(4): p. 901–910.

42. Guo, H., et al., *Ultrasound Produces Extensive Brain Activation via a Cochlear Pathway.* Neuron, 2018. **98**(5): p. 1020–1030.e4.

43. Sato, T., M.G. Shapiro, and D.Y. Tsao, *Ultrasonic Neuromodulation Causes Widespread Cortical Activation via an Indirect Auditory Mechanism.* Neuron, 2018. **98**(5): p. 1031–1041.e5.

44. Braun, V., et al., *Transcranial ultrasound stimulation in humans is associated with an auditory confound that can be effectively masked.* Brain Stimulation, 2020. **13**(6): p. 1527–1534.

45. Zou, J., et al., *Ultrasound Neuromodulation Inhibits Seizures in Acute Epileptic Monkeys.* iScience, 2020. **23**(5): p. 101066.

46. Lin, Z., et al., *Ultrasound Stimulation Modulates Voltage-Gated Potassium Currents Associated with Action Potential Shape in Hippocampal CA1 Pyramidal Neurons.* Frontiers in Pharmacology, 2019. **10**: p. 544. https://doi.org/10.3389/fphar.2019.00544

47. Lim, J.A., et al., *ASIC1a is required for neuronal activation via low-intensity ultrasound stimulation in mouse brain.* eLife, 2021. **10**: p. e61660. https://doi.org/10.7554/elife.61660

48. Yoo, S., et al., *Focused ultrasound excites cortical neurons via mechanosensitive calcium accumulation and ion channel amplification.* Nature Communications, 2022. **13**(1): p. 493.

49. Tufail, Y., et al., *Transcranial Pulsed Ultrasound Stimulates Intact Brain Circuits.* Neuron, 2010. **66**(5): p. 681–694.

50. O'Brien, W.D., *Ultrasound–biophysics mechanisms.* Progress in Biophysics and Molecular Biology, 2007. **93**(1): p. 212–255.

51. Hershkovitz, R., E. Sheiner, and M. Mazor, *Ultrasound in obstetrics: a review of safety.* European Journal of Obstetrics & Gynecology and Reproductive Biology, 2002. **101**(1): p. 15–18.

52. Kim, T., et al., *Thermal effects on neurons during stimulation of the brain.* Journal of Neural Engineering, 2022. **19**(5): p. 056029. https://doi.org/10.1088/1741-2552/ac9339

53. Owen, S.F., M.H. Liu, and A.C. Kreitzer, *Thermal constraints on in vivo optogenetic manipulations.* Nature Neuroscience, 2019. **22**(7): p. 1061–1065.

54. Kiyatkin, E.A., *Brain temperature and its role in physiology and pathophysiology: Lessons from 20 years of thermorecording.* Temperature, 2019. **6**(4): p. 271–333. https://doi.org/10.1080/23328940.2019.1691896

55. Kim, M.G., et al., *Image-guided focused ultrasound modulates electrically evoked motor neuronal activity in the mouse peripheral nervous system in vivo.* Journal of Neural Engineering, 2020. **17**(2): p. 026026. https://doi.org/10.1088/1741-2552/ab6be6

56. Collins, M.N., W. Legon, and K.A. Mesce, *The Inhibitory Thermal Effects of Focused Ultrasound on an Identified, Single Motoneuron.* eNeuro, 2021. **8**(2). https://doi.org/10.1523/ENEURO.0514-20.2021

57. Prieto, M.L., et al., *Dynamic response of model lipid membranes to ultrasonic radiation force.* PLoS One, 2013. **8**(10): p. e77115. https://doi.org/10.1371/journal.pone.0077115

58. Plaksin, M.A., E.A. Kimmel, and S.A. Shoham, *Cell-Type-Selective Effects of Intramembrane Cavitation as a Unifying Theoretical Framework for Ultrasonic Neuromodulation.* eNeuro, 2016. **3**(3). https://doi.org/10.1523/ENEURO.0136-15.2016

59. Lentacker, I., et al., *Understanding ultrasound induced sonoporation: Definitions and underlying mechanisms.* Advanced Drug Delivery Reviews, 2014. **72**: p. 49–64.

60. Hodgkin A.L. and A.F. Huxley, *A quantitative description of membrane current and its application to conduction and excitation in nerve.* Journal of Physiology, 1952. **117**(4): p. 500–544. https://doi.org/10.1113/jphysiol.1952.sp004764

61. Mosgaard, L.D., T. Zecchi, and T. Heimburg, *Mechano-capacitive properties of polarized membranes.* Soft Matter, 2015. **11**: 7899–7910. https://doi.org/10.1039/C5SM01519G

62. Prieto, M.L., et al., *Dynamic response of model lipid membranes to ultrasonic radiation force.* PLoS One, 2013. **8**(10): p. e77115.

63. Karthikesh, M.A. and X. Yang, *The effect of ultrasound cavitation on endothelial cells.* Experimental Biology and Medicine, 2021. **246**(7): p. 758–770. https://doi.org/10.1177/1535370220982301

64. Wang, S., et al., *Ultrasonic Neuromodulation and Sonogenetics: A New Era for Neural Modulation.* Frontiers in Physiology, 2020. **11**: p. 787. https://doi.org/10.3389/fphys.2020.00787

65. Chavan, P.A., et al., *Application of High-Intensity Ultrasound to Improve Food Processing Efficiency: A Review.* Food, 2020. **11**(1): p. 122. https://doi.org/10.3390/foods11010122

66. Thanh Nguyen, T., et al., *Dependence of cavitation, chemical effect, and mechanical effect thresholds on ultrasonic frequency.* Ultrasonics Sonochemistry, 2017. **39**: p. 301–306.

67. Tyler, W.J., *Noninvasive neuromodulation with ultrasound? A continuum mechanics hypothesis.* Neuroscientist, 2011. **17**(1): p. 25–36.

68. Krasovitski, B., et al., *Intramembrane cavitation as a unifying mechanism for ultrasound-induced bioeffects.* Proceedings of the National Academy of Sciences of the United States of America, 2011. **108**(8): p. 3258–3263. https://doi.org/10.1073/pnas.1015771108

69. Vykhodtseva, N.I., K. Hynynen, and C. Damianou, *Histologic effects of high intensity pulsed ultrasound exposure with subharmonic emission in rabbit brain in vivo.* Ultrasound in Medicine & Biology, 1995. **21**(7): p. 969–979.

70. Menz, M.D., et al., *Radiation Force as a Physical Mechanism for Ultrasonic Neurostimulation of the* Ex Vivo *Retina.* The Journal of Neuroscience, 2019. **39**(32): p. 6251. https://doi.org/10.1523/jneurosci.2394-18.2019

71. Sarvazyan, A.P., O.V. Rudenko, and W.L. Nyborg, *Biomedical Applications of Radiation Force of Ultrasound: Historical Roots and Physical Basis.* Ultrasound in Medicine & Biology, 2010. **36**(9): p. 1379–1394.

72. Verhaagen, B. and D. Fernández Rivas, *Measuring cavitation and its cleaning effect.* Ultrasonics Sonochemistry, 2016. **29**: p. 619–628.

73. McDannold, N. and S.E. Maier, *Magnetic resonance acoustic radiation force imaging.* Medical Physics, 2008. **35**(8): P. 3748–3758. https://doi.org/10.1118/1.2956712

74. Spasic, M., K. Maki, and C.R. Jacobs, *5.6 Effects of Mechanical Stress on Cells.* In *Comprehensive Biomaterials II*, *vol. 5,* P. Ducheyne, Editor. 2017, Elsevier: Oxford. p. 102–114.

75. Kubanek, J.A., et al., *Ultrasound Elicits Behavioral Responses through Mechanical Effects on Neurons and Ion Channels in a Simple Nervous System.* Journal of Neuroscience, 2018. **38**(12): p. 3081–3091. https://doi.org/10.1523/jneurosci.1458-17.2018

76. Kubanek, J., et al., *Ultrasound modulates ion channel currents.* Scientific Reports, 2016. **6**: p. 24170.

77. Sorum, B., et al., *Ultrasound activates mechanosensitive TRAAK K+ channels through the lipid membrane.* Proceedings of the National Academy of Sciences of the United States of America, 2021. **118**(6): p. e2006980118.

78. Qiu, Z., et al., *The Mechanosensitive Ion Channel Piezo1 Significantly Mediates In Vitro Ultrasonic Stimulation of Neurons.* iScience, 2019. **21**: p. 448–457.

79. Tyler, W.J., et al., *Remote excitation of neuronal circuits using low-intensity, low-frequency ultrasound.* PLoS One, 2008. **3**(10): p. e3511. https://doi.org/10.1371/journal.pone.0003511

80. Prieto, M.L., et al., *Spike frequency-dependent inhibition and excitation of neural activity by high-frequency ultrasound.* Journal of General Physiology, 2020. **152**(11): p. e202012672. https://doi.org/10.1085/jgp.202012672

81. Rydqvist, B., et al., *Mechanotransduction and the crayfish stretch receptor.* Physiology & Behavior, 2007. **92**(1): p. 21–28.

82. Ye, J., et al., *Ultrasonic Control of Neural Activity through Activation of the Mechanosensitive Channel MscL.* Nano Letters, 2018. **18**(7): p. 4148–4155. https://doi.org/10.1021/acs.nanolett.8b00935

83. Lin, J.W., et al., *Focused ultrasound transiently increases membrane conductance in isolated crayfish axon.* Journal of Neurophysiology, 2019. 1**21**(2): p. 480–489. https://doi.org/10.1152/jn.00541.2018

84. Morris, C.E. and U. Homann, *Cell surface area regulation and membrane tension.* Journal of Membrane Biology, 2001. **179(2)**: p. 79–102. https://doi.org/10.1007/s002320010040

85. Tieleman, D.P., et al., *Simulation of pore formation in lipid bilayers by mechanical stress and electric fields.* Journal of the American Chemical Society, 2003. **125**(21): p. 6382–6383. https://doi.org/10.1021/ja029504i

86. Morris, C.E. and U. Homann, *Cell surface area regulation and membrane tension.* Journal of Membrane Biology, 2001. **179**(2): p. 79–102. https://doi.org/10.1007/s002320010040

87. Leontiadou, H., A.E. Mark, and S.J. Marrink, *Molecular dynamics simulations of hydrophilic pores in lipid bilayers.* Biophysical Journal, 2004. **86**(4): p. 2156–2164. https://doi.org/10.1016/S0006-3495(04)74275-7

88. Alam Shibly, S.U., C. Ghatak, et al., *Experimental Estimation of Membrane Tension Induced by Osmotic Pressure.* Biophysical Journal, 2016. **111**(10): p. 2190–2201. https://doi.org/10.1016/j.bpj.2016.09.043

89. Hu, Q., R.P. Joshi, and K.H. Schoenbach, *Simulations of nanopore formation and phosphatidylserine externalization in lipid membranes subjected to a high-intensity, ultrashort electric pulse.* Physical Review. E, Statistical, Nonlinear, and Soft Matter Physics, 2005. **72**(3 pt. 1): p. 031902. https://doi.org/10.1103/physreve.72.031902

90. Lin, J.W., et al., *Focused ultrasound transiently increases membrane conductance in isolated crayfish axon.* Journal of Neurophysiology, 2019. **121**(2): p. 480–489.

91. Chapman, D., *Phase transitions and fluidity characteristics of lipids and cell membranes.* Quarterly Review of Biophysics, 1975. **8**(2): p. 185–235. https://doi.org/10.1017/s0033583500001797

92. Heller, H., M. Schaefer, and K. Schulten, *Molecular dynamics simulation of a bilayer of 200 lipids in the gel and in the liquid crystal phase.* Journal of Physical Chemistry, 1993. **97**(31): p. 8343–8360.

93. Ricchelli, F., et al., *Changes of the Fluidity of Mitochondrial Membranes Induced by the Permeability Transition.* Biochemistry, 1999. **38**(29): p. 9295–9300.

94. Faller, R. and S.J. Marrink, *Simulation of domain formation in DLPC-DSPC mixed bilayers.* Langmuir, 2004. **20**(18): p. 7686–7693. https://doi.org/10.1021/la0492759

95. Caron, B., A.E. Mark, and D. Poger, *Some Like It Hot: The Effect of Sterols and Hopanoids on Lipid Ordering at High Temperature.* The Journal of Physical Chemistry Letters, 2014. **5**(22): p. 3953–3957.

96. Reddy, S.T., et al., *Cholesterol-dependent thermotropic behavior and organization of neuronal membranes.* Biochimica et Biophysica Acta (BBA) - Biomembranes, 2016. **1858**(11): p. 2611–2616.

97. Goldstein, D.B., *The effects of drugs on membrane fluidity.* Annual Review of Pharmacology, 1984. **24**: p. 43–64. https://doi.org/10.1146/annurev.pa.24.040184.000355

98. Hodgkin A.L. and B. Katz, *The effect of sodium ions on the electrical activity of giant axon of the squid.* Journal of Physiology, 1949. **108**(1): p. 37–77. https://doi.org/10.1113/jphysiol.1949.sp004310

99. Thompson, S.M., L.M. Masukawa, and D.A. Prince, *Temperature dependence of intrinsic membrane properties and synaptic potentials in hippocampal CA1 neurons in vitro.* The Journal of Neuroscience, 1985. **5**(3): p. 817.

100. Volgushev, M., et al., *Membrane properties and spike generation in rat visual cortical cells during reversible cooling.* The Journal of Physiology, 2000. **522**(1): p. 59–76.

101. Wang, L., et al., *Temperature-dependent transitions of burst firing patterns in a model pyramidal neuron.* Neurophysiology, 2012. **44**(4): p. 265–273.

102. Elwassif, M.M., et al., *Bio-heat transfer model of deep brain stimulation induced temperature changes.* Conference Proceedings : ... Annual International Conference of the IEEE Engineering in Medicine and Biology Society, 2006. **2006**: p. 3580–3583. https://doi.org/10.1109/iembs.2006.259425

103. Lamas, J.A.., L. Rueda-Ruzafa, and S.A. Herrera-Pérez, *Ion Channels and Thermosensitivity: TRP, TREK, or Both?* International Journal of Molecular Sciences, 2019. **20**(10): p. 2371. https://doi.org/10.3390/ijms20102371

104. Noël, J., et al., *The mechano-activated K^+ channels TRAAK and TREK-1 control both warm and cold perception.* EMBO Journal, 2009. **28**(9): p. 1308–1318. https://doi.org/10.1038/emboj.2009.57

105. Bradacs H. R. Cooper, et al., *Differential physiology and morphology of phasic and tonic motor axons in a crayfish limb extensor muscle.* Journal of Experimental Biology, 1997. **200**(Pt 4): p. 677–691. https://doi.org/10.1242/jeb.200.4.677

106. Lin, J.W., *Electrophysiological events recorded at presynaptic terminals of the crayfish neuromuscular junction with a voltage indicator.* Journal of Physiology, 2008. **586**(Pt 20): p. 4935–4950. https://doi.org/10.1113/jphysiol.2008.158089

107. Lin, J.W., *Spatial variation in membrane excitability modulated by 4-AP-sensitive K+ channels in the axons of the crayfish neuromuscular junction.* Journal of Neurophysiology, 2012. **107**(10): p. 2692–2702. https://doi.org/10.1152/jn.00857.2011

108. Lin, J.W., *Spatial gradient in TTX sensitivity of axons at the crayfish opener neuromuscular junction.* Journal of Neurophysiology, 2012. **109**(1): p. 162–170. https://doi.org/10.1152/jn.00463.2012

109. Lin, J.W., *Na+ current in presynaptic terminals of the crayfish opener cannot initiate action potentials.* Journal of Neurophysiology, 2016. **115**(1): p. 617–621. https://doi.org/10.1152/jn.00959.2015

110. Vyshedskiy, A. and J.W. Lin, *Study of the inhibitor of the crayfish neuromuscular junction by presynaptic voltage control.* Journal of Neurophysiology, 1997. **77**(1): p. 103–115.

111. Wright, S.N., M.S. Brodwick, and G.D. Bittner, *Presynaptic calcium currents at voltage-clamped excitor and inhibitor nerve terminals of crayfish.* Journal of Physiology, 1996. **496** (Pt 2): p. 347–361.

112. Lin, J.W., *Spatial variation in membrane excitability modulated by 4-AP-sensitive K+ channels in the axons of the crayfish neuromuscular junction.* Journal of Neurophysiology, 2012. **107**(10): p. 2692–2702.

113. Miller, D.L., *Safety assurance in obstetrical ultrasound.* Seminars in Ultrasound, CT, and MR, 2008. **29**(2): p. 156–164.

114. Hodgkin, A.L. and A.F. Huxley, *A quantitative description of membrane current and its application to conduction and excitation in nerve.* Journal of Physiology, 1952. **117**(4): p. 500–544.

115. Tyler, W.J., Y. Tufail, and S. Pati, *Pain: Noninvasive functional neurosurgery using ultrasound.* Nature Reviews. Neurology, 2010. **6**(1): p. 13–14.

116. Tyler, W.J., et al., *Remote excitation of neuronal circuits using low-intensity, low-frequency ultrasound.* PLoS One, 2008. **3**(10): p. e3511.

117. Tufail, Y., et al., *Transcranial pulsed ultrasound stimulates intact brain circuits.* Neuron, 2010. **66**(5): p. 681–694.

118. Clement, G.T. and K. Hynynen, *A non-invasive method for focusing ultrasound through the human skull.* Physics in Medicine and Biology, 2002. **47**(8): p. 1219–1236.

119. Heimburg, T., *Lipid ion channels.* Biophysical Chemistry, 2010. **150**(1–3): p. 2–22.

120. Feng, B., L. Chen, and S.J. Ilham, *A review on ultrasonic neuromodulation of the peripheral nervous system: enhanced or suppressed activities?* Applied Sciences, 2019. **9**(8): p. 1637.

121. Zhang, T., et al., *Transcranial Focused Ultrasound Neuromodulation: A Review of the Excitatory and Inhibitory Effects on Brain Activity in Human and Animals.* Frontiers in Human Neuroscience, 2021. **15**: p. 749162.

122. Naor, O., S. Krupa, and S. Shoham, *Ultrasonic neuromodulation.* Journal of Neural Engineering, 2016. **13**(3): p. 031003. https://doi.org/10.1088/1741-2560/13/3/031003

123. Morris, C.E. and P.F. Juranka, *Nav channel mechanosensitivity: activation and inactivation accelerate reversibly with stretch.* Biophysical Journal, 2007. **93**(3): p. 822–833.

124. Kubanek, J., et al., *Ultrasound Elicits Behavioral Responses through Mechanical Effects on Neurons and Ion Channels in a Simple Nervous System.* Journal of Neuroscience, 2018. **38**(12): p. 3081–3091.

125. Wu, J., A.H. Lewis, and J. Grandl, *Touch, Tension, and Transduction – The Function and Regulation of Piezo Ion Channels.* Trends in Biochemical Sciences, 2017. **42**(1): p. 57–71.

126. Tieleman, D.P., et al., *Simulation of pore formation in lipid bilayers by mechanical stress and electric fields.* Journal of the American Chemical Society, 2003. **125**(21): p. 6382–6383.

127. Hu, Q., R.P. Joshi, and K.H. Schoenbach, *Simulations of nanopore formation and phosphatidylserine externalization in lipid membranes subjected to a high-intensity, ultrashort electric pulse.* Physical Review. E, Statistical, Nonlinear, and Soft Matter Physics, 2005. **72**(3 Pt 1): p. 031902.

128. Atwood, H.L. and W.A. Morin, *Neuromuscular and axoaxonal synapses of the crayfish opener muscle.* Journal of Ultrastructure Research, 1970. **32**(3–4): p. 351–369. https://doi.org/10.1016/S0022-5320(70)80015-6

129. Smith, D.O., *Extracellular potassium levels and axon excitability during repetitive action potentials in crayfish.* Journal of Physiology, 1983. **336**: p. 143–157.

130. Dai, J. and M.P. Sheetz, *Mechanical properties of neuronal growth cone membranes studied by tether formation with laser optical tweezers.* Biophysical Journal, 1995. **68**(3): p. 988–996.

131. Dai, J., H.P. Ting-Beall, and M.P. Sheetz, *The secretion-coupled endocytosis correlates with membrane tension changes in RBL 2H3 cells.* Journal of General Physiology, 1997. **110**(1): p. 1–10.

132. Böckmann, R.A., et al., *Kinetics, statistics, and energetics of lipid membrane electroporation studied by molecular dynamics simulations.* Biophysical Journal, 2008. **95(4)**(1542-0086 (Electronic)): p. 1837–1850.

133. Krasovitski, B., et al., *Intramembrane cavitation as a unifying mechanism for ultrasound-induced bioeffects.* Proceedings of the National Academy of Sciences of the United States of America, 2011. **108**(8): p. 3258–3263.

134. Leontiadou, H., A.L. Mark, and S.J. Marrink, *Molecular dynamics simulations of hydrophilic pores in lipid bilayers.* Biophysical Journal, 2004. **86**(4): p. 2156–2164.

135. Babakhanian, M., et al., *Effects of Low Intensity Focused Ultrasound on Liposomes Containing Channel proteins.* Scientific Reports, 2018. **8**(1): p. 17250.

136. Leontiadou, H., A.E. Mark, and S.J. Marrink, *Ion transport across transmembrane pores.* Biophysical Journal, 2007. **92**(12): p. 4209–4215.

137. Baek, H., et al., *Clinical Intervention Using Focused Ultrasound (FUS) Stimulation of the Brain in Diverse Neurological Disorders.* Frontiers in Neurology, 2022. **13**: p. 880814.

138. Lescrauwaet, E., et al., *Recent Advances in the Use of Focused Ultrasound as a Treatment for Epilepsy.* Frontiers in Neuroscience, 2022. **16**: p. 886584.

139. Rabut, C., et al., *Ultrasound Technologies for Imaging and Modulating Neural Activity.* Neuron, 2020. **108**(1): p. 93–110.

140. Douguet, D. and E. Honore, *Mammalian Mechanoelectrical Transduction: Structure and Function of Force-Gated Ion Channels.* Cell, 2019. **179**(2): p. 340–354.

141. Sorum, B., et al., *Ultrasound activates mechanosensitive TRAAK K(+) channels through the lipid membrane.* Proceedings of the National Academy of Sciences of the United States of America, 2021. **118**(6): p. e2006980118. https://doi.org/10.1073/pnas.2006980118

142. Thompson, M.J. and J.E. Baenziger, *Ion channels as lipid sensors: from structures to mechanisms.* Nature Chemical Biology, 2020. **16**(12): p. 1331–1342.

143. Babakhanian, M., et al., *Effects of Low Intensity Focused Ultrasound on Liposomes Containing Channel proteins.* Scientific Reports, 2018. **8**(1): p. 17250.

144. Yu, F., et al., *Effects of Osmolarity on Ultrasound-Induced Membrane Depolarization in Isolated Crayfish Motor Axon.* Ultrasound in Medicine & Biology, 2022. **48**(10): p. 2040-2051.

145. Plaksin, M., S. Shoham, and E. Kimmel, *Intramembrane Cavitation as a Predictive Bio-Piezoelectric Mechanism for Ultrasonic Brain Stimulation.* Physical Review X, 2014. **4**(1): p. 011004. https://doi.org/10.1103/PhysRevX.4.011004

146. Lundbaek, J.A., et al., *Regulation of sodium channel function by bilayer elasticity: the importance of hydrophobic coupling. Effects of Micelle-forming amphiphiles and cholesterol.* Journal of General Physiology, 2004. **123**(5): p. 599–621.

147. Sepulveda, F.V., et al., *Molecular aspects of structure, gating, and physiology of pH-sensitive background K2P and Kir K+-transport channels.* Physiological Reviews, 2015. **95**(1): p. 179–217.

148. Brohawn, S.G., *How ion channels sense mechanical force: insights from mechanosensitive K2P channels TRAAK, TREK1, and TREK2.* Annals of the New York Academy of Sciences, 2015. **1352**: p. 20–32.

149. Lengyel, M., P. Enyedi, and G. Czirjak, *Negative Influence by the Force: Mechanically Induced Hyperpolarization via K2P Background Potassium Channels.* International Journal of Molecular Sciences, 2021. **22**(16): p. 9062. https://doi.org/10.3390/ijms22169062

150. Mathie, A., et al., *Two-Pore Domain Potassium Channels as Drug Targets: Anesthesia and Beyond.* Annual Review of Pharmacology and Toxicology, 2021. **61**: p. 401–420.

151. Kang, D., C. Choe, and D. Kim, *Thermosensitivity of the two-pore domain K+ channels TREK-2 and TRAAK.* Journal of Physiology, 2005. **564**(Pt 1): p. 103–116.

152. Schneider, E.R., et al., *Temperature sensitivity of two-pore (K2P) potassium channels.* Current Topics in Membranes, 2014. **74**: p. 113–133.

153. Zhu, X., et al., *Single infrared light pulses induce excitatory and inhibitory neuromodulation.* Biomedical Optics Express, 2022. **13**(1): p. 374–388.

154. Maingret, F., et al., *TREK-1 is a heat-activated background K(+) channel.* EMBO Journal, 2000. **19**(11): p. 2483–2491.

155. Noel, J., et al., *The mechano-activated K+ channels TRAAK and TREK-1 control both warm and cold perception.* EMBO Journal, 2009. **28**(9): p. 1308–1318.

156. Frankenhaeuser, B. and L.E. Moore, *The Effect of Temperature on the Sodium and Potassium Permeability Changes in Myelinated Nerve Fibres of Xenopus Laevis.* Journal of Physiology, 1963. **169**: p. 431–437.

157. Volgushev, M., et al., *Membrane properties and spike generation in rat visual cortical cells during reversible cooling.* Journal of Physiology, 2000. **522**(Pt 1): p. 59–76.

158. Yu, F., et al., *Effects of Osmolarity on Ultrasound-Induced Membrane Depolarization in Isolated Crayfish Motor Axon.* Ultrasound in Medicine & Biology, 2022. **48**(10): p. 2040–2051.

159. Thompson, S.M., L.M. Masukawa, and D.A. Prince, *Temperature dependence of intrinsic membrane properties and synaptic potentials in hippocampal CA1 neurons in vitro.* Journal of Neuroscience, 1985. **5**(3): p. 817–824.

160. Trevelyan, A.J. and J. Jack, *Detailed passive cable models of layer 2/3 pyramidal cells in rat visual cortex at different temperatures.* Journal of Physiology, 2002. **539**(Pt 2): p. 623–636. https://doi.org/10.1113/jphysiol.2001.013291

161. Rueda-Ruzafa, L., et al., *Are TREK Channels Temperature Sensors?* Frontiers in Cellular Neuroscience, 2021. **15**: p. 744702.

162. Kennard, L.E., et al., *Inhibition of the human two-pore domain potassium channel, TREK-1, by fluoxetine and its metabolite norfluoxetine.* British Journal of Pharmacology, 2005. **144**(6): p. 821–829.

163. Abraham, S., et al., *Effect of Temperature on the Structure, Electrical Resistivity, and Charge Capacitance of Supported Lipid Bilayers.* Langmuir, 2019. **35**(26): p. 8709–8715.

164. Rawicz, W., et al., *Elasticity, strength, and water permeability of bilayers that contain raft microdomain-forming lipids.* Biophysical Journal, 2008. **94**(12): p. 4725–4736.

165. Lemaire, T., et al., *MorphoSONIC: A morphologically structured intramembrane cavitation model reveals fiber-specific neuromodulation by ultrasound.* iScience, 2021. **24**(9): p. 103085.

166. Plaksin, M., E. Kimmel, and S. Shoham, *Cell-Type-Selective Effects of Intramembrane Cavitation as a Unifying Theoretical Framework for Ultrasonic Neuromodulation.* eNeuro, 2016. **3**(3). https://doi.org/10.1523/ENEURO.0136-15.2016

167. Pan, J., et al., *Temperature dependence of structure, bending rigidity, and bilayer interactions of dioleoylphosphatidylcholine bilayers.* Biophysical Journal, 2008. **94**(1): p. 117–124.

168. Leung, S.S.W., et al., *Measuring molecular order for lipid membrane phase studies: Linear relationship between Laurdan generalized polarization and deuterium NMR order parameter.* Biochimica et Biophysica Acta – Biomembranes, 2019. **1861**(12): p. 183053.

169. Lin, J.W., *Electrophysiological events recorded at presynaptic terminals of the crayfish neuromuscular junction with a voltage indicator.* Journal of Physiology, 2008. **586**(20): p. 4935–4950.

170. Lin, J.W., *Na+ current in presynaptic terminals of the crayfish opener cannot initiate action potentials.* Journal of Neurophysiology, 2016. **115**(1): p. 617–621.

171. Tufail, Y., et al., *Ultrasonic neuromodulation by brain stimulation with transcranial ultrasound.* Nature Protocols, 2011. **6**(9): p. 1453–1470.

172. Blackmore, J., et al., *Ultrasound Neuromodulation: A Review of Results, Mechanisms and Safety.* Ultrasound in Medicine & Biology, 2019. **45**(7): p. 1509–1536.

173. Feng, B., L. Chen, and S.J. Ilham, *A review on ultrasonic neuromodulation of the peripheral nervous system: enhanced or suppressed activities?* Applied Sciences, 2019. **9**(8): p. 1637. https://doi.org/10.3390%2Fapp9081637

174. Clennell, B., et al., *Transient ultrasound stimulation has lasting effects on neuronal excitability.* Brain Stimulation, 2021. **14**(2): p. 217–225.

175. Lin, Z., et al., *Ultrasound Stimulation Modulates Voltage-Gated Potassium Currents Associated with Action Potential Shape in Hippocampal CA1 Pyramidal Neurons.* Frontiers in Pharmacology, 2019. **10**: p. 544.

176. Prieto, M.L., et al., *Spike frequency-dependent inhibition and excitation of neural activity by high-frequency ultrasound.* Journal of General Physiology, 2020. **152**(11): p. e202012672. https://doi.org/10.1085/jgp.202012672

177. Qi, X., et al., *Low-Intensity Ultrasound Causes Direct Excitation of Auditory Cortical Neurons.* Neural Plasticity, 2021. **2021**: p. 8855055.

178. Kanda, H., et al., *TREK-1 and TRAAK Are Principal K(+) Channels at the Nodes of Ranvier for Rapid Action Potential Conduction on Mammalian Myelinated Afferent Nerves.* Neuron, 2019. **104**(5): p. 960–971 e7.

179. Schwarz, J.R., *Function of K2P channels in the mammalian node of Ranvier.* Journal of Physiology, 2021. **599**(19): p. 4427–4439.

180. Atwood, H., *Parallel `Phasic' and `Tonic' Motor Systems of the Crayfish Abdomen.* Journal of Experimental Biology, 2008. **211**(14): p. 2193–2195.

181. Lin, J.W., *Spatial gradient in TTX sensitivity of axons at the crayfish opener neuromuscular junction.* Journal of Neurophysiology, 2013. **109**(1): p. 162–170.

182. Delaney, K.R., R.S. Zucker, and D.W. Tank, *Calcium in motor nerve terminals associated with posttetanic potentiation.* Journal of Neuroscience, 1989. **9**(10): p. 3558-3567. https://doi.org/10.1523/jneurosci.09-10-03558.1989

183. Mulkey, R.M. and R.S. Zucker, *Calcium released by photolysis of DM-nitrophen triggers transmitter release at the crayfish neuromuscular junction.* Journal of Physiology, 1993. **462**: p. 243–260.

184. Zhu, X., J.-W. Lin, and M.Y. Sander, *Infrared inhibition and waveform modulation of action potentials in the crayfish motor axon.* Biomedical Optics Express, 2019. **10**(12): p. 6580–6594.

185. Colucci, V., et al., *Focused ultrasound effects on nerve action potential in vitro.* Ultrasound in Medicine & Biology, 2009. **35**(10): p. 1737–1747.

186. Buzatu, S., *The temperature-induced changes in membrane potential.* Rivista di Biologia, 2009. **102**(2): p. 199–217.

187. Vasan, A., et al., *Ultrasound Mediated Cellular Deflection Results in Cellular Depolarization.* Advanced Science, 2022. **9**(2): p. e2101950. https://doi.org/10.1002/advs.202101950

188. Gheorghita, E., C. Bucur, and L. Neagoe, *Control of fluid balance and osmolarity disorders in the cerebral pathology.* Romanian Journal of Neurology, 2009. **9**: p. 5–12.

189. Wang, H., et al., *Brain temperature and its fundamental properties: a review for clinical neuroscientists.* Frontiers in Neuroscience, 2014. **8**: p. 307. https://doi.org/10.3389/fnins.2014.00307

CURRICULUM VITAE